An Energy-Based Constitutive Model for the In-Plane Mechanical Behavior of Woven Fabrics

by
Michael J. King

B.S.M.E. Northeastern University
(2001)

Submitted to the Department of
Mechanical Engineering
in Partial Fulfillment of the Requirements
for the Degree of

MASTER OF SCIENCE IN MECHANICAL ENGINEERING

at the
Massachusetts Institute of Technology
June 2003

© Massachusetts Institute of Technology, 2003
All rights reserved

Signature of Author _____
Department of Mechanical Engineering
June, 2003

Certified by _____
Assistant Professor Simona Socrate, Mechanical Engineering
Thesis Supervisor

Accepted by _____
Professor Ain A. Sonin, Chairman
Department Graduate Committee, Department of Mechanical Engineering

BARKER

MASSACHUSETTS INSTITUTE OF TECHNOLOGY
JUL 0 8 2003
LIBRARIES

An Energy-Based Constitutive Model for the In-Plane Mechanical Behavior of Woven Fabrics

by
Michael J. King

Submitted to the Department of Mechanical Engineering
on May 28, 2003 in partial fulfillment of the requirements
for the Degree of Master of Science in Mechanical Engineering

ABSTRACT

We propose a new approach for developing a continuum model for the behavior of woven fabrics in planar deformation. The intent is to generate a physically motivated model that can both simulate existing fabrics and predict the mechanical behavior of novel fabrics based on the properties of the yarns and the weave. The continuum model captures the response of the fabric structure without explicitly modeling the yarns. The approach relies on the selection of a geometric model for the fabric weave, coupled with models of the mechanical responses of the yarns and the effects of yarn interactions. The fabric configuration is related to the macroscopic deformation gradient through an energy minimization method, and is then used to calculate the internal forces carried by the yarn families. The macroscopic stresses are determined from the internal forces using equilibrium arguments. Using this approach, we develop a model for the analysis of plain weave ballistic fabrics such as Kevlar. The model is based on a pin-joined beam geometry and includes the effects of axial and bending compliance of the yarns, crimp-interchange, rate dependent shear, and locking. Numerical implementation into the finite element code ABAQUS allows the simulation of fabric under different modes of deformation. We present comparisons between model predictions and experimental findings for quasi-static modes of in-plane loading. The model qualitatively captures all the behaviors exhibited in the experiments, and quantitatively predicts the experimentally measured fabric response for behaviors dominated by directly measurable fabric parameters, indicating that the model can serve as an effective predictive tool. Finally, the capability of the model to track variables that describe the behavior of the fabric at the structural level is demonstrated, and it is shown that these variables can be used to accurately predict the onset of failure.

Thesis Supervisor: Simona Socrate
Title: Assistant Professor of Mechanical Engineering

Acknowledgements

Writing a thesis is an extraordinary amount of work, and I could not have done it without the support of many people. This space is too small to acknowledge them all, but I would like to thank some of them here.

First and foremost, I would like to thank my advisor, Professor Simona Socrate, for all the support she has given me. She has not only guided my research and helped me solve innumerable problems that inevitably and unexpectedly arise, but she has also been exactly the sort of person that one always hopes to work for. I would also like to thank Professor Mary C. Boyce for advice and support she has given me, and I would like to thank both Professors Boyce and Socrate for involving me in this project.

Funding for this research was provided by the United States Army through the Institute for Soldier Nanotechnologies [ISN] at MIT. I would like to thank Phil Cunniff of the Natick Soldier Center for his technical insights regarding ballistic fabrics. DuPont Inc. provided us with fabric samples and technical information about ballistic armors. I want to thank James Singletary of DuPont for the information he provided regarding DuPont's ballistic fabrics.

I received valuable support from my fellow researcher Petch Jearanaisilawong, who conducted most of the experiments that contributed to this research. Without him, this thesis would not have been possible. I would also like to thank all my past and present friends and officemates here at MIT, who have helped me with everything from technical problems and office crises to studying for qualifying exams and keeping the stress level low.

I would like to acknowledge some of the excellent professors who have helped me understand the theoretical concepts vital to my research—Professor David Parks, Professor Lallit Anand, Professor Klaus-Jurgen Bathe, Professor John Hutchinson, Professor David Roylance, and Professor Nicholas Hadjiconstantinou.

Of course I must thank my all friends who, while they lent me no technical aid, were always there for me—especially my close friends Andy and James. My family, too, has been there for me. Thanks to my father Robert and my mother Margaret, and my sisters Laura and Alice.

I reserve my final thank you for the one person that changed my life and made my time at MIT a happy experience from the very start. Thank you, Carol. You are the most incredible person I have ever met.

Contents

Abstract **2**

Acknowledgements **3**

Table of Contents **4**

List of Figures **7**

List of Tables **10**

Chapter 1 – Introduction **11**

Chapter 2 – Background **14**

2.1 Mechanical Behavior of Fabrics 14

2.2 Modeling Background 17

2.3 Requirements for a General Approach to Model the Response of Woven Fabrics 21

Chapter 3 – The General Fabric Modeling Approach Applied to Develop a Ballistic Fabric Continuum Model **30**

3.1 Scope and Description of the Modeling Approach 30

3.1.1 Mechanics of a Planar Continuum Model for Woven Fabric 30

3.1.2 Overview of Approach 33

3.1.3 Definition of the Unit Cell 35

3.1.4 Selection of Component Constitutive Relations 36

3.1.5 Determination of the Fabric Configuration 36

3.1.6 Calculation of the Internal Forces 37

3.1.7 Determination of Macroscopic Stresses 37

3.1.8 Advantages and Disadvantages of the Proposed Approach 37

3.2 Definition of a Unit Cell 39

3.3 Component Constitutive Relations 43

3.3.1 Yarn Extension 44

3.3.2 Yarn Bending 46
3.3.3 Interference 47
3.3.4 Locking 50
3.3.5 Shear 52
3.4 Determining the Fabric State 55
3.4.1 Parameters from the Deformation Gradient 57
3.4.2 Parameters from Energy Minimization 58
3.5 Internal Forces and Macroscopic Stresses 60
3.5.1 Methods of Determining Stress 61
3.5.2 Strain Energy of a Simplified Model 62
3.5.3 Material Frame Indifference Constraints on the Strain Energy Function 63
3.5.4 Derivation of the Cauchy Stress 66
3.5.5 Interpretation of the Stress Tensor 68
3.5.6 Stress in the Complete Model. 70
Chapter 4 – Numerical Implementation of the Fabric Model. 82
4.1 Input and Output Requirements of the Finite Element Code 82
4.2 Overview of the Algorithm 83
4.2 Integration of Dissipative Shear Rotation 84
4.4 Energy Minimization 85
4.4.1 Newton's Method 85
4.4.2 The Downhill Simplex Method 88
4.4.3 Simulated Annealing 91
4.5 Numerical Jacobian Matrix 93
4.6 Local Buckling and Inertial Stabilization 94
4.7 Element Selection and Nonlinear Strain Gradients 98
Chapter 5 – Analysis of Boundary Value Problems 110
5.1 Testing the Behavior of the Model 110
5.2 Measuring the Fabric Properties 113
5.2.1 List of Model Parameters 113
5.2.2 Geometric Parameters 115
5.2.3 Component Constitutive Parameters 117

5.3 Experimental Comparison of Macroscopic Behavior 120
5.4 Predicting the Response of the Fabric Structure 125
Chapter 6 – Conclusions and Future Work 137
6.1 Conclusions 137
6.2 Future Work 140
Bibliography 142
Appendix – Model Source Code 145

List of Figures

2-1 Examples of woven fabrics 24
2-2 Knitted and non-woven fabrics 25
2-3 Crimp parameters 26
2-4 Twill weave showing crimp interchange leading to cross locking and shear rotation ("trellising") leading to shear locking 27
2-5 Plain weave fabric in a shear-locked state 27
2-6 Fabric geometry proposed by Pierce 27
2-7 Fabric geometry proposed by Kawabata 28
2-8 Roylance's ballistic fabric model 28
2-9 Finite element model of fabric structure 29
2-10 Trapezoidal fabric lattice model 29

3-1 Fabric treated as an anisotropic continuum with unit thickness 75
3-2 Ballistic fabric geometry and selection of unit cell 76
3-3 Typical stress-strain curves for Kevlar yarns from S706 ballistic fabric 77
3-4 Schematic of sandwich compression test and results for S706 ballistic fabric with exponential and power law fits 78
3-5 Typical behavior of fabrics in shear 79
3-6 Decomposition of shear angle into elastic and dissipative components (initially orthogonal) 79
3- 7 Typical energy surface for fabric in even biaxial tension 80
3-8 Energy function for buckling fabric geometry, at different states of even biaxial tension and shear. 80
3-9 Forces on the unit cell resulting from the simplified model's stress tensor 81

4-1 UMAT algorithm 102
4-2 Energy function in even biaxial extension 103
4-3 Convergence of $\{L_1, L_2\}$ in Newton's method for different initial guesses 103
4-4 Basic simplex algorithm 104
4-5 Newton's method and circulating simplex algorithm paths for uneven biaxial extension 104
4-6 Modified downhill simplex algorithm 105
4-7 Modified downhill simplex algorithm path for uneven biaxial extension 105
4-8 Simulated annealing and modified downhill simplex algorithm paths for uneven biaxial extension 106
4-9 Modes of local buckling for ballistic fabric geometry, with stabilizing inertia 107
4-10 Optimal warp strain for zero interference as a function of weft strain, with integration point strains of 4-node elements in element strip test 108
4-11 σ_{xx} stress contours showing oscillations in element strip test with linear strain elements 108
4-12 Work required to deform element strips of different element types with equivalent meshes 109
4-13 Stress patterns in a tensile test model that appear for different element types .109

5-1 Single element results showing crimp interchange capabilities of model 128
5-2 Single element results showing locking capabilities of model 129
5-3 Stress contours in simulated tensile test using locking dummy material 130
5-4 Stress-strain curve in simulated tensile test using locking dummy material 130
5-5 Fabric cross sections showing microstructure 131
5-6 Deformation and stresses in warp direction tensile test 132
5-7 Warp direction tensile test load-extension curves compared to model prediction 133
5-8 Weft direction tensile test load-extension curves compared to model prediction 133

5-9 Deformation of fabric strip in bias extension test.....134
5-10 Bias-extension load-extension curves compared to model prediction.....135
5-11 Contours of contact force between yarns.....136
5-12 Predicting fabric failure through yarn tensions.....136

List of Tables

3:1 Model Nomenclature 73
3:2 Summary of fabric deformation mechanisms 74

5:1 Dummy material properties used to test model behavior 127
5:2 Material data for S706 Kevlar 127

Chapter 1
Introduction

Fabrics are used in a wide variety of applications, including apparel, portable structures, architecture, parachutes, structural reinforcement, and body armor. Common features inherent to the mechanical response of woven fabrics are relevant for many of these applications. Despite this fact, fabric mechanics is not typically viewed as a unified field of study; rather, researchers working on each particular fabric application develop and use specific theories and models. Ballistic researchers use models that predict the behavior of fabric armors in response to ballistic impact, aeronautical engineers have developed theories that describe the behavior of fabric-reinforced composites, engineers in the textile industry have a good understanding of the behaviors of apparel fabrics relevant for the weaving process, and so forth. As advanced fabric technologies are developed, researchers seek a better understanding of fabric behavior in order to apply these technologies. They look beyond their respective fields and apply lessons from other fabric applications to solve problems in their own fields. Textile mechanics is becoming increasingly less specialized.

At the same time, new technologies permit the use of fabrics in novel applications as well as the improvement of fabrics used in conventional applications. These technologies are not limited to new weaving techniques that permit tighter weaves or better manufacturing processes that result in superior yarn materials. In particular, the emergence of micro- and nanotechnologies has opened the door to novel fabric applications. For example, flexible electronics can be woven among the yarns, and electronic components can be embedded within conventional yarns to create "smart" apparel. Microfluidic technologies could be used to create apparel or fabric structures that could regulate

temperatures or transport fluids. More advanced applications might integrate emerging "smart" materials—adaptive, actuated or shape-memory materials—into fabrics to obtain textiles with properties that can actively be controlled—e.g. to change the stiffness of a fabric armor or to create clothing that augments human muscles. Such novel fabric technologies could have a wide variety of applications, from enhanced protective clothing to superior portable structures.

In order to develop such advanced materials, it is necessary to understand the mechanical behavior of fabrics, both at the continuum scale and at the scale of the yarn structure. This understanding requires theoretical or computational tools to relate the macroscopic response of the fabric to the underlying behaviors of its yarns. The effect of macroscopic loads on the fabric structure must be understood. For example, if a yarn contains microfluidic tubes, it might be important to quantify the yarn deformation when the fabric is macroscopically loaded. If a fabric contains embedded electronics, it may be necessary to predict the transverse contact forces that the fabric weave will exert on those electronics when the fabric is loaded. Conversely, the effects that changes to the fabric structure have on its macroscopic response are also of interest. If a fabric contains an actuated material that can change its stiffness, a means of predicting how the stiffened fabric will behave macroscopically—for example, whether or not it could deflect a bullet—would be of interest. Novel woven materials might be combined with other materials in multi-component structures, so the nature of the fabric contributions to the mechanical behavior of a hierarchical ensemble needs to be understood as well.

While a wide variety of methods for modeling fabrics have been proposed in the literature, most of these methods are specific to a single field or application, and lack the generality necessary to aid the development and application of new technologies. This thesis presents a general approach to fabric modeling that can be used in a variety of specific applications. The proposed approach is capable of capturing both the macroscopic continuum behavior of woven fabrics as well as the response of the fabric internal structure with a sufficient decree of accuracy.

This document is structured as follows. **Chapter 2** presents background information regarding the mechanical behavior of fabrics, including common fabric behaviors and differences between fabrics and other materials. Existing fabric models are then outlined, and their strengths and weaknesses are discussed. Finally, the specific requirements that the new modeling approach proposes to meet are defined. **Chapter 3** presents the details of the fabric modeling approach, and describes how each step is applied to the development of a model for woven ballistic fabrics. **Chapter 4** reviews numerical challenges that arise in the implementation of the model into a finite element framework. **Chapter 5** discusses the procedure by which the model is experimentally validated. First, the model is tested for a range of materials properties designed to explore the model capabilities and ensure that it can capture all intended fabric behaviors. Next, real properties of a ballistic Kevlar fabric are measured experimentally, and these properties are used to simulate the macroscopic response of the fabric. The simulation results are compared to experimental data in order to test the validity of the proposed model. Finally, in **Chapter 6**, the conclusions from this research are reviewed and future work regarding this research is discussed.

Chapter 2
Background

2.1 Mechanical Behavior of Fabrics

A fabric is defined as a material formed by weaving families of yarns together. These yarns may be solid structures, but often are composed of many twisted or untwisted fibers spun together. This thesis is primarily concerned with woven fabrics, as opposed to knitted or non-woven fabrics. A woven fabric has a very well defined repeating structure and two clearly defined yarn families. The "warp" family tends to be the "primary" yarn family in the weave and is often the stronger, straighter, or stiffer of the two yarn families. The "weft" or "fill" yarn family tends to be woven across the warp yarns. Thus the weaving process determines the yarn families. There are several different types of weaves used in woven fabrics, such as "plain", "basket", "twill", and "satin" weaves; the principal difference between these is the number of adjacent yarns that cross above and below the yarns of each family. **Figure 2-1** shows examples of some common woven fabrics. For comparison, **Figure 2-2** shows knitted fabrics, which have a repeating pattern but no clearly defined yarn families, and a nonwoven fabric where the yarns have no repeating pattern or preferred orientation and are held together through friction and entanglements.

When considered as a macroscopic continuum, a woven fabric has a number of unique mechanical behaviors that sets it apart from other materials. One important mechanical characteristic is anisotropy. Due to the directionality of the yarns, woven fabrics are highly anisotropic, like long-fiber composites with two fiber families. However, there are several important differences between fabric behaviors and composite behaviors. A

fabric typically has no matrix to support its yarns in compression and distribute the load from one yarn to its neighbors or to the other family. The macroscopic bending stiffness is controlled by the very low bending stiffness of the yarns. Because of this, fabrics tend to buckle very easily and typically cannot bear any practical in-plane compressive loads. Even when a fabric is constrained to remain planar, preventing macroscopic buckling of the continuum (for example, if the fabric were sandwiched between two plates in a multi-layer structure), the yarns themselves will buckle locally. Consequently, fabrics are generally used in structural applications only to carry in-plane tensile loads. They behave like anisotropic membranes.

Instead of interacting through a matrix, yarns in a woven fabric interact because they cross over and under one another in an alternating pattern as they undulate through the weave. At the point where two yarns cross, one yarn has a peak in its undulation while the other has a trough. These undulations are referred to as "crimp" and are shown in **Figure 2-3**. The amplitude of undulation is referred to as the "crimp amplitude" and the angle that the yarn makes with the midplane of the fabric as the "crimp angle". A yarn family is said to have increased crimp when its crimp amplitude (and consequently its crimp angle) are increased. When yarns of one family are loaded in tension, they tend to straighten, decreasing their crimp. This mechanism allows significant elongation along the loaded yarns. If the decrease in crimp is not constrained, this elongation can occur at very low loads, due to the low bending stiffness of the yarns. However, when yarns of one family straighten and decrease their crimp, yarns of the crossing family are forced to increase their crimp and shorten their undulations, thereby causing the fabric to contract in the direction of the crossing yarns. Hence load in one direction is transferred to both yarn families, and elongation along one yarn direction requires contraction in the other direction to minimize load levels. This Poisson-like effect is referred to as "crimp interchange" and is an important behavior unique to woven fabrics, which introduces significant nonlinear effects in the mechanical response.

The behavior of woven fabrics in shear is unique as well. The primary mechanism for fabric shear is rotation of the yarns at the crossover points, as shown in **Figure 2-4**. The

two yarn families, which are initially orthogonal in most fabrics, become increasingly skewed as the angle between them changes. This mechanism is sometimes referred to as "trellising". It is interesting to note that, if the fabric is modeled as a continuum, shear deformation of this type is not volume conservative. Shear deformation is primarily resisted by friction at the crossover points, which counteracts the rotation of the yarns. In some fabrics it is also resisted by wrapping effects, as greater yarn lengths are required to wrap helically around crossing yarns at non-orthogonal angles. This causes contraction of both yarn families; if this contraction is prevented, yarn wrapping result in a stiffening effect that counteracts shear deformation.

At large shear angles, shear deformation is also resisted by locking. "Locking", also referred to as "jamming", is another important behavior unique to fabrics. During any mode of homogeneous planar deformation, yarns of the same family remain approximately parallel but may draw closer together, either due to shear deformation or to crimp interchange. However, yarns of the crossing family must still be able to pass between them. Sufficient deformation causes yarns to draw so close that they jam against the crossing yarns. This tends to arrest further deformation. When this condition arises because of shear deformation it is referred to as "shear locking"; when it arises due to crimp interchange during extension it is referred to as "cross locking". These phenomena are shown in **Figures 2-4** and **2-5**.

While the physical motivations for these behaviors are well understood, these deformation mechanisms raise significant challenges for models that do not explicitly include the underlying yarn structure. Approaches that have been used to develop classical material models need to be re-examined and modified to take a woven fabric's unique continuum behavior into account.

2.2 Modeling Background

As woven fabrics have been used in a variety of engineering applications, many fabric models have been proposed. Most of these models assume that yarns do not slip in the weave, since this assumption greatly facilitates model development, although it limits models to cases where the fabric has not begun to fail. Hearle, Grosberg and Backer [1969] describe a number of classical fabric models. One of the most widely adopted model geometries, proposed by Pierce in 1937, is shown in **Figure 2-6**. It models a plain weave fabric woven from yarns with solid, circular cross-sections. Pierce demonstrated that different geometric parameters of the weave (amplitude, crimp angle, yarn wrapping angle, etc.) can be related through various kinematic relations, thereby providing a means of analyzing the relationship between macroscopic deformation and changes to the fabric's internal structure. This model captures many important details of the fabric geometry that affect its mechanical behavior, but its complexity requires numerical methods to obtain solutions to the corresponding systems of nonlinear equations. Also, certain constraints, such as the assumption of solid, circular yarns, limit its applicability to a small range of fabrics.

Some researchers have suggested generalizing Pierce's geometry, at the cost of increased complexity. Others have proposed simpler alternative geometries to decrease the computational requirements. Realff [1992] discusses several of these alternative geometries. One of the simpler geometric models, proposed by Kawabata in 1973, is shown in **Figure 2-7**. It models the yarns as straight spars connected by pin joints at the yarn crossover points. This geometry is much simpler than Pierce's, and hence is easier to analyze, but does not capture certain fabric behaviors. While it can capture crimp interchange, yarn directionality, and shear, Kawabata's geometry can not include wrapping effects since it assumes straight-length distances between peaks and troughs in the yarn undulations. However, it is a popular model because these effects are not important in many applications, and Kawabata's geometry is one of the simplest possible models that still captures many fundamental fabric behaviors.

Many of the early mechanical models were developed before modern computers and finite element or finite difference methods were available, so they tend to be analytical in nature, consisting only of a set of equations that, given a set of input parameters and specific load and boundary conditions, could predict one or two aspects of the resulting fabric behavior. For example, one model might predict the effective warp direction modulus as a function of a uniform weft load, given the material properties of the fabric, while another might predict the warp direction load that will cause warp yarns to begin to break, provided the weft direction boundary conditions are known. These models, whether based on a simple geometry such as Kawabata's or a more complex geometry such as Pierce's, have limited versatility.

Recent fabric modeling efforts have attempted to formulate more universal material models that can be implemented into a numerical analysis code, with special emphasis on finite element applications. Some researchers, such as Ruan et. al. have considered a fabric to be an anisotropic continuum with two preferred material orientations [Raun et. al., 1996]. This approach is frequently used in the analysis of fabric-reinforced composites, and is equivalent to approximating the fabric as a long-fiber composite with two families of fibers. For non-reinforced fabrics, the isotropic "matrix" can be taken to have a very low or even negligible stiffness, since a non-reinforced fabric has no matrix. This approach has the advantage that existing material models for long-fiber composites have been developed and are already implemented into commercial finite element packages. However, it does not capture potentially important fabric behaviors such as crimp interchange or locking, since the fibers in a composite do not interweave. It is more appropriate for composites reinforced by knitted fabrics, but should not be used for any analysis of woven fabrics where crimp interchange or locking have a significant effect on the fabric response.

A number of researchers have abandoned the idea of a continuum model entirely. Breen et. al. proposes to model fabric as an array of interacting particles, and has shown this model to be very effective for simulating the low-stress behavior of fabrics, such as draping [Breen et. al., 1994]. Draping is typically a low stress behavior involving large

shear and out-of-plane deformations, and is important in both fabric-composite forming applications and in computer animation. Breen's approach has not been thoroughly explored as an alternative in high rate, high stress ballistic applications, and does not include any provisions for dissipative deformation. This model requires empirical testing to determine the potential fields that govern the particle interactions and therefore determine the mechanical behavior of the fabric, which limits its use as a predictive tool for the development of novel fabrics. It is also not well suited to directly provide information about the fabric structure, such as the tension in a yarn family or contact force between yarns.

The model most frequently used for ballistic analysis, proposed by Roylance [1995], is also a discrete model. Roylance's fabric model consists of a planar array of point masses, used to capture the inertial response of the fabric. The point masses are connected by a rectangular planar grid of massless spars oriented in the directions of the yarns. These spar elements capture the in-plane stiffness of the fabric and the directionality of the yarns. This model has no bending stiffness, since ballistic impacts are typically dominated by the out-of-plane inertia of the fabric and the in-plane stiffness. **Figure 2-8** shows the deformed shape that results in a ballistic analysis using this model. Roylance's model has been refined since it was originally proposed by various researchers, such as by Shim et. al. [1995], who proposes a modification that includes rate-dependent yarn behavior. This class of models has been proven effective at predicting the ballistic properties of fabric armors, such as the so-called "V_{50}" ballistic limit (the impact speed at which a projectile has a 50% chance of penetration) and the energy absorbed for penetrating projectiles, but it lacks the capability of capturing several features of fabric behavior, which renders it unsuitable for a more general study of fabrics. Because the spars lie in the same plane and have zero cross sectional area, this model cannot capture crimp interchange or locking. Also, while it can predict the macroscopic response of a fabric continuum, it contains no information about the fabric structure.

One obvious approach for capturing a fabric structure is to build a detailed finite element model that explicitly simulates every yarn, or even every fiber of every yarn, and the

interactions between them. A model of this type, discussed by Ng et. al. [1998], is shown in **Figure 2-9**. The advantages of such an approach are evident—it is completely physically based and enables an exact understanding of the predominant effects that contribute to the fabric macroscopic behavior. Failure of yarns can be exactly modeled, and the approach does not require limiting assumptions such as no-slip or negligible wrapping. However, this approach has two practical disadvantages. First, very detailed material characteristics are necessary. Some of this required data, such as relations describing the frictional forces between yarns or the forces involved in cross sectional deformation, are very difficult to measure. The second problem is that it is a very computationally intensive approach. The computational power required to analyze such a complex model for even a small sample of fabric—a few hundred crossover points corresponding to a fabric sample a few centimeters square—is substantial. This approach is not computationally efficient enough to be practical for general engineering applications within the current computational framework.

The approach discussed in this work—namely the derivation of a continuum model based on an assumed unit cell geometry and a set of material parameters describing component behaviors—has recently been considered in a more limited context by other researchers. Kato et. al. [1999] proposed a model for plain weave coated structural fabrics assuming the so called "trapezoidal fabric lattice" unit cell structure shown in **Figure 2-10.** This structure is composed of a network of spar elements arranged so as to have the same mechanical characteristics as a "unit cell" of a real fabric (the yarns around a single crossover point). Kato et. al. propose measuring the mechanical behavior of the fabric under different states of deformation, and then choosing the mechanical behavior of the different spars in the fabric lattice so as to conform to this behavior. The force contributions from the various spars can be combined and converted into continuum stresses. Kato et. al. show that a specific model derived for the low shear-angle behavior of a particular coated fabric predicts the mechanical behavior of that material with good approximation. However, it is important to note that the spars in the trapezoidal fabric lattice model do not directly correspond to yarns, but simply provide stiffening mechanisms against every possible mode of deformation. For example, the lattice model

includes diagonal spar elements to provide stiffness in shear that do not correspond to actual physical members in a real fabric. In Kato's model, these elements represent the stiffness of the coating material, but in an uncoated fabric they would have no direct physical analog. Because the lattice geometry does not directly correspond to real fabric geometry, the material properties of the spars cannot be predicted by measuring the individual yarn properties. Hence this model, like Breen's, cannot predict the behavior of a novel fabric. Because the unit cell structure does not directly imitate an actual fabric structure, it does not directly track all the internal structural parameters of interest. Also, like many other fabric models, Kato's model only captures specific behaviors—for example it does not include shear dissipation or locking—rather than employing a more general approach amenable to further expansions.

2.3 Requirements for a General Approach to Model the Response of Woven Fabrics

A number of models and modeling approaches describing the response of woven fabrics have been proposed in the literature. Some of these are very effective at predicting specific behaviors or fabric characteristics, and many are well suited to specific classes of fabric materials and load conditions. However, evolving technologies, especially micro- and nano-technologies, have begun to create opportunities for new fabric applications, and to make novel fabrics with superior capabilities for current applications possible. There is a need for a more general approach to fabric modeling in order to facilitate the growth of these technologies. It is difficult to predict what specific aspects of fabric behavior will be important for novel applications.

Development of such novel fabric technologies demands a more comprehensive approach for modeling the mechanical behavior of woven fabrics that satisfies three requirements. First, it should produce models that are accurate simulation tools. Fabric models must include all of the mechanical behaviors that affect the performance of the fabric of

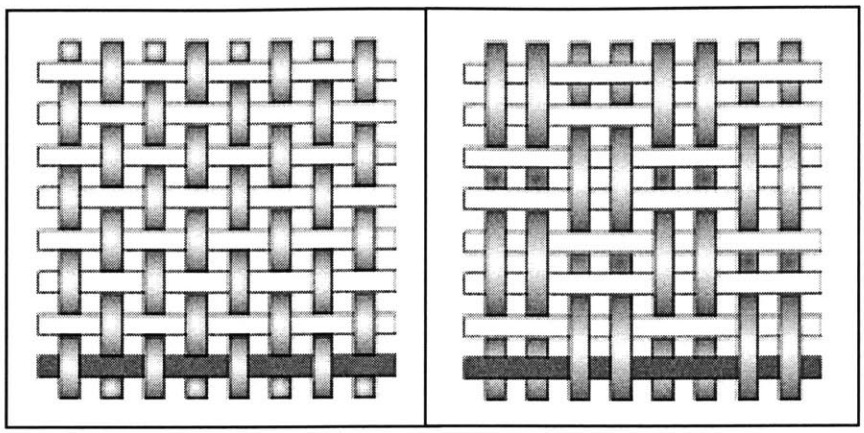
interest, such as yarn directionality, crimp interchange, locking, or shear dissipation. They must also predict not only the macroscopic mechanical response—i.e. the stress-strain curve that results from different loading conditions—but also predict the behavior of the fabric internal structure, tracking geometric parameters (such as crimp angle and yarn spacing) and force parameters (such as yarn tension and compressive forces between interacting yarns). This capability allows fabric models to be used as mechanical analysis tools for novel technologies.

The second requirement is that the approach should produce models that can serve as design tools. In other words, a model should predict the fabric material behavior if the behaviors of the simple materials that compose it, the yarns, are known. Ideally, if the mechanical behaviors of the fabric components are well understood, a model should be able to completely predict the behavior of the fabric itself. Of course, measuring and understanding all relevant aspects of yarn behavior including yarn interactions is not possible, so in practice some of the fabric model parameters will need to be fit to data gathered from tests on the fabric itself. However, the model should be predictive to the point where, if some change to the component yarn behavior is quantitatively known (for example, if a stiffer yarn material is used), the effects that this change will have on the macroscopic fabric behavior can be accurately predicted. The impact of possible modifications to the fabric structure or components can then be evaluated without the need to develop, manufacture, and test actual material samples. This capability allows fabric models that can be used to aid in the development of novel woven materials

The third requirement is that the model should be practical to use. This has two ramifications. A significant amount of mechanical engineering analyses are currently performed using the finite element method. Therefore, it is convenient to implement the fabric constitutive model into a finite element framework. A continuum model is preferable to a discrete yarn model, since continuum models are generally easier to interface with other material models and to use in the construction of multi-component models of large systems. For example, woven fabrics are often used in multilayer structures, and the other layers frequently are composed of different materials that

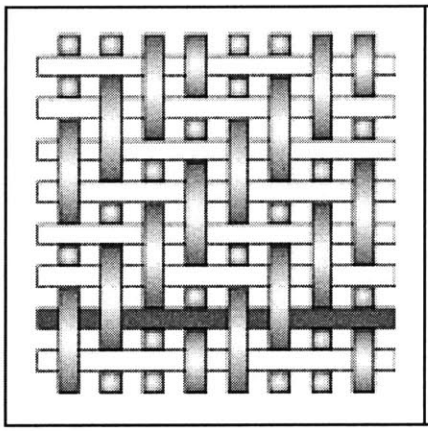
interact with the fabrics but exhibit very different constitutive behaviors. The second ramification is that the model should be computationally efficient. Since fabrics are frequently used in structures (from apparel and body armor to parachutes and architectural components) that are subjected to complex loadings and extend over areas much larger than the characteristic length of the internal fabric structure, large computational models will be required, and hence the fabric material model must be computationally efficient. Here again a continuum model is preferable to a discrete yarn model. However, an excessively complex continuum model may become computationally inefficient.

While the models should be specific to a particular application, in order to maximize their speed and accuracy, the approach used should be general and provide a systematic methodology to develop models for a wide variety of fabric materials and applications. Obviously, the requirements of the approach will sometimes compete. A more accurate model might require greater complexity and therefore be less computationally efficient, while increased computational efficiency might be achieved through limiting the applicability of a specific model. The needs of any given analysis will dictate the required speed, complexity, and accuracy of the models developed. However, the general approach should allow the development of models that can meet any efficiency, complexity, or accuracy requirements.

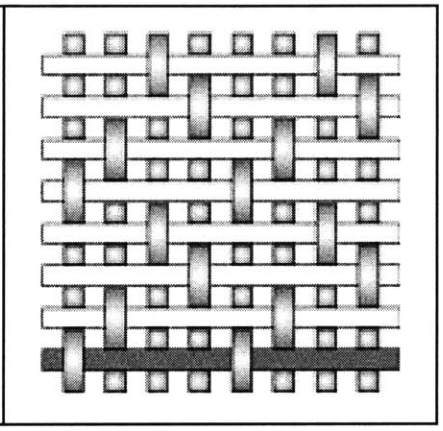


Plain Weave

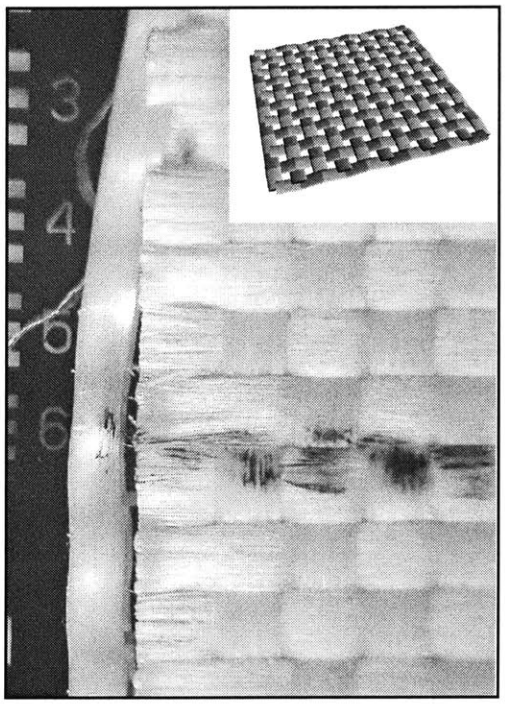
Basket Weave



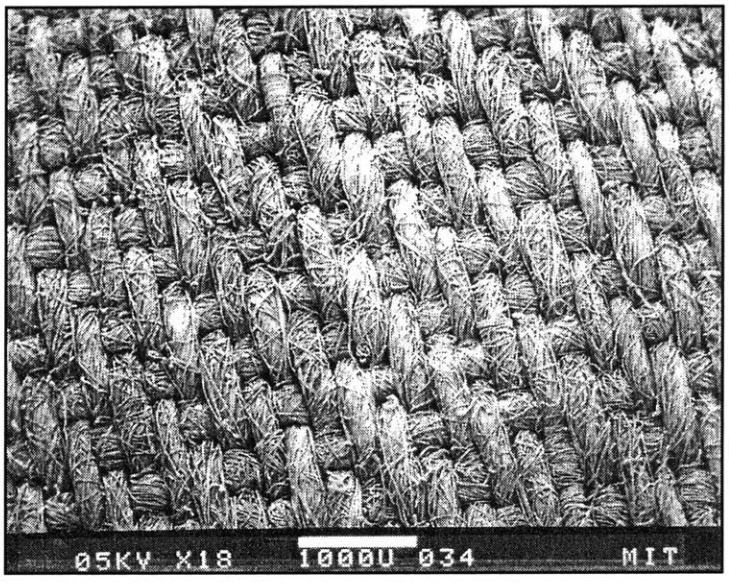
2-2 Twill Weave



Satin Weave

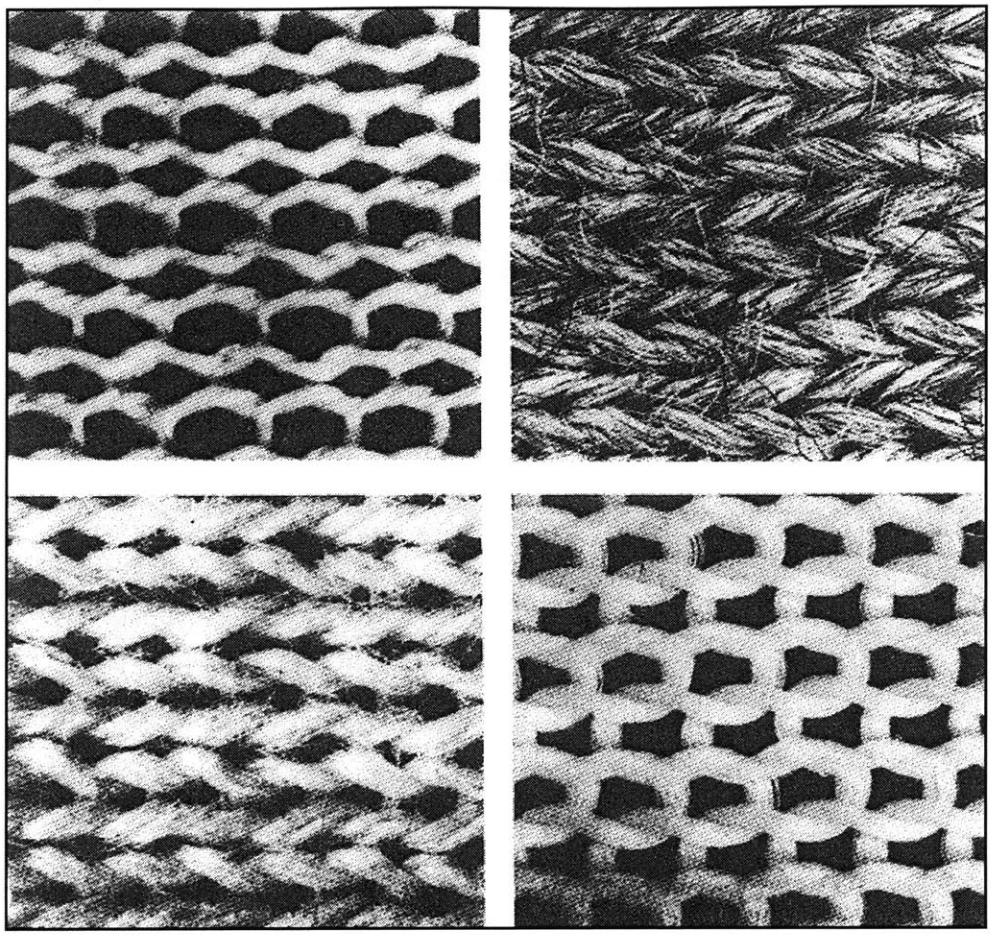


Plain Weave S706 Kevlar
with Weave Schematic
(Jearanaisilawong, 2003)

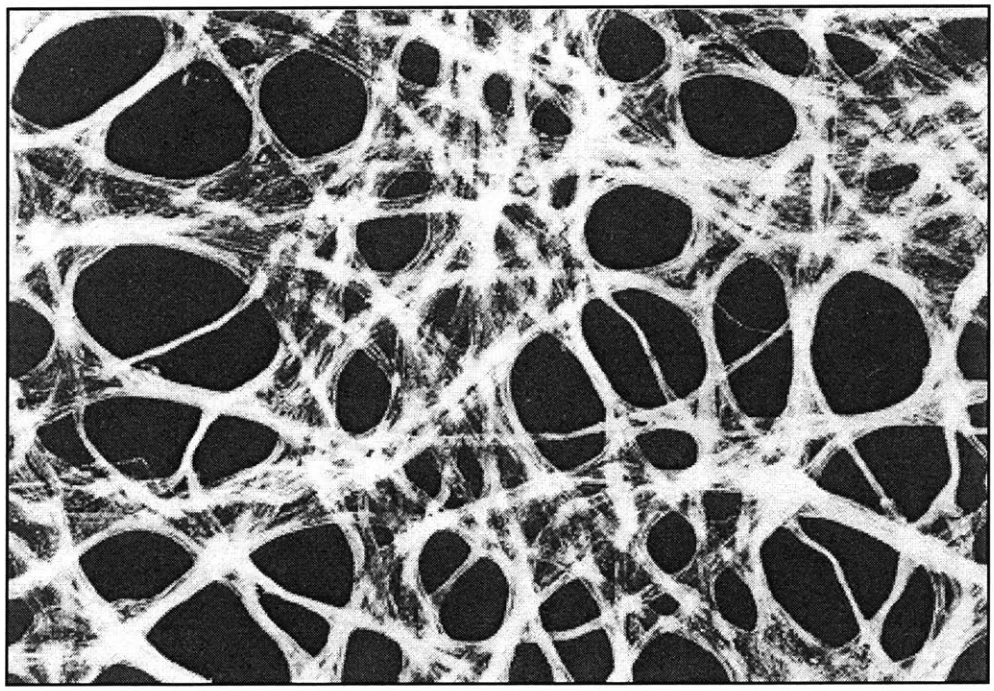


2-1 Twill Weave Fabric
(Realff, 1992)

Figure 2-1 - Examples of woven fabrics



Various Plain Knitted Fabrics
(Hearle et. al., 1969)



Nonwoven Fabric
(Hearle et. al., 1969)

Figure 2-2 - Knitted and nonwoven fabrics

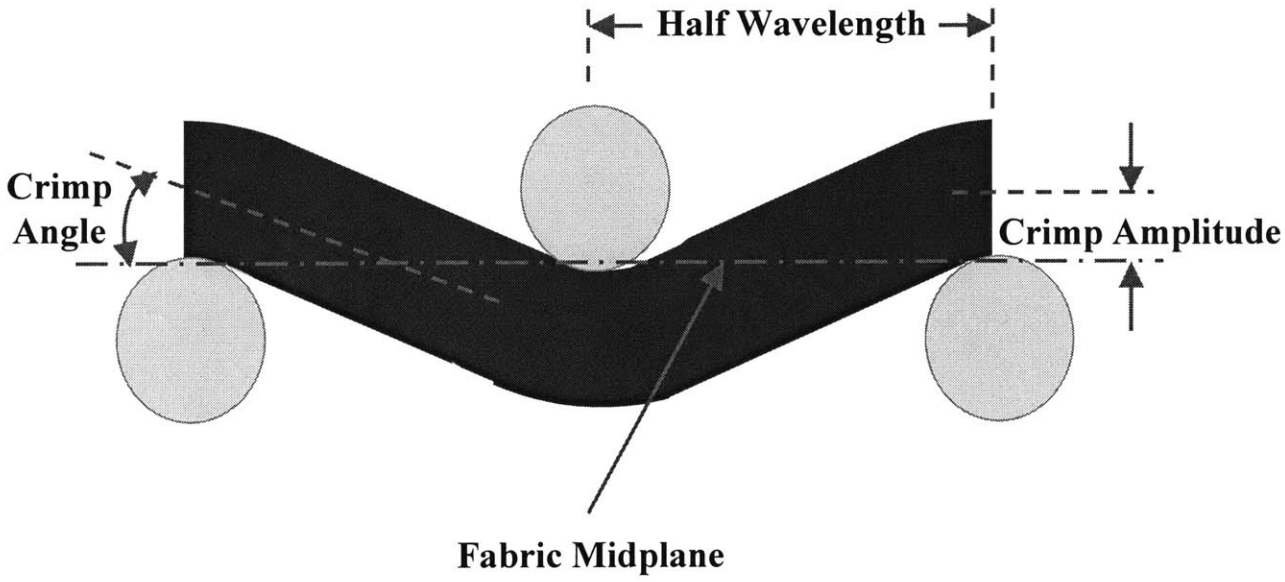


Figure 2-3 – Crimp parameters

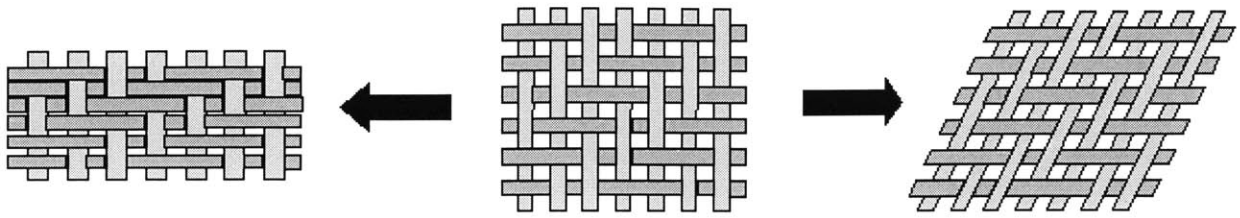


Figure 2-4 – Twill weave showing crimp interchange leading to cross locking and shear rotation ("trellising") leading to shear locking

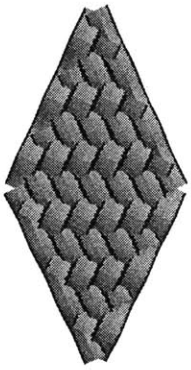


Figure 2-5 – Plain weave fabric in a shear locked state

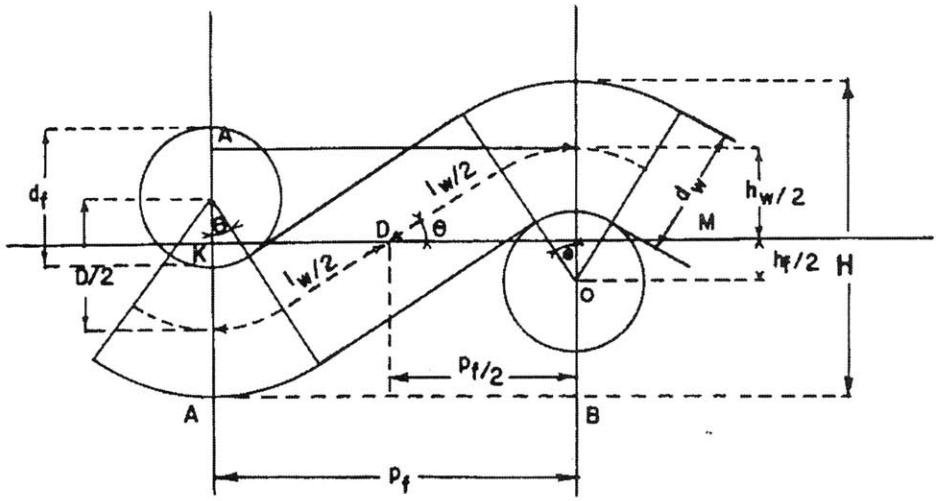


Figure 2-6 – Fabric geometry proposed by Pierce (1937)

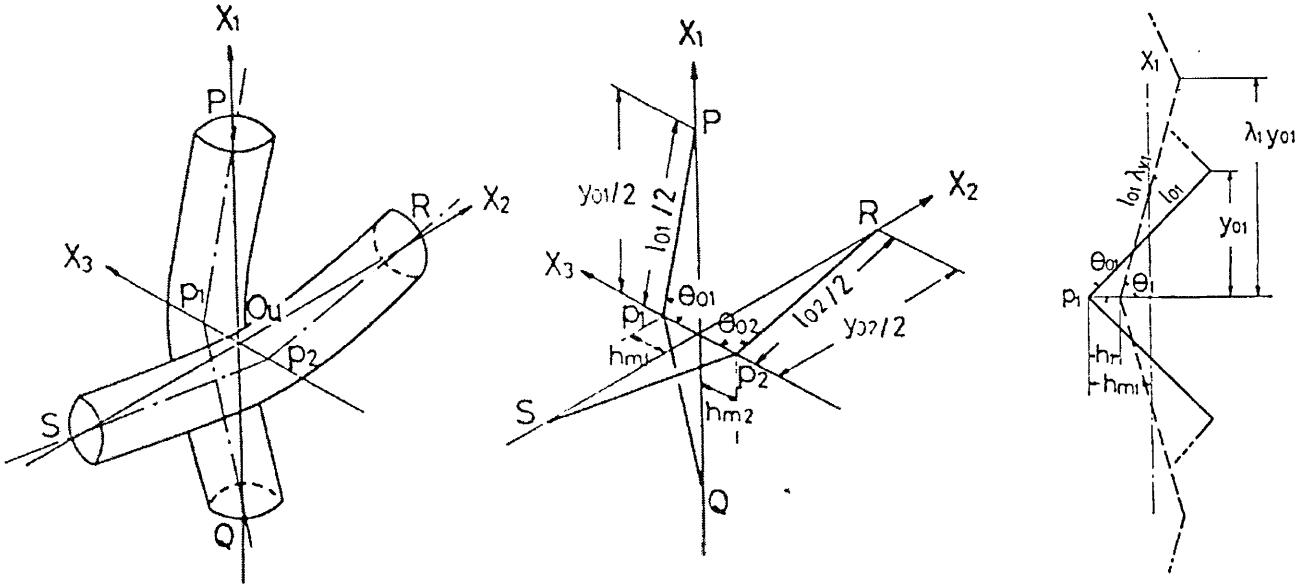


Figure 2-7 - Fabric geometry proposed by Kawabata
(Kawabata et. al., 1973)

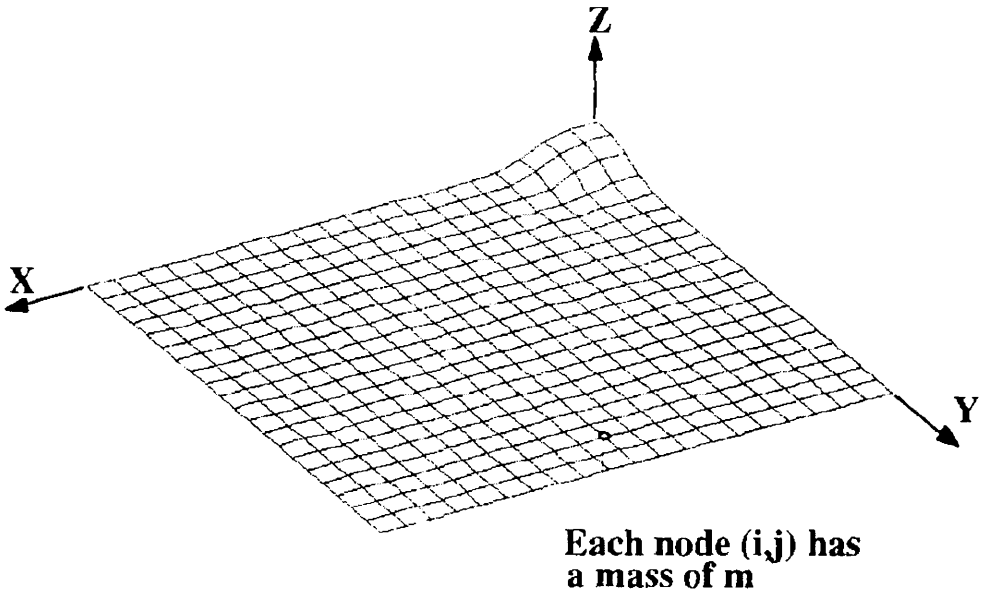


Figure 2-8 - Roylance's ballistic fabric model
(Roylance et. al., 1995)

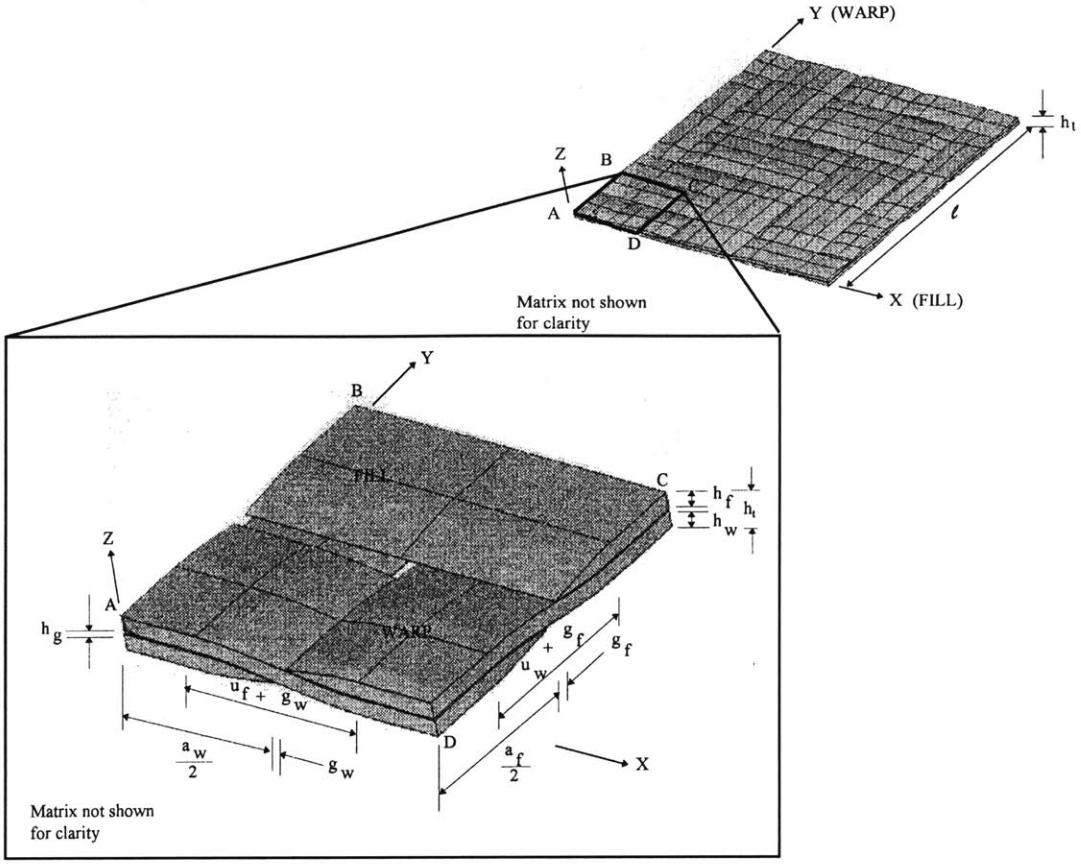


Figure 2-9 - Finite element model of fabric structure
(Ng et. al, 1998)

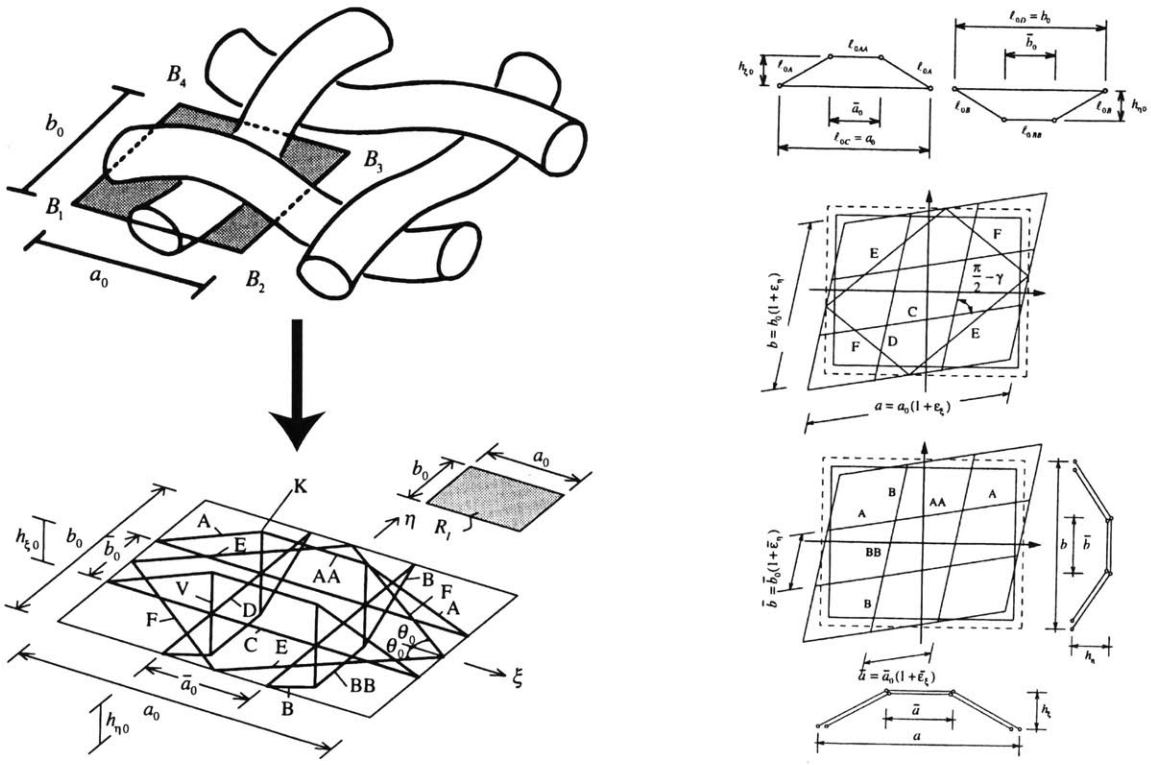


Figure 2-10 - Trapezoidal fabric lattice model
(Kato et. al., 1999)

Chapter 3

The General Fabric Modeling Approach Applied to Develop a Ballistic Fabric Continuum Model

3.1 Scope and Description of the Modeling Approach

3.1.1 Mechanics of a Planar Continuum Model for Woven Fabric

Our intent is to develop a continuum material model for woven fabrics. In a continuum description, a woven fabric is treated as homogenized anisotropic material, as is shown in **Figure 3-1**. In the anisotropic continuum, two preferred directions are defined by the unit vectors $\mathbf{g}_1$ and $\mathbf{g}_2$, which indicate the orientation of the yarns. The deformed configuration of the actual fabric structure is related to the macroscopic state of deformation of the anisotropic continuum, and the loads within the structure are related to the macroscopic state of stress. In continuum mechanics, the macroscopic state of deformation is typically described using the deformation gradient, designated by **F**. This is a tensor that evolves with time, and which describes how "material lines" in the neighborhood of a specific point are transformed when the material is deformed. In a given Cartesian coordinate system with unit vectors **i, j,** and **k**, it can be expressed in terms of Cartesian components defined as follows.

$$F_{ij}(t) = \frac{\partial x_i(t)}{\partial X_j} \tag{3.1}$$

Here $x_i(t)$ is the i-coordinate of a point at time t, and X_i is the i-coordinate of that point in the undeformed configuration. The deformation gradient **F** is a linear operator, describing the transformation of material lines with deformation: a line that moves and deforms with the material, described in the undeformed configuration by a vector $^0\mathbf{a}$, is transformed by deformation into a vector **a** according to **Equation 3.2**.

$$\mathbf{a} = \mathbf{F}\,{}^0\mathbf{a} \tag{3.2}$$

The deformed length a of this vector is determined by finding the magnitude of the vector.

$$a = \sqrt{\mathbf{a}\cdot\mathbf{a}} = \sqrt{\left(\mathbf{F}\,{}^0\mathbf{a}\right)\cdot\left(\mathbf{F}\,{}^0\mathbf{a}\right)} = \sqrt{{}^0\mathbf{a}\cdot\left(\mathbf{F}^{\mathrm{T}}\mathbf{F}\right){}^0\mathbf{a}} \tag{3.3}$$

It is often convenient to express the state of deformation using the right Cauchy-Green stretch tensor **C** (also known as the Green deformation tensor), defined as $\mathbf{C} = \mathbf{F}^{\mathrm{T}}\mathbf{F}$.

The angle θ between two material lines **a** and **b** at the same point can be determined from the dot product of the two.

$$\mathbf{a}\cdot\mathbf{b} = \left(\mathbf{F}\,{}^0\mathbf{a}\right)\cdot\left(\mathbf{F}\,{}^0\mathbf{b}\right) = ab\cos\theta \tag{3.4}$$

These relations imply that if the deformation gradient at a point is known, the deformed length, orientation, and angles between material lines at that point can be calculated.

Various different measures of macroscopic strain have been defined in terms of the deformation gradient, but these different measures are approximately equivalent as long as strains remain small. One commonly used strain measure is the Green-Lagrange strain, defined in **Equation 3.5**.

$$\mathbf{E} = \frac{1}{2}\left(\mathbf{F}^{\mathrm{T}}\mathbf{F} - \mathbf{I}\right) \tag{3.5}$$

When **E** is expressed in Cartesian coordinates, its components ε_{ij} correspond to the strains in the different Cartesian directions.

The "true" stress measure in the loaded configuration is the Cauchy stress, $\boldsymbol{\sigma}$. This is the stress acting in the loaded (deformed) configuration. If a small surface with area dS within a body is defined by a vector $\mathbf{n}dS$, where **n** is the unit normal to the surface, and the Cauchy stress in the body at that point is $\boldsymbol{\sigma}$, the traction force vector **t** acting on dS is given by **Equation 3.6**.

$$\mathbf{t} = \boldsymbol{\sigma}\mathbf{n}dS \tag{3.6}$$

This is the macroscopic stress measure that must be determined from the applied deformation history in order to define a continuum constitutive model.

In three dimensions, the deformation gradient and the stress and strain tensors have nine components, with six independent components for the symmetric stress and strain tensors. In a fabric, the out-of-plane response is not strongly coupled to the in-plane response: the out-of-plane bending response typically has little effect on the in-plane responses and vise versa, and out-of-plane compression and shear are assumed to be negligible. Furthermore, many interesting characteristic aspects of fabric behavior (such as crimp interchange and locking) control only the fabric in-plane response. Accordingly, the approach proposed here pertains to capturing only the in-plane fabric response. After an effective model has been developed to describe the in-plane behavior of fabrics, a three dimensional model can be created through the use of modeling approaches for thin shell structures—especially "membrane with bending" structures, where the membrane behavior is governed by the in-plane response of the fabric. The bending behavior, which is decoupled and typically orders of magnitude less stiff, is anisotropic and is controlled by the bending behavior of the yarns.

Therefore, the continuum description of the fabric can be considerably simplified to include only the in-plane response in the two-dimensional plane of the fabric. The

deformation gradient will have only four components, and the only relevant stresses and strains will be the in-plane normal components $\{\sigma_{11}, \sigma_{22}\}$ and $\{\varepsilon_{11}, \varepsilon_{22}\}$ and the in-plane shear components σ_{12} and ε_{12}. In the present formulation, the out-of-plane response is entirely decoupled from the in-plane response—in-plane extension and contraction do not result in through-thickness strains or stresses. Under these assumptions, plane stress and plane strain conditions are equivalent, as σ_{33} and ε_{33} are both identically zero. The choice of the out of plane model dimension is arbitrary and so, for simplicity, a constant unit thickness is assumed. Therefore, stresses can be interpreted as loads per unit in-plane length, obtained by multiplying the stresses by the unit model thickness. Because of the unit thickness assumption, the "area" upon which stresses act will have the same numerical value as the in-plane length, and the "volume" of a section of fabric will have the same numerical value as the area of the section.

3.1.2 Overview of Approach

Modeling fabric behavior under all modes of deformation is an exceedingly complicated task, well beyond the scope of this writing. Instead, this thesis will concentrate on modeling a subset of fabric behaviors. Fabric behavior is drastically altered once yarns begin to fail, because under these conditions yarns begin to slip out of the weave and pull-out behaviors become important. Capturing this failure process and post-failure mechanical behavior with a continuum model poses significant difficulties and is a topic for failure study. The model discussed here does not include failure mechanisms, which permits simplifying continuum and no-slip assumptions to be made. The continuum assumption implies that the length scale of the modeled structure should be significantly larger than the length scale of the fabric weave structure, and allows the homogenized response of the local fabric structure to be considered representative of the macroscopic response of the fabric. The no-slip assumption implies that yarns do not slide at the crossover points, and hence the yarn undulations may expand or contract, but the crossover points deform with the fabric continuum. This assumption facilitates the mathematical description of the fabric state.

While the proposed approach is applicable to most woven fabrics, it is applied here to develop a model for ballistic armor fabrics such as Kevlar™. Consequently, certain simplifying assumptions are made throughout the model development process, as some fabric behaviors are more critical than others in ballistic analyses. During a ballistic impact, the material at the point of impact is displaced out of the plane of the fabric, and the resulting elongation of the fabric around the impact zone causes large stresses to develop along the yarns. Typically, these stresses propagate along yarns away from the impact zone at high speeds and increase until yarns begin to fail as the projectile penetrates the fabric. Yarns not impacted are affected through the interweaving nature of the fabric. Due to the large velocities involved in the process and the fact that the in-plane fabric stiffness is much higher than the fabric bending stiffness, out-of-plane inertial effects and in-plane stiffness effects dominate the fabric response. Out-of-plane shear and bending have little effect. In-plane shear behavior is important, as it affects the flow of material inwards towards the impact point, but shear angles typically remain small to moderate (less than 30°) before failure occurs. Locking can be important as it may arrest the inward flow of material, and crimp interchange is important since it directly affects the in-plane stiffness and the propagation of the stress wave front. Yarn bending effects typically have a negligible effect on the ballistic response of a fabric due to the extremely small bending stiffness of the yarns; however, these effects are included in a fabric models to stabilize the low-stress response of the fabric. Accurate modeling of these behaviors is essential; other behaviors are less critical for this particular application.

The long-term goal of this project is to model the high-rate response of ballistic fabrics to projectile impact. This work represents a first step towards this goal, as it proposes a model that accurately captures fabric behavior under in-plane, quasi-static loading conditions.

There are five basic steps in developing a model to predict the in-plane fabric behavior. Note that, in this context, predicting a fabric "behavior" implies that, if the macroscopic homogenized in-plane deformation history of a fabric structure is known, the stress and

the fabric state parameters that result from that deformation can be predicted. The five steps are summarized below.

- Definition of a suitable unit cell to represent the yarn and weave geometry.
- Selection of component constitutive relations and associated properties governing the yarn deformations and yarn interactions.
- Definition of a procedure to determine the fabric configuration from the macroscopic deformation history.
- Determination of the unit-cell internal forces from the fabric configuration.
- Selection of a homogenization scheme to determine the macroscopic state of stress from the internal forces.

Most of the simplifying assumptions for the model are established in the first two steps. Each of these steps is briefly outlined below, and detailed discussion of each step as it is applied to the development of a ballistic fabric model follows in subsequent sections.

3.1.3 Definition of the Unit Cell

In the first step, an idealized geometry is selected to represent the structure of the fabric. By assuming an idealized geometry, the mathematical representation of the fabric response and its numerical implementation can be greatly simplified. However, the simpler the geometry, the fewer fabric behaviors the resulting model will be able to capture accurately, so this step involves balancing the complexity of captured behavior against the simplicity, ease of implementation, and computational efficiency of the model. Once a suitable geometry is selected and a repeating unit cell has been identified, mathematical relations between the geometric parameters within the unit cell must be derived. For instance, a relation between crimp amplitude, yarn wavelength, and yarn length per wave might be a geometrically necessary consequence of the selected geometry.

3.1.4 Selection of Component Constitutive Relations

The next step is to postulate the form of the constitutive relations for the fabric components. For example, the yarns may be observed to behave in a linear elastic manner when extended. The exact form of the component constitutive relations should be based upon experimental observation of the behavior of the fabric components if the model is to be used in a predictive capacity, or, if the model is to be fitted to a real fabric behavior, designed to capture the fabric's response to a specific mode of loading. The fabric model will only be accurate if the component behavior models are accurate in the load range of interest. A component constitutive relation should be established for every mechanism of energy storage or dissipation in the fabric. Also, these component constitutive relations should be expressed in terms of geometric variables defined in the context of the idealized unit cell.

3.1.5 Determination of the Fabric Configuration

The third step is to relate the fabric configuration to the deformation history. For a fabric whose components all behave in an elastic manner, the instantaneous deformation gradient is sufficient to determine the fabric state; but most fabrics have dissipative modes of deformation and therefore the corresponding models require internal state variables that evolve with the deformation history. For example, many fabrics, when subjected to shear, take on a permanent deformation, so a state variable that tracks the amount of inelastic shear may be required. Even for completely elastic models, the in-plane components of the macroscopic deformation only directly determine a maximum of three parameters relating to the fabric configuration. Any additional free independent parameters must be related to the deformation state as well. This can be accomplished using a minimum energy argument. The free independent parameters that are not directly determined by the deformation gradient or by the laws of evolution of the state variables will tend to take values that result in the fabric configuration with smallest amount of stored energy.

3.1.6 Calculation of Internal Forces

Once the fabric configuration is known, the loads carried within the unit cell—e.g. axial loads carried by yarn, contact forces where yarns cross, moment forces between yarns of different families resulting from shear rotation, etc.—can be calculated from the component constitutive relations. This is why it is convenient to express the constitutive relations in terms of the geometry of the fabric configuration, as this geometry is determined from the deformation history. The unit cell forces are necessary to determine the macroscopic state of stress, and may also be parameters of direct interest for the analysis. For example, it may be important to track the tension in the yarns in order to predict failure conditions.

3.1.7 Determination of the Macroscopic Stresses

The final step is to calculate the state of macroscopic stress from the internal forces in the unit cell. The form of the relation will depend on the assumed unit cell geometry. For simple elastic models where the geometry and internal forces can be calculated exactly from the deformation gradient, this equilibrium relation can be derived by differentiation of the strain energy function. For more complicated models, the macroscopic stresses must be derived through force equilibrium arguments.

3.1.8 Advantages and Disadvantages of the Proposed Approach

The proposed approach provides a means of determining the fabric state, the internal fabric forces, and the state of macroscopic stress from the applied deformation history and therefore provides a complete continuum constitutive model for the in-plane fabric behavior, without requiring the explicit modeling of each yarn or fiber. This approach has several advantages. It is a computationally efficient alternative to fabric modeling techniques that simulate every thread of a weave. It also has the advantage of being

easily integrated with continuum models of other materials, an important requirement for simulating multilayer fabric systems such as ballistic armor. Unlike more simplistic continuum approaches, this approach is capable of capturing real fabric behaviors, such as crimp interchange and shear dissipation, and is capable of tracking the evolution of mechanical parameters that describe the fabric structure, such as yarn orientation, crimp angle, yarn tension, and yarn contact force.

The fabric properties required to define the model are of two types. Some characterize the geometry of the yarns and weave, while others characterize the component constitutive relations. The former type can be measured directly from a woven fabric sample; the latter type can be measured by performing tests on the component yarns. This underlines another advantage of this approach. If the individual yarn properties can be accurately measured, the model can serve as a predictive tool. Models developed using this approach can predict the behavior of a woven fabric based on the properties of its component yarns and its weave types, and hence can be a valuable design tool for developing novel fabrics. In practice, measuring constitutive yarn properties, especially those governing yarn interactions, may be difficult, and some adjustment may be necessary to match the simulations results and the experimentally measured fabric responses. However, once these parameters are established, the relative effects of varying individual properties can be easily predicted. For example, it may be necessary to test an actual fabric to find the compliance of a yarn cross section, but once this is established, it becomes possible to predict the behavior of a fabric with an increased cross sectional stiffness. This allows the evaluation of the net effect of new yarn or weaving technology will have on a woven fabric without actually having to manufacture and test the new fabric. This predictive capability sets this modeling approach apart from approaches that require fitting of model parameters to experimental data without establishing a connection between the model parameters and the fabric structure.

Another advantage of the proposed approach is its flexibility. Since the general approach makes no assumptions about a particular fabric characteristic, it can be applied equally well to a wide variety of fabric applications. Since most of the derivations involved in

the model development depend strongly on the geometric assumptions, models for fabrics with similar weave geometries will require only changes to the assumed component constitutive relations and the measured fabric properties, even if the fabrics are used in very different applications. Fabrics with different weave structures will require new models to be developed, but the approach provides a flexible procedure to attain this goal.

The proposed approach has some disadvantages as it relies on the "continuum" and "no-slip" assumptions, and so it suffers from the limitations that these assumptions impose. The continuum assumption is only valid so long as the length scale of the modeled structure is significantly larger than characteristic length scale of the weave structure. The no-slip assumption limits the model to fabric analyses prior to failure, since fabric failure mechanisms involve significant yarn slippage. Another disadvantage arises because complex fabrics can entail constitutive or geometric relations that have no closed form solution, so numerical solution techniques become necessary. While this approach is computationally more efficient than approaches that simulate each thread, numerical solution techniques can decrease its efficiency and render this approach significantly more costly than simpler approaches. However, even with these limitations, this approach provides a flexible, powerful means of modeling fabric behavior.

3.2 Definition of a Unit Cell

The first, and arguably most important, step in developing the fabric model is the selection of a suitable geometry to represent the fabric, and the definition of a unit cell within that geometry. Selection of an excessively complex geometry leads to difficulty in the subsequent derivation of the model, and to a less computationally efficient model, especially if the geometry is so complex relations between its parameters cannot be expressed in closed form. On the other hand, choosing too simplistic a geometry makes it impossible to capture certain fabric behaviors. It is important to decide which fabric

behaviors are important to a particular model, and then select the simplest possible geometry capable of accurately representing these behaviors.

The model currently being developed is intended for ballistic fabrics. Ballistic fabrics, such as Kevlar™, are typically plain-weave fabrics woven from multi-fiber untwisted yarns. Accurate prediction of the tension in the yarns is necessary so that the initiation of failure can be predicted, and crimp interchange can affect this significantly, so both the capabilities to track yarn tension and to capture crimp interchange must be included in the model. Ballistic fabrics typically have fairly tight weaves, so locking can be an important factor. Ballistic yarns are multi-fiber yarns with an oval cross section, so it may be desirable to be able to capture cross-sectional deformation and the contact force between yarns, both at the crossover points and where the fabric locks. Also, ballistic fabrics typically are loaded at different rates so time dependent behavior, especially in shear, needs to be considered. On the other hand, shear angles under ballistic loading tend to remain small, so large shear-angle phenomena such as shear stiffening and wrapping are less critical. Yarn bending stiffness is not likely to be a significant factor, but it is typically included in numeric analysis of ballistic fabrics because it improves model stability.

Based on these considerations, a geometry similar to that proposed by Kawabata [1973] has been adopted. This geometry, shown in **Figure 3-2**, is a simple and physically motivated variation of a "fabric lattice" geometry. It represents the yarns as a network of beams connected by pin-joints at their crossover points. Unlike Roylance's geometry, these beams do not lie in the fabric plane, but rather undulate in an interweaving lattice to capture the crimp interchange effects of the yarns. These beams have axial compliance, which allows for yarn extension, but are infinitely stiff in bending. Yarn bending compliance is achieved through the presence of torsional springs at the pin joints that resist a change in bending angle. Interactions between yarns at the crossover points are captured by the inclusion of spring elements connecting the pin joints. These spring elements have two modes of deformation. They are capable of extending and contracting to simulate the effects of cross-sectional deformation that allows the yarns to change their

undulation amplitude while remaining in contact. The spring elements also offer resistance (both elastic and dissipative) to twist, which allows the geometry to capture the effects of shear through yarn rotation at the crossover points. The proposed geometry is one of the simplest fabric representations that is capable of capturing yarn orientations, yarn extension, crimp interchange, cross-sectional deformation, yarn bending, and both elastic and dissipative shear behavior. The geometry contains no explicit information about the cross sections of the yarns other than the values of parameters that relate to yarn compression (or cross sectional interference) at the crossover points. In spite of this, the effects of locking can be easily included through the introduction of spar elements that contribute to the material response only when their configurations reflect the onset of locking conditions. These spar elements resist further deformation once locking has occurred. **Figure 3-2** shows the spar elements in a case where the yarn angle is non-orthogonal.

The chief assumption of this geometry (in addition to the no-slip and continuum assumptions, which are expected to hold provided no failure has occurred) is that the true yarn length between crossover points (which is the sum of a straight length and a length required to wrap around the crossing yarns) does not differ substantially from a straight-line length from peak to trough. In other words, the effects of yarn wrapping are neglected. Inclusion of wrapping would require a significantly more complicated geometry tracking exact cross sectional shapes. However, wrapping effects, such as shear stiffening, become significant only in very tight weaves with solid yarns, or at high shear angles. In analysis of ballistic fabrics, with multi-fiber yarns and typically low shear angles, these effects are not likely to impact the fabric response significantly, so the simpler geometry is adopted.

Another simplification inherent to this geometry is the assumption that all yarn bending occurs at the crossover points. This is not physically accurate, as the yarns will actually have continuous and varying curvatures. However, if wrapping effects are negligible, the curvature at the crossover points will dominate. Even if the "negligible wrapping" assumption does not hold, the bending stiffness of the yarns is so small compared to the

stiffnesses associated with other modes of deformation (yarn extension, cross section interference, etc.) that modeling bending as concentrated at the crossover points will not affect the fabric response significantly.

A single unit cell of the fabric is taken as a representative volume element for the purposes of the continuum model derivation. This cell, shown in **Figure 3-2**, contains a single crossover point and the yarn quarter-wavelengths that surround this crossover point. Throughout this thesis, subscripts designate the yarn family (1-warp, 2-weft). The geometry of this unit cell can be described by nine parameters: the quarter-wavelengths p_i, the yarn lengths (per quarter-wavelength) L_i, the crimp angles β_i, the crimp amplitudes A_i, and the included angle between the yarn families θ. The geometric parameters describing the yarn geometry, along with all other parameters relevant to the deformation and loads in the model, are summarized in **Table 3:1**.

Several of these parameters are related through geometric constraints, so that of the nine parameters that describe the fabric, only five are independent. Amplitude and crimp angle can be described by functions of wavelength and yarn length:

$$A_i = \sqrt{L_i^2 - p_i^2} \ , \tag{3.7}$$

$$\cos\beta_i = \frac{p_{(i)}}{L_{(i)}} \ . \tag{3.8}$$

Hence, only the two wavelengths, the two yarn lengths, and the yarn angle are required to completely determine the geometrical configuration of the unit cell. For models that include locking, it is necessary to evaluate the (half) distance between two adjacent yarns (the length of the locking spar) and the direction of the locking force relative to the fabric plane. If the yarns are orthogonal, this distance d_i and angle α_i are given by relatively simple relations:

$$d_i = \sqrt{p_i^2 + A_j^2} \ , \tag{3.9a}$$

$$\alpha_i = \tan^{-1}\left(\frac{A_j}{p_i}\right). \tag{3.10a}$$

If nonorthogonal yarns are considered, a slightly more complex expression can be derived:

$$d_i = \sqrt{p_i^2 \sin^2\theta + A_j^2 \xi_{ij}^{\ 2}} \qquad \text{(no sum) } i = (1,2);\ i \neq j\ ,$$

$$\text{with} \quad \xi_{ij} = \left|1 - \frac{|p_i \cos\theta|}{p_j}\right| \qquad |p_i \cos\theta| \leq 2p_j\ , \tag{3.9b}$$

$$\alpha_i = \tan^{-1}\left(\frac{\xi_{ij} A_j}{p_i \sin\theta}\right). \tag{3.10b}$$

Note that this relation is only defined over a certain range of $|\, p_i \cos\theta \,|$ relative to p_j; a very unbalanced weave at very high shear angles would require a different relation.

It is important to note that these relations are specific to the geometry selected for the current model; a different geometry would involve different expressions. Their definition completes the first phase of the development of the fabric constitutive model—the selection and mathematical characterization of an appropriate approximation for the fabric geometry.

3.3 Component Constitutive Relations

The next step in the development of a fabric model is the selection of appropriate component properties. Along with the selection of a geometric model, this choice determines the complexity and accuracy of the fabric model. More elaborate component

constitutive laws will yield a more accurate model at the cost of increased complexity. The goal of the component constitutive laws is to provide a means of calculating the forces internal to the fabric unit cell, and the energy stored and dissipated, from a given geometry of the unit cell. These relations should reflect the actual physical behavior of the components. The constants in these relations, which will comprise the material properties of the fabric model (along with geometric constants), should be obtained through mechanical tests on the fabric components.

A component constitutive law is required for every mode of energy storage or dissipation in the model. Eight are necessary for the proposed ballistic fabric model. Two relations describe the extension of the warp and weft yarns, and two describe the bending of the warp and weft yarns at the crossover points. A fifth relation describes the interference between the warp and weft yarns at the crossover points, and another describes the interference that occurs when the warp yarns lock against the weft or when the weft yarns lock against the warp. Finally, a seventh relation describes the elastic shear response and an eighth describes the dissipative shear response of the fabric as the yarns rotate past each other. These relations are summarized in **Table 3:2**.

3.3.1 Yarn Extension

Figure 3-3 shows typical results of stress-strain tests on yarns obtained from Kevlar ballistic armor [Jearanaisilawong, 2003]. These data indicate that the responses of the yarns are predominantly linear up to their breaking stress, past an initial "toe regime" where the yarns uncrimp and align in the loading direction. Most ballistic fabrics are woven of materials (such as Kevlar™) that display this linear behavior. Therefore, the yarn extension behavior implemented in the model is assumed to be linear elastic. Here the force in the yarn is proportional to the change in its length. No energy is dissipated and the stored energy is proportional to the square of the change in yarn length:

$$F_i = k_i(L_i - {}^0L_i) \quad , \tag{3.11a}$$

$$\phi_i = \frac{1}{2}k_i(L_i - {}^0L_i)^2 \ . \tag{3.11b}$$

The constants of proportionality k_i are the stiffnesses of the yarn segments in the unit cell, which have initial length ${}^0L_i$, and may be different for the different yarn families. They can be measured from the slopes of the curves in **Figure 3-3**, which give the effective moduli E_i of the yarns of each family, since $k_i = E_iA_i / {}^0L_i$, where A_i are the cross sectional areas of the yarns of each family.

This relation assumes that no dissipation occurs and that the yarn response is not rate dependent. This is a simplifying assumption of the current model. Some sources [Shim, 1995 and 2001] suggest that the mechanical response of Kevlar may display rate dependent behavior. As additional data from single yarn tests becomes available, the rate dependence of the yarn extensile behavior can be quantified and, if necessary, included in the model.

One potential shortcoming of this constitutive law is that it implies that the yarns are equally stiff in tension and compression. This is not accurate since both yarns and individual fibers placed in compression tend to buckle. The proposed model only captures the in-plane response of the fabric and therefore does not allow out-of-plane buckling of the fabric. However, the possibility of yarn buckling is allowed for by the geometry of the model, through bending at the crossover points. Because the bending stiffness of the yarns is typically small compared to their axial stiffness, the yarns in the model will tend to buckle by bending at the crossover points before a large compressive load can build up. Hence, the exact compressive stiffness of the yarns is of little practical importance as long as it is significantly larger than the bending stiffness, since the yarns will never be subjected to large compressive loads.

3.3.2 Yarn Bending

For most yarns, tensile stiffness is much larger than bending stiffness, so the energy associated with yarn bending is typically small compared to that associated with the yarn extension. However, prior to locking or yarn straightening, bending resistance is typically the dominant resistance to deformation (other than inertia) in fabrics that are free to undergo crimp interchange. Therefore, bending tends to dominate the low-stress deformation regime of the fabric. Even in cases where the response in this low-stress regime is not important, the inclusion of bending energy in a fabric model is desirable in order to impart a nonzero stiffness at low strains and prevent numerical difficulties.

The pinned beam geometry selected assumes that all bending occurs at the pin joints at the crossover points. Bending resistance is imparted through rotational springs at these points. For the sake of simplicity, bending is assumed to be linear elastic as well, with the bending moment M_{bi} exerted on the yarns at the crossover point proportional to the change in the crimp angle β_i.

$$\begin{aligned} M_{bi} &= k_{bi}(\beta_i - {}^0\beta_i) \\ \phi_{bi} &= \frac{1}{2}k_{bi}(\beta_i - {}^0\beta_i)^2 \end{aligned} \tag{3.12}$$

The constant of proportionality k_{bi} carries units of moment per radian, and can be estimated or measured from the low-load regime of load-extension tests on individual yarns or from uniaxial tensile tests on a loose-weave fabric in each yarn direction. The constant ${}^0\beta_i$ represents the degree of initial "set" the yarns have and affects the amount of initial load carried by the unstressed fabric in cases where ${}^0\beta_i$ is different from the initial value of β_i in the weave. This can be easily measured by pulling a yarn from the fabric, allowing it to relax, and measuring the angle that its residual crimps take.

Bending is included primarily for stability reasons. Small deformations in the yarn directions can be accommodated primarily through crimp interchange, and unless the

fabric is constrained in both yarn directions, only bending resists crimp interchange. If bending were not included, small, unconstrained deformations would be possible and the model would be unstable. A linear moment relation may not be the most accurate relation to describe yarn bending, but since bending typically has a small effect on the fabric's response after the yarns straighten and the stresses become large (the "high stress regime"), inaccuracy in the bending relation does not greatly affect the model response. Given that crimp angles tend to be small, a linear assumption is even more justifiable. In ballistic Kevlar, the initial crimp angle is approximately 15° and the strains that occur while the response is dominated by bending (the "low stress regime") are less than 3%, or even smaller if the fabric is constrained in multiple directions. Consequently, the bending effects will not significantly affect the model response in most analyses.

3.3.3 Interference

Interference relations are generally difficult to measure exactly and to model, since they involve interactions between yarns, under specific constraints, on a very small scale. Ballistic fabrics are typically woven from yarns that are composed of a large number of untwisted fibers, rather than solid yarns. The cross sections of these yarns are capable of deformation. The interaction behavior of crossing yarns is governed by fiber-scale mechanics and tends to be very complex. In general, the magnitude of cross sectional deformation will be a nonlinear function of the force applied and may also exhibit other dependencies. For example, it may depend on the relative diameters and angles of the crossing yarns, or the tension carried by the yarns, or on a host of other factors such as temperature, rate of deformation, moisture content of the yarns, etc.

Understanding the complexities of this response would require detailed modeling of yarn-to-yarn interactions on the fiber level, or extensive experimental observation. Trying to capture the details of these effects with a continuum scale model would be impractical and would reduce the computational advantages of a continuum model. Instead, a simplified approach has been adopted for the proposed model. The fabric mechanical

behavior is governed by competing modes of energy storage and dissipation, including yarn extension, bending, and shear response, in addition to cross sectional deformation. The low-stress behavior of the fabric is dominated by yarn bending and by the shear response, while the high-stress behavior of the fabric will be dominated by the yarn stiffness and the locking geometry. Cross sectional deformation as it affects interference at the crossover points is typically a far stiffer phenomenon—the displacement magnitudes associated with cross sectional deformation will tend to be small compared to the changes in the other relevant fabric geometry parameters, such as wavelength or crimp amplitude. Consequently, the exact cross-sectional deformation response is not expected to have a significant effect on the behavior of the fabric. Therefore, the details of the relation are not important as long as the relative magnitude of the cross sectional deformation compared to the magnitudes of the deformations associated with the other modes of energy storage and dissipation is correct.

Therefore, in the model the cross section interactions are replaced with a nonlinear "interference spring" with a compliance that permits the peaks of the yarn undulations to move closer together at the crossover points. This spring simulates the effect of allowing the cross sections to deform at the crossover points. One experiment designed to investigate the nature of this spring is performed by sandwiching layers of fabric between metal plates and conducting a compression test. **Figure 3-4** shows a schematic of such an experiment, along with experimental results for a typical Kevlar ballistic fabric [Jearanaisilawong, 2003]. The results of this test indicate that under increasing loads the initially small stiffness increases as the cross sections become compacted. The interference relation is similar to contact relations. Therefore, an offset exponential relationship (often used to model contact problems) is used to describe the yarn interaction relationship:

$$F_I = K_I(e^{aI} - 1) \ , \tag{3.13a}$$

$$\phi_I = \frac{K_I}{a}(e^{aI} - aI - 1) \ . \tag{3.13b}$$

In this equation, I is the interference at the crossover points, defined to be positive when the cross sections overlap, resulting in a compressive force F_I. It is related to the unit cell variables through **Equation 3.14**:

$$I = (r_1 + r_2) - (A_1 + A_2) \ . \tag{3.14}$$

Here r_1 and r_2 are the minor radii of the yarns measured perpendicular to the fabric plane, which are fixed material properties (see **Figure 3-2**), and A_1 and A_2 are crimp amplitudes given by **Equation 3.7**. This implies that interference I is a function of the quarter-wavelengths p_i and the quarter yarn lengths L_i of both the warp and weft yarns. The model parameters for this relationship, the "interference stiffness" K_I and the "interference exponent" a, can be estimated from the compressive "sandwich" test described above, by normalizing the data to reflect load per crossover point as a function of compressive displacement per fabric layer, and choosing K_I and a so that the exponential force expression in **Equation 3.13** fits the measured data. **Figure 3-4** shows an exponential fit to the experimental data. Of course, this test does not exactly recreate the conditions that occur in a fabric subject to in-plane deformation, since the crossover points experience compression from both sides in this test, instead of just from one side. However, the test results yield properties that give a reasonable estimate of the magnitude and functional dependence of the stiffness response. A more accurate method to determine the interference relation would be to perform an equal biaxial extension test on the fabric, which would allow the interference relation to be quantified provided the yarn extension and bending stiffnesses were properly accounted for.

It is arguable that the interference behavior could exhibit additional dependencies, such as on yarn angle or tension. These dependencies could be included in the model by replacing **Equation 3.13** with an appropriate expression, once experiments or detailed numeric simulations have established the exact nature of these dependencies. Inclusion of these effects might increase the model's accuracy, at the cost of numeric efficiency. These effects are not included in the current model.

3.3.4 Locking

When the fabric locks, yarns of one family jam against yarns of the other family that pass between them. Because the cross sections are not rigid, this jamming has compliance and is a phenomenon similar to crossover interference. It is included in the model by the addition of spar elements in the unit cell that arrest deformation, as is shown in **Figure 3-2**. The compliance of these spar elements should be based on the compliance associated with the jamming of the yarn cross sections against each other.

Unfortunately, recreating this jamming phenomenon in a test involving individual yarns is very difficult. Three alternatives are possible. Detailed numeric simulations of the jamming phenomenon at the length scale of the fibers that compose the yarns may provide insight into the nature of the locking relation. Alternately, an approximate locking relation can be inferred from the crossover interference relation, since both are similar phenomena involving yarn cross sections deforming against each other. In the particular case where the yarn cross sections are circular and where the interference relation does not depend on yarn angle, the locking relation should be identical to the interference relation and the same relation and physical constants can be used. However, fabrics woven from highly non-circular yarns will have a very different, and generally far more compliant locking response, and the non-orthogonal angles involved in the locking process may also affect the response. The third option is to infer a phenomenological form for the locking relation and then fit model parameters to data from fabric tests that are dominated by locking, such as large-displacement shear. This approach is less desirable as it limits the usefulness of the model as a predictive tool; however, it is the most accurate approach to simulate fabrics whose response is dominated by locking when no direct method to measure or estimate the fabric locking behavior is available.

The current model uses the third method. The locking relation is assumed to have a form similar to the interference relation fit to the data in **Figure 3-4**. However, since the ballistic fabric of interest has very broad, flat yarns, the locking response is more

compliant than the interference response at the crossover points, and the magnitude of the locking interference can be significantly larger than that of the crossover point interference. Therefore, an exponential model, which becomes extremely stiff as interference increases, is unsuitable. Instead, a more compliant piecewise power-law/linear relation was fit to data from the "sandwich tests" and used to predict the locking force from the locking interference:

$$F_{Li} = \begin{cases} 0 & I_{Li} < 0 \\ K_d (I_{Li})^c & 0 \le I_{Li} < I_L^* \\ m^* (I_{Li}) + d^* & I_L^* \le I_{Li} \end{cases}, \tag{3.15a}$$

$$\phi_{Li} = \begin{cases} 0 & I_{Li} < 0 \\ \frac{K_d}{c+1} (I_{Li})^{c+1} & 0 \le I_{Li} < I_L^* \\ \frac{m^*}{2} \left(I_{Li} - I_L^*\right)^2 + d^* \left(I_{Li} - I_L^*\right) + \phi_i \left(I_L^*\right) & I_L^* \le I_{Li} \end{cases}. \tag{3.15b}$$

Here F_{Li}, the force that results from the yarns of family i locking against the crossing yarns, depends only in I_{Li}, the locking interference associated with direction i. It is calculated from inter-yarn distance in **Equation 3.9** and from the initial cross section geometry. The model parameters are the "locking stiffness" K_d (which has units of force/(length)^c), the locking exponent c (adimensional), and the transition locking interference I_L^* (length), the interference value where the relation transitions from power law to linear. These parameters are chosen to fit the locking response to the measured curve from the fabric compression test. This relation is also shown fit to the data in **Figure 3-4**. The linear constants m^* and d^* are determined by the three model parameters and are calculated to generate a continuous function with a continuous slope.

Use of this relation has a number of advantages. It has continuous derivatives, which makes it numerically stable. It gives zero force, energy, and stiffness when locking interference is negative—i.e. no locking is occurring. It allows for a stiffness that increases with locking interference to a maximum stiffness level, and the three

parameters provide the flexibility to adjust the model response to a wide variety of observed behavior.

3.3.5 Shear

The last relation to be established governs the response of the fabric to in-plane yarn rotation, which is the principal mechanism for fabric shear and which is referred to as "shear rotation". The larger the angle of rotation between yarn families (referred to as the "shear angle"), the larger the corresponding macroscopic shear strain. Shear frame experiments, which measure the load required to increase shear angle while keeping extension in the yarn directions constant, have shown that fabrics typically exhibit three regimes of shear rotation behavior, shown schematically in **Figure 3-5**. A very stiff initial elastic response is recovered if the load is removed. Some or all of this elastic response may be physically accommodated by "s-shaped" bending of the yarns between crossover points, shown in **Figure 3-6**. At a small shear angle, the moments exerted about the crossover points overcome friction and the fabric begins to shear dissipatively as yarns rotate in "trellising" manner. This rotation is resisted by frictional forces. Finally, locking effects (and, in some fabrics, wrapping effects) begin to resist shear and the shear stiffness dramatically increases. In the locking regime, macroscopic shear stresses become large and approach or exceed the magnitude of other in-plane stresses. In an unconstrained fabric, this increased stiffness typically leads to out-of-plane buckling, leading to visible wrinkling. In this model it is assumed that the fabric is constrained to remain planar and no wrinkling is possible.

Some shear stiffening occurs during the dissipative regime due to elastic deformation, which continues to increase even after the material begins to deform dissipatively. A portion of the shear stiffening may also be caused by wrapping effects: as the fabric is sheared, a larger yarn lengths are required to wrap around crossing yarns due to the increasingly helical nature of the wrapping, which results in contraction of the fabric. If contraction is prevented (for example, if the fabric is being tested in a shear frame),

wrapping effects results in shear stiffening. This wrapping-induced contraction can also cause shear locking at a shear angle smaller than that predicted by the simple linear geometry considered by this model. This effect is most noticeable at large shear angles in tight weaves with large diameter yarns; thus this behavior is not expected to have a significant effect on ballistic fabrics at the relatively low shear angles of interest.

In general, the extent to which rate dependence affects the mechanical response of a fabric will depend on the yarn and weave properties. Rate-dependent effects need to be included in a model developed to capture the effects of very high (ballistic) rates of deformation, but only certain regimes of shear deformation will exhibit rate dependence. Wrapping and locking effects result from geometric constraints and will not be modeled as rate dependent. It is further assumed that the elastic yarn rotation response, which typically entails very small deformations, is also rate-independent. Rate dependence in the shear response of the fabric is included only in the relations that govern dissipative shear rotation.

Resistance to shear rotation due to locking is decoupled from the resistance to the elastic and dissipative shear mechanisms, and is captured through the locking relations described in the previous section. The shear stresses that result from locking will be combined with the shear stresses that result from the elastic and dissipative responses to shear rotation. Typically, the initial elastic response is very stiff compared to the more compliant response observed once frictional rotation at the crossover points begins. In general, the dissipative rotation is resisted by small moments at the crossover points between the yarn families, which correspond to macroscopic shear stresses that are small compared to the macroscopic axial stresses. The magnitude of the macroscopic shear stresses necessary to cause dissipative shear rotation is referred to as the "shear strength", and is a function of the fabric material, the diameter, roughness, and structure of the yarns, the tightness of the weave, and possibly the contact force at the crossover points. Because the elastic resistance to shear is relatively large and the "shear strength" is small, the amount of elastic shear that occurs will be very small, and a rate-independent linear elastic shear relation should be able to accurately capture the elastic portion of the response. This

relation is expressed at the fabric structural level in terms of the moment at the crossover points and the elastic component of the rotation angle:

$$M = K_s \gamma_e$$
$$\phi_s = \frac{K_s}{2} \gamma_e^{\,2} = \frac{K_s}{2} \left({}^0\theta - \theta_e \right)^2 \cdot \tag{3.16}$$

Here the moment M at the crossover point between the two yarn families depends only on the elastic shear angle $\gamma_e = {}^0\theta - \theta_e$. (see **Figure 3-6**). The constant of proportionality, K_s, which has units of moment per radian, can be readily calculated from simple beam theory, assuming that elastic shear deformation is accommodated through s-bending of the yarns between crossover points. However, as in the case of the interference stiffness, the exact value of K_s will have little effect on the overall fabric response because the elastic shear angles will be small, since they are limited by the shear strength.

Once the moment between yarn families exceeds the frictional resistance to yarn rotation at the crossover points, a portion of the shear deformation will be accommodated through dissipative mechanisms. To capture these effects, the shear angle is decomposed additively into elastic and dissipative portions, as is shown in **Figure 3-6**.

$$\gamma = {}^0\theta - \theta = \gamma_e + \gamma_f \tag{3.17}$$

The elastic-dissipative model used is a Maxwell type model, with the elastic and dissipative compliances acting in series. The response of the fabric at any given time will depend not only on the instantaneous state of imposed macroscopic deformation, but also on the deformation history. The magnitude of the accumulated dissipative shear rotation γ_f and the dissipative shear rotation rate are considered internal state variables that describe the current state of the fabric.

Because the relationship between the moment from the applied shear stress and the resulting dissipative rotation rate may be rate dependent, a general power-law relation has been implemented into the model:

$$\dot{\gamma}_f = \dot{\gamma}_0 \left(\frac{M}{M_0} \right)^b . \tag{3.18}$$

The power law relation in **Equation 3.18** involves two material parameters—a rate-sensitivity exponent b and a reference point on a moment-strain rate curve $\gamma_0/(M_0)^b$. In physical terms, M_0 is a "strength" parameter, and when the fabric crossover points are subjected to a moment M_0 between the yarn families, they will dissipatively rotate at rate $\dot{\gamma}_0$. These parameters are difficult to measure directly from single yarn tests; they must be determined either by detailed numeric simulations of the yarn interactions or by fitting the model results to controlled experiments.

Once the fabric geometry and the component constitutive relations have been selected, the elements of the fabric model are completely defined. The following section discusses methods of relating the macroscopic deformation state and history to the fabric configuration. Then the internal loads can be determined and related to the macroscopic stresses.

3.4 Determining the Fabric State

The geometry for the unit cell provides a means of characterizing the configuration of the fabric, and the component constitutive relations describe how energy is stored or dissipated through changes to the unit cell geometric parameters, and what forces result from these processes. Though there are many variables that describe the fabric state, many of them are related to each other through the geometric constraints discussed in

Section 3.2. Therefore, it is only necessary to determine the independent parameters to describe the fabric configuration and hence to determine the forces in the unit cell.

The modified fabric lattice geometry assumed for the ballistic fabric model requires only five independent parameters. For this geometry with the no-slip assumption, the (quarter) wavelengths of each yarn family p_i and angle θ between yarn families are good choices as independent parameters, since these are easily determined from the deformation gradient. For the other two independent parameters, it is convenient to choose the quarter wavelength yarn lengths L_i, since these directly relate to the yarn tensions, a force that must be tracked. Once these parameters are known, all other geometric parameters can be determined through the geometric constraint equations, such as those in **Equations 3.7** and **3.8**.

Different geometric models would require different numbers of independent parameters. For example, a simpler model that includes crimp interchange but does not allow yarn extension requires only three parameters to completely define its geometry, since yarn lengths are held constant. A model which tracks yarn cross sectional shapes, say by assuming an oval cross section of constant area but with variable major and minor axes, would require an additional independent parameter relating to the amount of deformation each cross section undergoes, since the cross sectional shapes could not be determined by the wavelengths, yarn lengths, and yarn angle alone. A model that includes wrapping and yarn bending between crossover points would require additional independent parameters describing the wrapping angle and the curvature of the yarns. For all cases that require more than three parameters, the same energy-based approach described here can be used to determine the fabric state from the macroscopic state of deformation, though different energy-minimization algorithms may become more efficient for different models with different numbers of parameters.

3.4.1 Parameters from the Deformation Gradient

The following derivation rests on the assumption that the crossover points define a material lattice that deforms in an affine manner with the macroscopic deformation gradient. Three of the independent fabric parameters can then be determined from the deformation gradient using the relations in **Equations 3.3** and **3.4**. The yarn families in a fabric can be described using "wavelength vectors" $\mathbf{p}_i$, vectors that originate and terminate at adjacent crossover points and that are parallel to the yarn families. At a given location, the length of one of these vectors describing yarn family i will be equal to the quarter wavelength of that yarn family p_i, and its orientation will correspond to the orientation of the yarn family in the plane of the fabric. The angle between the wavelength vectors of the different yarn families is the yarn angle. Provided that the no-slip condition holds, these wavelength vectors will be material lines—they will rotate with the yarn families and stretch as the fabric stretches in the directions of the yarn families. Furthermore, it is assumed that the initial condition of the fabric in the undeformed state is known, so the initial wavelength vectors ${}^0\mathbf{p}_i$ are known at every location. Therefore, both the quarter wavelengths p_i and the yarn angle θ can be calculated at any time from the deformation gradient using **Equations 3.19** and **3.20**, which follow directly from **Equations 3.3** and **3.4**:

$$p_i = \sqrt{\left(\mathbf{F}^0\mathbf{p}_i\right)\cdot\left(\mathbf{F}^0\mathbf{p}_i\right)}\ , \tag{3.19}$$

$$\cos\theta = \frac{\left(\mathbf{F}^0\mathbf{p}_1\right)\cdot\left(\mathbf{F}^0\mathbf{p}_2\right)}{p_1 p_2}\ . \tag{3.20}$$

These relations also imply the interesting property that the macroscopic axial strain in a direction parallel to one of the yarn families is related to the change in wavelength of that yarn family, and that the macroscopic shear strain is related to the change in the angle between the yarns. **Equation 3.5** can be combined with **Equations 3.19** through **3.20** to express the strain at a point in the fabric continuum in terms of the wavelengths and the yarn angle.

It is important to note that the yarn angle θ determined by the deformation gradient is the total angle between yarns and its variation must be decomposed into elastic and dissipative components as shown in **Figure 3-6** in order to calculate local moments from the elastic-dissipative constitutive law.

3.4.2 Parameters from Energy Minimization

Three of the independent parameters are therefore directly determined by the deformation gradient; however, additional independent parameters, such as L_1 and L_2, are not. Indeed, for a given deformation gradient the ballistic fabric geometry has an infinite number of possible configurations achieved by varying the remaining parameters. For example, at a given deformation gradient the warp yarn length L_1 could be increased while the wavelengths and yarn angle are kept constant. This would require an increase in the warp crimp angle and amplitude, and a decrease in the interference at the crossover points. Therefore, the deformation gradient alone cannot determine the fabric state.

The fabric configuration is determined here using energetic arguments. Changing any of the parameters not fixed by the deformation gradient will change the amount of energy stored in the fabric unit cell. In the above example, if the yarns were under tension and the interference spring was under compression, increasing L_1 would increase this tension and store a larger amount of energy in warp yarn extension. However, from **Equation 3.7** the change in configuration would increase the warp amplitude, which would in turn both increase bending energy and decrease the crossover point interference and reduce the amount of energy stored in the interference spring. Or, if the interference was kept constant a decrease in the weft amplitude A_2 would be required, corresponding to a decrease in the weft yarn length L_2 and in the energy stored through weft yarn extension. By varying the free parameters, different amounts of energy will be stored by different mechanisms within the unit cell, but since the rates of energy exchange will not be equal for all the different mechanisms, the total amount of energy with vary as the free

parameters are varied. At a fixed deformation gradient, energy is a scalar function of the free independent parameters.

This concept is illustrated in **Figure 3-7**. This is a plot of total energy stored in a fabric unit cell at a fixed deformation gradient corresponding to even biaxial extension. Since the deformation gradient is fixed, p_1, p_2, and θ are held constant and the amount of energy depends only on the parameters L_1 and L_2. The function is bounded on two sides by the wavelengths—L_i cannot be smaller than p_i since the limiting case for completely flat yarns corresponds to the yarn lengths equaling the wavelengths. The function has a single minimum close to its bounds, which corresponds to a certain crimp amplitude. At this configuration the fabric unit cell has the minimum possible energy, and any other values of the free parameters that result in different amounts of energy stored in the various mechanisms result in a larger total energy level. Though this graph represents only one conditional energy surface corresponding to one particular deformation gradient, its shape with a single minimum is typical, though the gradients tend to become steeper and the minimum moves closer to the bounds ($L_i = p_i$) as the amount of deformation is increased.

Thermodynamically, any system will tend to adopt the configuration corresponding to the state of minimum energy. Therefore, even though there are infinitely many possible fabric states corresponding to a particular deformation gradient (represented by the entire energy surface), the fabric will tend to take on the state that minimizes the energy, with the corresponding values of the free parameters. As the various constitutive relations have been established, the form of the energy function is known. The yarn lengths are determined by minimization of this energy function at fixed values of wavelength and yarn angle.

The full procedure for calculating the fabric state from the deformation gradient is therefore a two-step process. First, the three parameters directly determined by the deformation gradient—p_1, p_2, and θ—are calculated. Next, the values of the free independent parameters (in this case, L_1 and L_2) that minimize the energy function with

p_1, p_2, and θ held constant are determined. Even for simple component constitutive relations, it is difficult or impossible to find a closed form expression for the free parameters that will minimize the energy function, so in practice this minimization must be performed numerically.

One final consideration with regard to this minimization argument concerns the effects of dissipative mechanisms. The fabric is assumed to "choose" the state that minimizes stored energy and this choice is instantaneous—the fabric does not take on a non-favorable state and change its configuration until it finds its energetic minimum. Because this process is instantaneous, energy dissipation should not affect the conditional energy surface. This issue does not arise in the current model, as only shear has a dissipative portion and the shear angle is fixed by the deformation gradient and therefore is held constant during the minimization process.

3.5 Internal Forces and Macroscopic Stresses

The preceding sections have discussed the assumptions of geometry and component constitutive relations, and how to determine the fabric state from the deformation history. The geometric relations allow all the geometric variables to be determined from the independent fabric state parameters, and the component constitutive relations allow the forces internal to the unit cell to be calculated from the geometric variables. These forces, which include yarn tensions, contact forces at crossover points and locking points, and moments acting between the yarn families at the crossover points, may be quantities required to predict local failures. However, a complete continuum constitutive model that can be implemented into a finite element code also requires a means of determining the state of macroscopic stress that corresponds to these internal forces.

3.5.1 Methods of Determining Stress

There are several ways of determining the macroscopic stress acting on a unit cell of material. For hyperelastic constitutive models, the stress can be derived by differentiating the strain energy density function expressed in terms of the deformation gradient (or other deformation tensors derived from it). This approach is effective for elastic materials where the strain energy density can be expressed in a closed analytic form, but cannot be applied to cases where the strain energy density does not have a closed form (for example, because a numeric minimization is required to find the energy state at a given deformation gradient). An alternate approach is to realize that the macroscopic stress exerts tractions on the faces of the unit cell, and that equilibrium demands that these tractions must exactly balance the tractions derived from the internal forces. This approach requires only knowledge of the forces and geometry of a unit cell at a given time to determine the macroscopic stress state.

To demonstrate that the two methods yield the same results and to gain insight into the physical meaning of the terms in a fabric stress expression, the energy differentiation method is used to rigorously derive the macroscopic stress for a simplified fabric model with no dissipation and a closed form energy function. The resulting stress is expressed as the sum of different terms, each with a single scalar measure of one of the fabric internal forces, along with various parameters describing the geometric state of the fabric. This expression is shown to generate tractions on the unit cell faces that exactly counteract the internal unit cell forces, with each term in the stress expression contributing to counteract a different component. This provides a physical understanding of the terms required in the stress expression to balance each component of force. In the following section, a more complicated stress expression of similar form is derived by equilibrium arguments for the complete ballistic fabric model.

3.5.2 Strain Energy of a Simplified Model

A simplified model with no shear dissipation, locking or bending stiffness, and with inextensible yarns and a linear-elastic interference spring is considered to demonstrate the energy differentiation method. The exclusion of shear dissipation means that the model will be completely elastic, while the exclusion of locking and bending stiffness and the consideration of a linear-elastic interference spring significantly simplifies the mathematical derivations. To simplify calculations further, it is also assumed that the yarns are initially orthogonal. Most importantly, the assumption of inextensible yarns eliminates two of the five independent parameters needed to establish the fabric state, leaving only the three parameters that are explicitly determined by the deformation gradient. This eliminates the need for numerical minimization to determine the fabric state, and allows the strain energy density function to be expressed as a closed form function of the deformation gradient. Note that even though the yarns are inextensible, they can still carry load and must do so to counteract forces in the interference spring, since force equilibrium at the point where the yarn bends and joins the interference spring demands that $F_I = 2\,T_i \sin(\beta_i)$, for a positive yarn tension T_i with crimp angle β_i and a positive interference compressive force F_I.

The strain energy density function $\phi(\mathbf{F})$ for the homogenized continuum model of the simplified fabric is given in **Equation 3.21:**

$$\phi = \frac{1}{4\,{}^0p_1\,{}^0p_2}\left\{\frac{1}{2}K_I I^2 + \frac{1}{2}K_s\gamma^2\right\}. \tag{3.21}$$

Here ${}^0p_1$ and ${}^0p_2$ are the initial wavelengths, so the undeformed volume of the unit cell is $4\,{}^0p_1\,{}^0p_2$, since the homogenized continuum model assumes unit thickness in the direction orthogonal to the plane of the fabric. K_I and K_s are the stiffnesses in response to interference I and yarn rotation γ respectively, where I is given by **Equation 3.14** and γ by **Equation 3.17**.

3.5.3 Material Frame Indifference Constraints on the Strain Energy Function

The fabric is modeled as a continuum material with two preferred directions given by the unit vectors $\mathbf{g}_1$ and $\mathbf{g}_2$, which coincide with the orientations of the yarn families. Yarn directions in the undeformed configuration are given by ${}^0\mathbf{g}_1$ and ${}^0\mathbf{g}_2$. The fabric configuration can therefore be characterized by the "structural tensors" $\mathbf{g}_1 \otimes \mathbf{g}_1$ and $\mathbf{g}_2 \otimes \mathbf{g}_2$. The principle of material frame indifference requires that the strain energy, expressed as a function of the deformation gradient and of these structural tensors, be objective—that is, it must be independent of the coordinate system of the observer and therefore be unchanged if the fabric in the reference configuration undergoes a rotation defined by a proper orthogonal tensor $\mathbf{Q}$. In mathematical terms, this implies that

$$\phi\left(\mathbf{C},\left({}^0\mathbf{g}_1\otimes{}^0\mathbf{g}_1\right),\left({}^0\mathbf{g}_2\otimes{}^0\mathbf{g}_2\right)\right)=\phi\left(\mathbf{Q}\mathbf{C}\mathbf{Q}^{\mathrm{T}},\mathbf{Q}\left({}^0\mathbf{g}_1\otimes{}^0\mathbf{g}_1\right)\mathbf{Q}^{\mathrm{T}},\mathbf{Q}\left({}^0\mathbf{g}_2\otimes{}^0\mathbf{g}_2\right)\mathbf{Q}^{\mathrm{T}}\right) \tag{3.22}$$

This requirement is satisfied when the energy function is expressed in terms of invariants of the right Cauchy-Green stretch tensor $\mathbf{C} = \mathbf{F}^{\mathrm{T}}\mathbf{F}$ and so called "pseudo-invariants" of $\mathbf{C}$ and the structural tensors [Spencer, 1971].

The energy function in **Equation 3.21** is expressed in terms of physical parameters (the interference I and the shear angle γ). These physical parameters can be related to pseudo-invariants of $\mathbf{C}$ and the structural tensors. The following three invariants are used:

$$\begin{aligned} I_4 &= {}^0\mathbf{g}_1\cdot\mathbf{C}\,{}^0\mathbf{g}_1 = \lambda_1^{\,2} = \left(\frac{p_1}{{}^0p_1}\right)^2, \\ I_6 &= {}^0\mathbf{g}_2\cdot\mathbf{C}\,{}^0\mathbf{g}_2 = \lambda_2^{\,2} = \left(\frac{p_2}{{}^0p_2}\right)^2, \\ I_8 &= {}^0\mathbf{g}_1\cdot\mathbf{C}\,{}^0\mathbf{g}_2 = {}^0\mathbf{g}_2\cdot\mathbf{C}\,{}^0\mathbf{g}_1 = \lambda_1\lambda_2\cos\theta\ . \end{aligned} \tag{3.23}$$

Here θ is the angle between the preferred directions (the angle between the yarn families) with the initial value of ${}^0\theta$, and λ_1 and λ_2 are the amounts of stretch in each of the preferred directions along the yarns. For a fabric deforming in accordance with the no-slip assumptions, the amount of stretch along a yarn direction is equal to the ratio of the current wavelength of that yarn family to its initial wavelength. These expressions follow from **Equations 3.19** and **3.20**.

I_4 and I_6 are standard invariants conventionally used in constitutive formulations of hyperelastic materials with two preferred directions [Holzapfel, 2000; Spencer, 1971]. I_8 is a modification of the conventional invariant I_8^* proposed by Spencer:

$$I_8^* = \left({}^0\mathbf{g}_1 \cdot {}^0\mathbf{g}_2\right) I_8 \ . \tag{3.24}$$

Spencer's invariant I_8^* is identically zero for a fabric with initially orthogonal yarns. The proposed I_8 defined in **Equation 3.23** is invariant with respect to a change in observer—that is, $I_8({}^0\mathbf{g}_1, {}^0\mathbf{g}_2, \mathbf{C}) = I_8(\mathbf{Q}\,{}^0\mathbf{g}_1, \mathbf{Q}\,{}^0\mathbf{g}_2, \mathbf{Q}\mathbf{C}\mathbf{Q}^T)$ for any proper orthogonal tensor $\mathbf{Q}$, as proved by **Equation 3.25**:

$$\begin{aligned} &I_8(\mathbf{Q}\,{}^0\mathbf{g}_1, \mathbf{Q}\,{}^0\mathbf{g}_2, \mathbf{Q}\mathbf{C}\mathbf{Q}^T) = \mathbf{Q}\,{}^0\mathbf{g}_1 \cdot \mathbf{Q}\mathbf{C}\mathbf{Q}^T\mathbf{Q}\,{}^0\mathbf{g}_2 \\ &= \mathbf{Q}^T\mathbf{Q}\,{}^0\mathbf{g}_1 \cdot \mathbf{C}\,{}^0\mathbf{g}_2 = {}^0\mathbf{g}_1 \cdot \mathbf{C}\,{}^0\mathbf{g}_2 = I_8({}^0\mathbf{g}_1, {}^0\mathbf{g}_2, \mathbf{C}) \ . \end{aligned} \tag{3.25}$$

I_8 is not identically zero for fabrics with initially orthogonal weaves, so in this case it can be used to describe the dependency of the strain energy function on yarn rotation, since the shear angle γ can be expressed in terms of I_4, I_6, and I_8.

$$\cos\theta = \frac{I_8}{\sqrt{I_4 I_6}} = \cos\left(\frac{\pi}{2} - \gamma\right) = \sin\gamma \tag{3.26}$$

Therefore, the geometric parameters in the strain energy function can be completely expressed in terms of the three pseudo-invariants listed in **Equation 3.23**.

$$I = \left({}^0A_1 + {}^0A_2\right) - \left(L_1{}^2 - p_1{}^2\right)^{1/2} - \left(L_2{}^2 - p_2{}^2\right)^{1/2}$$
$$= \left({}^0A_1 + {}^0A_2\right) - \left({}^0L_1{}^2 - I_4\,{}^0p_1{}^2\right)^{1/2} - \left({}^0L_2{}^2 - I_6\,{}^0p_2{}^2\right)^{1/2} \tag{3.27}$$

$$\gamma = \frac{\pi}{2} - \cos^{-1}\left(\frac{I_8}{\sqrt{(I_4 I_6)}}\right) \tag{3.28}$$

One final note on the choice of the modified pseudo-invariant I_8 concerns issues of convexity of the strain energy function. The selection of a conventional set of invariants [I_4, I_6, I_8^*] to express a strain energy function ensures that the function will be convex (downward) and therefore the material response will be stable (i.e. a material described using these invariants will not capture internal instabilities such a local yarn buckling). However, the strain energy function given by **Equation 3.21** is not strictly convex. This is evident in **Figure 3-8**, which shows the strain energy from **Equation 3.21** when the fabric is placed in biaxial extension or compression and then deformed in shear. The strain energy function remains convex when the fabric is subjected to biaxial tension, but becomes concave under biaxial compression, which reflects the tendency of the yarns to buckle in a shearing mode when subjected to compression. This buckling phenomenon is further discussed in **Section 4.6**. The set of invariants [I_4, I_6, I_8^*] is unable to capture this fabric behavior. For a fabric with initially orthogonal yarns, the invariant I_8^* is identically zero; this ensures that a model with an I_8^* dependency cannot buckle in shear, since shear buckling only occurs when the yarns are initially orthogonal and capable of snapping to either side. The strain energy function in **Equation 3.21** is therefore expressed using the set [I_4, I_6, I_8] and is not strictly convex, reflecting the instabilities of the initially orthogonal weave under in-plane compressive loading. This buckling behavior is stabilized by the introduction of inertia terms in the complete fabric model, as discussed in **Section 4.6**.

3.5.4 Derivation of the Cauchy Stress

The second Piola-Kirchhoff stress tensor **S**, a measure of stress applied to the undeformed configuration, can be found by differentiating the strain energy function ϕ with respect to the right Cauchy stretch tensor **C**, or equivalently (by the chain rule) by differentiating ϕ with respect to the invariants of **C**, and then by differentiating those invariants with respect to **C**.

$$\mathbf{S} = 2\frac{\partial \phi}{\partial \mathbf{C}} = 2\sum_k \frac{\partial \phi}{\partial I_k}\frac{\partial I_k}{\partial \mathbf{C}} \tag{3.29}$$

The Cauchy stress $\boldsymbol{\sigma}$ is related to **S** through a push-forward relation.

$$\boldsymbol{\sigma} = J^{-1}\mathbf{F}\mathbf{S}\mathbf{F}^{\mathbf{T}} \tag{3.30}$$

The coefficient J is the Jacobian, the ratio of the volume in the deformed configuration to the volume in the undeformed configuration. For this fabric model, the Jacobian is given by **Equation 3.31**.

$$J = \frac{4p_1p_2\sin\theta}{4^0p_1{}^0p_2\sin{}^0\theta} = \frac{p_1p_2\sin\theta}{{}^0p_1{}^0p_2} \tag{3.31}$$

The partial derivatives of ϕ with respect to the invariants can be calculated by combining **Equations 3.27** and **3.28** with **Equation 3.21**. Differentiating with respect to the invariants gives the following relations:

$$\frac{\partial \phi}{\partial I_4} = \phi_4 = \frac{K_I I^0 p_1}{8^0 p_2 A_1} - \frac{K_s \gamma^0 p_1 \cos\theta}{8^0 p_2 p_1^{\,2} \sin\theta}$$
$$\frac{\partial \phi}{\partial I_4} = \phi_6 = \frac{K_I I^0 p_2}{8^0 p_1 A_2} - \frac{K_s \gamma^0 p_2 \cos\theta}{8^0 p_1 p_2^{\,2} \sin\theta} \qquad (3.32)$$
$$\frac{\partial \phi}{\partial I_8} = \phi_8 = \frac{K_s \gamma}{4 p_1 p_2 \sin\theta}$$

Differentiating the invariants from **Equation 3.23** with respect to **C** gives the tensorial directions for the respective contributions to the stress tensor.

$$\frac{\partial I_4}{\partial \mathbf{C}} = \frac{\partial}{\partial \mathbf{C}}\left({}^0\mathbf{g}_1 \cdot \mathbf{C}\,{}^0\mathbf{g}_1\right) = {}^0\mathbf{g}_1 \otimes {}^0\mathbf{g}_1$$
$$\frac{\partial I_6}{\partial \mathbf{C}} = \frac{\partial}{\partial \mathbf{C}}\left({}^0\mathbf{g}_2 \cdot \mathbf{C}\,{}^0\mathbf{g}_2\right) = {}^0\mathbf{g}_2 \otimes {}^0\mathbf{g}_2 \qquad (3.33)$$
$$\frac{\partial I_8}{\partial \mathbf{C}} = \frac{\partial}{\partial \mathbf{C}}\left({}^0\mathbf{g}_1 \cdot \mathbf{C}\,{}^0\mathbf{g}_2\right) = \frac{1}{2}\left({}^0\mathbf{g}_1 \otimes {}^0\mathbf{g}_2 + {}^0\mathbf{g}_2 \otimes {}^0\mathbf{g}_1\right)$$

Here ${}^0\mathbf{g}_i \otimes {}^0\mathbf{g}_j$ are structural tensors that relate to the directions of the yarn families in the undeformed configuration. Now **Equations 3.29 – 3.33** can be combined to obtain the Cauchy stress in terms of fabric parameters and component constitutive properties.

$$\boldsymbol{\sigma} = \left(\frac{K_I I p_1}{4 A_1 p_2 \sin\theta} - \frac{K_s \gamma \cos\theta}{4 p_1 p_2 \sin^2\theta}\right)\mathbf{g}_1 \otimes \mathbf{g}_1$$
$$+ \left(\frac{K_I I p_2}{4 A_2 p_1 \sin\theta} - \frac{K_s \gamma \cos\theta}{4 p_1 p_2 \sin^2\theta}\right)\mathbf{g}_2 \otimes \mathbf{g}_2 \qquad (3.34a)$$
$$+ \frac{K_s \gamma}{4 p_1 p_2 \sin^2\theta}\left(\mathbf{g}_1 \otimes \mathbf{g}_2 + \mathbf{g}_2 \otimes \mathbf{g}_1\right)$$

The push forward operation has scaled the results to take into account the change in volume associated with deformation and has converted the initial configuration structural tensors ${}^0\mathbf{g}_i \otimes {}^0\mathbf{g}_j$ to deformed configuration structural tensors $\mathbf{g}_i \otimes \mathbf{g}_j$. The geometric relations, component constitutive constants, and fabric parameters can be combined so that the Cauchy stress can be expressed in terms of internal force scalars and unit cell

geometric parameters, eliminating the component constitutive relation coefficients K_I and K_S from the expression.

$$\begin{aligned}\boldsymbol{\sigma} = &\left(\frac{T_1 \cos\beta_1}{2p_2 \sin\theta} - \frac{M\cos\theta}{4p_1 p_2 \sin^2\theta}\right)\mathbf{g}_1 \otimes \mathbf{g}_1 \\ &+ \left(\frac{T_2 \cos\beta_2}{2p_1 \sin\theta} - \frac{M\cos\theta}{4p_1 p_2 \sin^2\theta}\right)\mathbf{g}_2 \otimes \mathbf{g}_2 \\ &+ \frac{M}{4p_1 p_2 \sin^2\theta}(\mathbf{g}_1 \otimes \mathbf{g}_2 + \mathbf{g}_2 \otimes \mathbf{g}_1)\end{aligned} \tag{3.34b}$$

Here T_1 and T_2 are the axial tensions carried by the yarns, and M is the moment load from the elastic rotation spring at the crossover points.

3.5.5 Interpretation of the Stress Tensor

By applying the stress tensor in **Equation 3.34b** to the faces of the unit cell, using **Equation 3.6**, the physical meaning of each term in **Equation 3.34b** becomes clear. For example, **Equation 3.35** gives the forces that result from the stress tensor when it is applied to the positive warp face $\mathbf{A}_1$, which has area $2p_2$ and unit normal $\mathbf{n}_2$, defined as the unit normal perpendicular to the weft yarn direction $\mathbf{g}_2$.

$$\begin{aligned}\mathbf{t}_{A_1} &= \boldsymbol{\sigma}\mathbf{A}_1 \\ &= \left(\frac{T_1 \cos\beta_1}{2p_2 \sin\theta} - \frac{M\cos\theta}{4p_1 p_2 \sin^2\theta}\right)2p_2(\mathbf{g}_1 \cdot \mathbf{n}_2)\mathbf{g}_1 \\ &+ \left(\frac{T_2 \cos\beta_2}{2p_1 \sin\theta} - \frac{M\cos\theta}{4p_1 p_2 \sin^2\theta}\right)2p_2(\mathbf{g}_2 \cdot \mathbf{n}_2)\mathbf{g}_2 \\ &+ \frac{M}{4p_1 p_2 \sin^2\theta}2p_2((\mathbf{g}_2 \cdot \mathbf{n}_2)\mathbf{g}_1 + (\mathbf{g}_1 \cdot \mathbf{n}_2)\mathbf{g}_2) \\ &= T_1 \cos\beta_1 \mathbf{g}_1 - \frac{M\cos\theta}{2p_1 \sin\theta}\mathbf{g}_1 + \frac{M}{2p_1 \sin\theta}\mathbf{g}_2\end{aligned} \tag{3.35}$$

Note that the dot product of $\mathbf{g}_2$ and $\mathbf{n}_2$ is zero, and the dot product of $\mathbf{g}_1$ and $\mathbf{n}_2$ is $\sin(\theta)$. The forces that result from the application of the stress tensor to each unit cell face are shown in **Figure 3-9**

The physical meanings of the terms can now be elucidated. The tensor dyad that multiplies the first two terms indicates that these terms generate forces that act on an area perpendicular to the warp yarns and act outward (for positive terms) in the in-plane direction of the warp yarns. The area per unit thickness of the unit cell face that cuts the warp yarns, projected on a plane perpendicular to $\mathbf{g}_1$ is $2p_2\sin(\theta)$. This means that the first term of the stress tensor generates a forces on the warp faces of the unit cell acting in-plane in the outward warp directions with magnitude $T_1\cos(\beta_1)$. This is exactly the magnitude of the in-plane component of the yarn tensile forces that pull inward on the unit cell faces in the warp direction. Hence the first term of the stress tensor counteracts the tensile forces in the warp yarns internal to the unit cell. Similarly, the third term of the stress tensor counteracts the tensile forces in the weft yarns, as a similar application of the stress tensor to the weft area $\mathbf{A}_2$ shows.

The fifth term is a shearing term that applies components of the loads $\mathbf{F}_{M1}$ and $\mathbf{F}_{M2}$ to the warp faces acting in the weft directions and to the weft faces acting in the warp directions, respectively. These are the loads required to generate the moments between the yarns M; by definition $\mathbf{F}_{Mi} = (M/(2p_i))\mathbf{n}_i$ so $\mathbf{F}_{M1}$ and $\mathbf{F}_{M2}$ generate equal and opposite moments and moment equilibrium on the unit cell is maintained. This ensures the symmetry of the stress tensor. However, since the unit cell does not remain square (and hence $\mathbf{n}_1$ and $\mathbf{n}_2$ do not remain parallel to $\mathbf{g}_2$ and $\mathbf{g}_1$ respectively), and because the structural dyads $\mathbf{g}_i \otimes \mathbf{g}_j$ can only resolve forces acting parallel to the $\mathbf{g}$ directions, the forces $\mathbf{F}_{Mi}$ required to generate moment M must be resolved into components, as shown in **Figure 3-9**. This is the origin of the $\sin(\theta)$ dependence in the fifth term, and of the second and fourth terms. The moment generating forces are projected onto the unit cell faces so they can be expressed in terms of the structural tensors; however, the projection also adds a component of force in the direction parallel to the yarns since the yarns and

hence the unit cell faces do not remain orthogonal. Therefore, these extra axial force contributions must be subtracted from the axial components of the stress tensor.

This simple model has only three types of internal forces that act on the unit cell faces—tension in the yarns and moment between them. The in-plane components of the yarn tensions give the first and third terms of the stress tensor, which are axial terms, while the forces needed to generate the moment, projected onto the unit cell faces, give the last terms, which are symmetric shear terms, and require corrections to the axial terms because the yarns do not remain orthogonal. The interference force does not appear explicitly in the stress tensor because this force does not act on the unit cell faces and hence does not need to be counteracted by the macroscopic stresses, though it does drive the tensile forces that appear in the yarns. The stress tensor balances the in-plane unit cell forces that act on the faces of the unit cell to maintain equilibrium. It can be shown also that the out-of-plane forces cancel out and hence no out-of-plane stress is generated. With an understanding of how the macroscopic stresses counteract the unit cell forces, the stress tensor in **Equation 3.34b** could have been determined without a strain energy differentiation, provided some means of determining the fabric state and the relevant forces was available. This is the method used to determine the stress tensor for the complete fabric model, for which strain energy differentiation is not possible.

3.5.6 Stress in the Complete Model

The stress tensor for the full ballistic fabric model can be derived using the following procedure:

1). Determine all load-bearing structural members "cut" by the boundaries of the unit cell.
2). Develop detailed free-body diagrams to determine the forces the fabric inside the unit cell exerts on the unit cell faces.
3). Find the in-plane components of these forces. The out-of-plane components should cancel.

4). Resolve the in-plane forces along vectors $\mathbf{g}_1$ and $\mathbf{g}_2$ parallel to the yarn directions.

5). Divide the resolved forces by the appropriate projected areas to obtain stresses. Express the results in tensorial form in terms of structural tensors $\mathbf{g}_i \otimes \mathbf{g}_j$.

6). Check to ensure that the resulting stress tensor is symmetric, and hence generates zero net moment.

The full fabric model has a number of additional contributions to the internal forces. The forces that contribute to the stresses are summarized below:

- Yarn tensions, which have an in-plane component that contributes to the axial stresses, as in the simplified model discussed above.
- Yarn bending moment at the yarn crossover points. These moments require a perpendicular shear force to counteract them, which has an in-plane component that contributes to the axial stresses, provided that the yarns are not fully extended.
- Moment between the yarns, which is calculated from the elastic-dissispative shear relation. This moment requires perpendicular forces that contribute to the shear stresses and also contributes corrections to the axial stresses, as discussed for the simplified model.
- Forces from the spars that capture locking and act on the unit cell faces. The in-plane component of these forces will have both an axial and a shear component.
- The locking spars also act against the crossing yarns provided that the crossing yarns are non-orthogonal. This will create additional moments on these yarns, which must be counteracted by perpendicular shear forces with in-plane contributions to both axial and shear stresses.

The complete stress tensor can therefore be calculated with knowledge of the scalar force magnitudes and an understanding of the fabric geometry.

$$\boldsymbol{\sigma} = \frac{1}{2p_2 \sin\theta}\begin{bmatrix} T_1 \cos\beta_1 - \dfrac{M_{b1}\sin\beta_1}{L_1} - F_{L1}\dfrac{p_1}{d_1} - \dfrac{M\cos\theta}{2p_1\sin\theta} \\ - F_{L2}\left(\dfrac{{p_2}^2\cos^2\theta}{p_1 d_2} + \sin\alpha_2 \dfrac{p_2}{L_1}\left|\cos\theta\right|\sin\beta_1\right) \end{bmatrix}(\mathbf{g}_1 \otimes \mathbf{g}_1)$$

$$+ \frac{1}{2p_1 \sin\theta}\begin{bmatrix} T_2 \cos\beta_2 - \dfrac{M_{b2}\sin\beta_2}{L_2} - F_{L2}\dfrac{p_2}{d_2} - \dfrac{M\cos\theta}{2p_2\sin\theta} \\ - F_{L1}\left(\dfrac{{p_1}^2\cos^2\theta}{p_2 d_1} + \sin\alpha_1 \dfrac{p_1}{L_2}\left|\cos\theta\right|\sin\beta_2\right) \end{bmatrix}(\mathbf{g}_2 \otimes \mathbf{g}_2) \qquad (3.36)$$

$$+ \left[\frac{M}{4p_1 p_2 \sin^2\theta} + F_{L1}\frac{p_1\cos\theta}{2p_2 d_1 \sin\theta} + F_{L2}\frac{p_2\cos\theta}{2p_1 d_2 \sin\theta}\right](\mathbf{g}_1 \otimes \mathbf{g}_2 + \mathbf{g}_2 \otimes \mathbf{g}_1)$$

The scalars F_{Li} reflect the compressive force in the locking spars, and the parameters d_i and α_i give the length and out-of-plane inclination of the locking spars as defined by **Equations 3.9** and **3.10**. This tensor is derived assuming the locking spars remain perpendicular to the in-plane projections of the yarns rather than the yarns themselves, which greatly simplifies the formulation. As long as both the shear angle and the crimp angles do not become extremely large, this is a very good approximation, especially considering that the locking relations themselves contain a significant degree of approximation. The terms from the stress tensor for the simplified model in **Equation 3.34b** appear in **Equation 3.36**, along with other terms that include the effects of the other force mechanisms within the unit cell. This stress tensor counteracts the in-plane components of the internal forces that act on the unit cell faces, satisfying in-plane equilibrium. The out-of-plane forces cancel, satisfying out-of-plane equilibrium. This tensor is symmetric, so it also satisfies moment equilibrium. As in the simplified model, interference does not appear because it does not act on any of the unit cell faces. Given the state and geometry of the unit cell and the force scalars from the component constitutive relations, macroscopic continuum stress can be calculated. This is the final component necessary to complete the fabric model.

Table 3:1 – Model Nomenclature

Note that subscripts *i* refer to yarn family

Geometric Parameters	
r_i	Minor radii of yarn cross section
R_i	Major radii of yarn cross section
p_i	Quarter wavelength
A_i	Crimp amplitude
β_i	Crimp angle
L_i	Yarn length per quarter wavelength
I	Cross section interference at crossover points
θ	Yarn angle
γ	Shear angle
γ_e	Elastic portion of shear angle
γ_f	Dissipative portion of shear angle
$\dot{\gamma}_f$	Rate of dissipative shear rotation
α_i	Out-of-plane inclination of locking force
ξ_i	Amplitude correction factor
d_i	(Half) distance between adjacent yarns (length of locking spar)
I_{Li}	Interference due to locking
Component Constitutive Parameters	
k_i	Axial yarn stiffness per unit length
k_{bi}	Yarn bending stiffness
K_I	Interference stiffness
a	Interference exponent
K_d	Locking stiffness
c	Locking exponent
I_L^*	Power law-linear transition locking interference
m^*	Linear locking stiffness
d^*	Linear locking offset
K_S	Elastic shear stiffness
M_0	Reference "shear strength"
$\dot{\gamma}_0$	Reference dissipative rotation rate
b	Dissipative rotation rate sensitivity factor
Internal Force Parameters	
T_i	Yarn tension
M_{bi}	Yarn bending moment at crossover points
F_I	Contact force from interference at crossover points
F_{Li}	Compressive locking force in locking spars
M	Moment between yarn families at crossover points

Table 3:2 – Summary of fabric deformation mechanisms

Deformation Mechanism	Load Relation	Equation Number	Contribution to Energy Function	Model Parameters	Properties Can Be Obtained By:
Axial Yarn Extension	$F_i = k_i(L_i - {}^0L_i)$	3.11	$\phi_i = \frac{1}{2}k_i(L_i - {}^0L_i)^2$	k_i	Measure from single yarn tension tests
Yarn Bending	$M_{bi} = k_{bi}(\beta_i - {}^0\beta_i)$	3.12	$\phi_{bi} = \frac{1}{2}k_{bi}(\beta_i - {}^0\beta_i)^2$	k_{bi}	Measure from tension tests on crimped yarn
Cross Sectional Interference	$F_I = K_I(e^{aI} - 1)$	3.13	$\phi_I = \frac{K_I}{a}(e^{aI} - aI - 1)$	K_I, a	Estimate by fitting data from "sandwich" compression test
Locking	$F_{Li} = \begin{cases} 0 & I_{Li} < 0 \\ K_d(I_{Li})^c & 0 \le I_{Li} < I_L^* \\ m^*(I_{Li}) + d^* & I_L^* \le I_{Li} \end{cases}$	3.15	$\phi_{Li} = \begin{cases} 0 & I_{Li} < 0 \\ \frac{K_d}{c+1}(I_{Li})^{c+1} & 0 \le I_{Li} < I_L^* \\ \frac{m^*}{2}(I_{Li} - I_L^*)^2 + d^*(I_{Li} - I_L^*) + \phi_i(I_L^*) & I_L^* \le I_{Li} \end{cases}$	K_d, c, I_L^*	Estimate by fitting data from "sandwich" compression test
Elastic Shear Rotation	$M = K_s\gamma_e$	3.16	$\phi_s = \frac{K_s}{2}\gamma_e^{\,2} = \frac{K_s}{2}({}^0\theta - \theta_e)^2$	K_S	Measure from shear frame experiments OR estimate by fitting data from bias-extension test
Dissipative Shear Rotation	$\dot{\gamma}_f = \dot{\gamma}_0\left(\frac{M}{M_0}\right)^b$	3.18	N/A	$\dot{\gamma}_0, M_0, b$	Measure from shear frame experiments OR estimate by fitting data from bias-extension test

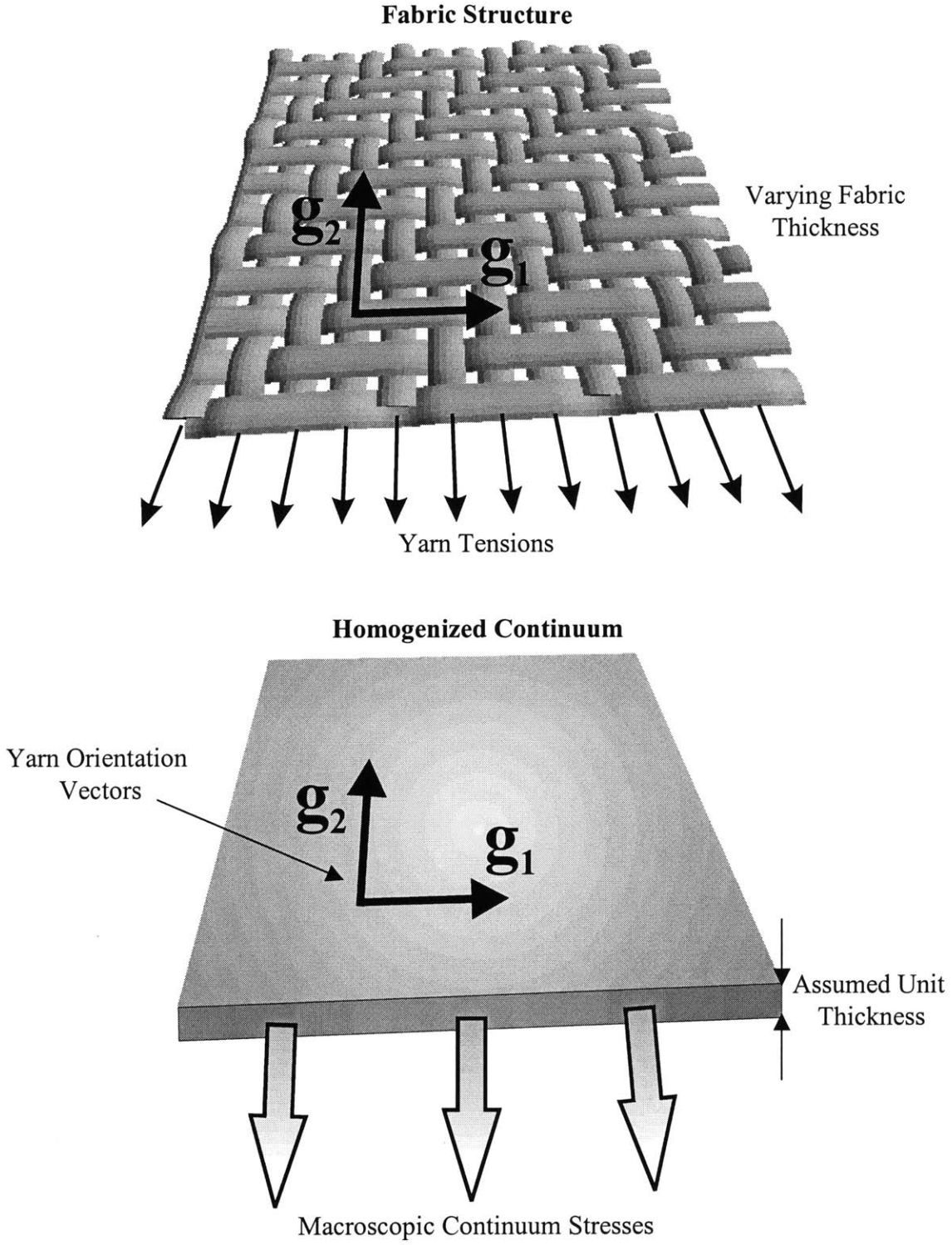


Figure 3-1 – Fabric treated as an anisotropic continuum with unit thickness

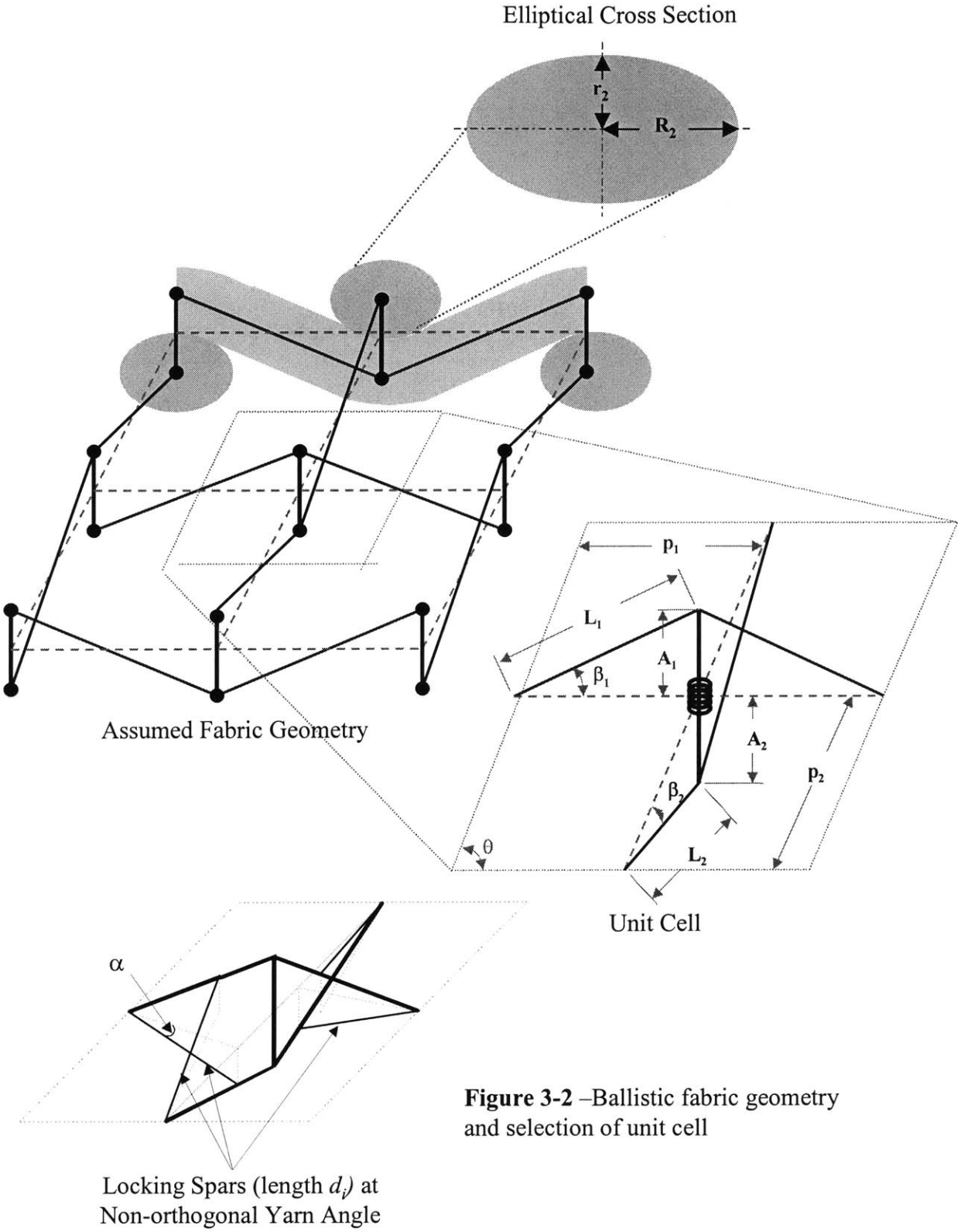


Figure 3-2 –Ballistic fabric geometry and selection of unit cell

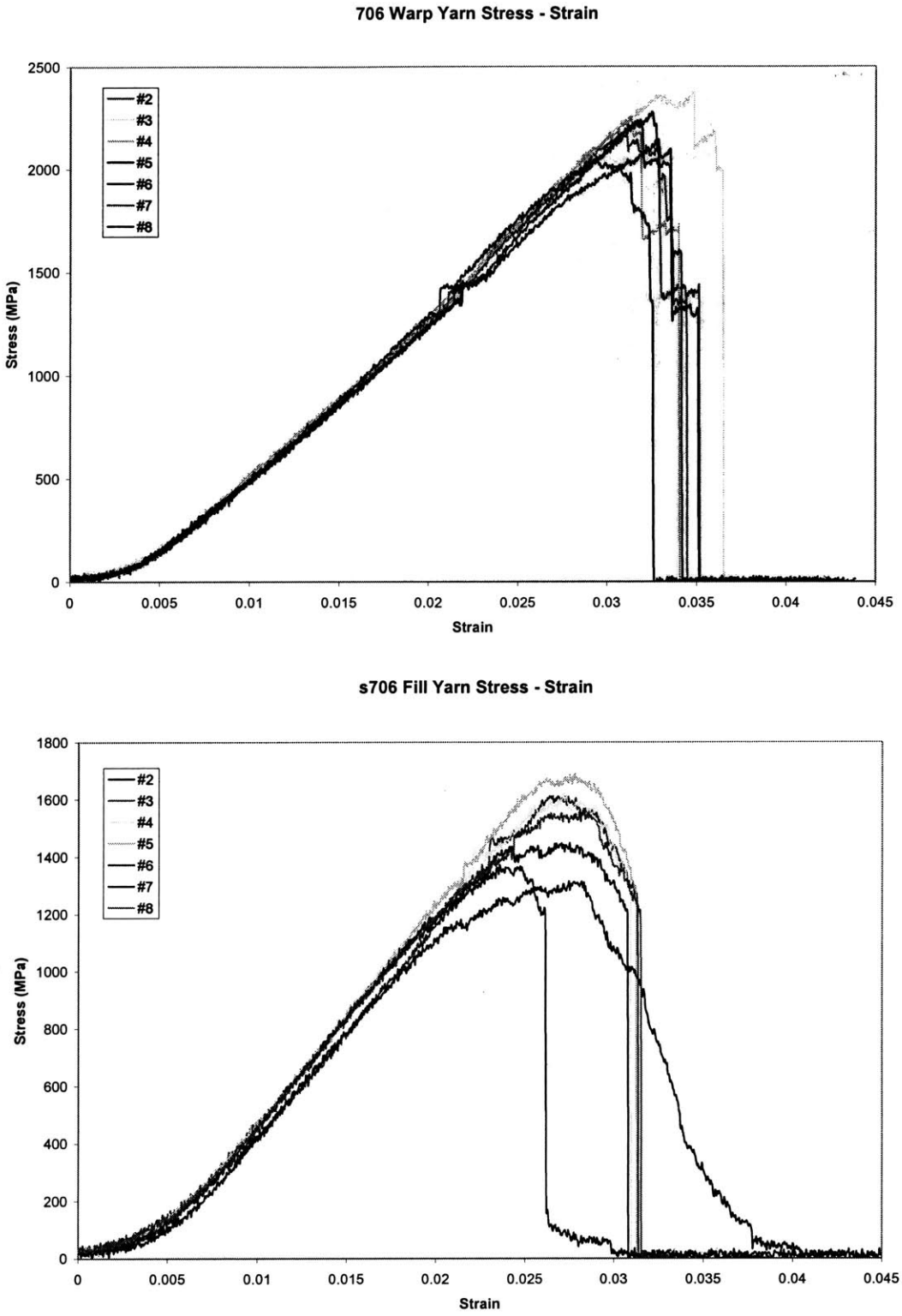


Figure 3-3 – Typical stress-strain curves
for Kevlar yarns from S706 ballistic fabric
(Jearanaisilawong, 2003)

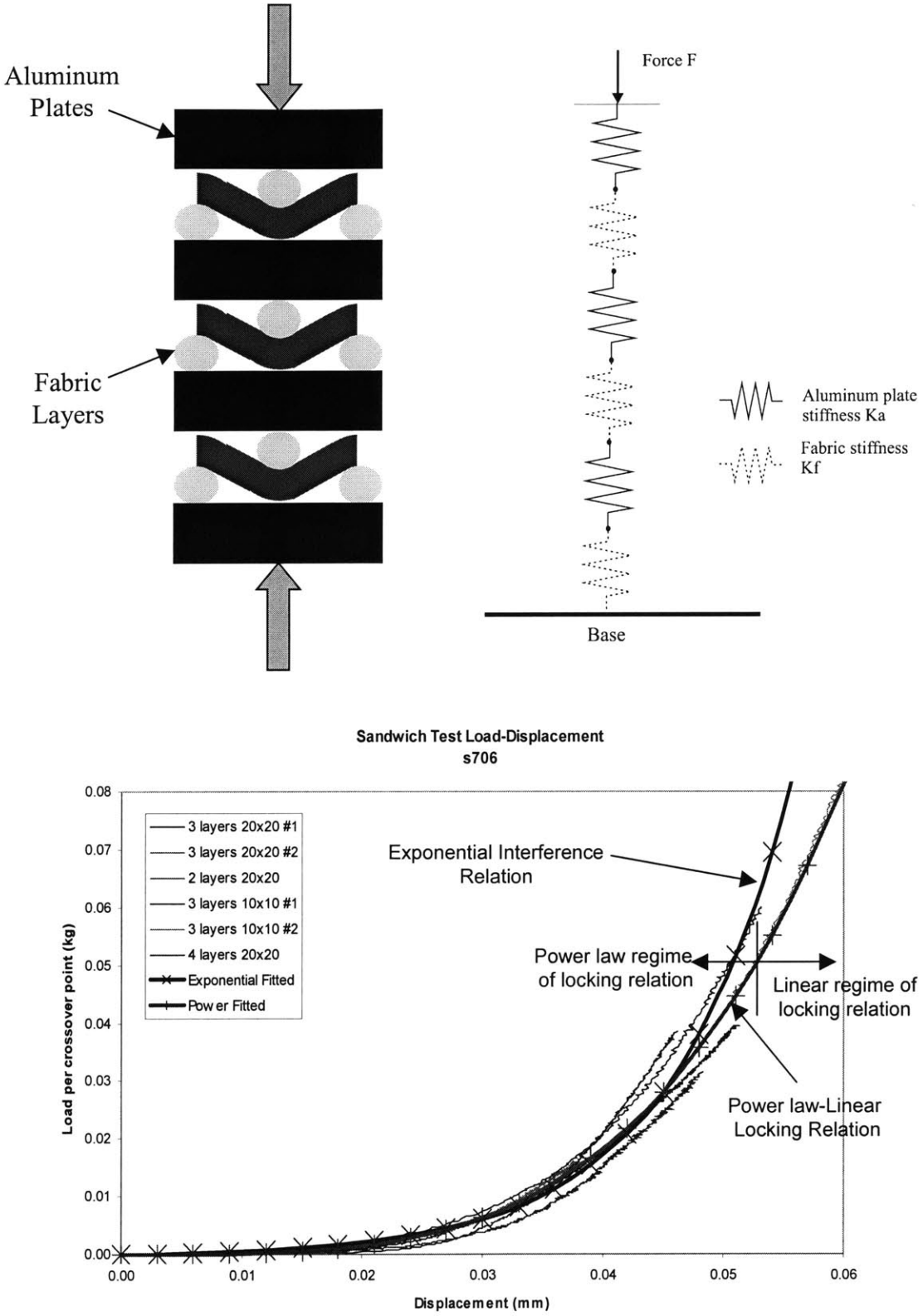


Figure 3-4 – Schematic of sandwich compression test and results for S706 ballistic fabric with exponential and power law fits (experimental data from Jearanaisilawong, 2003)

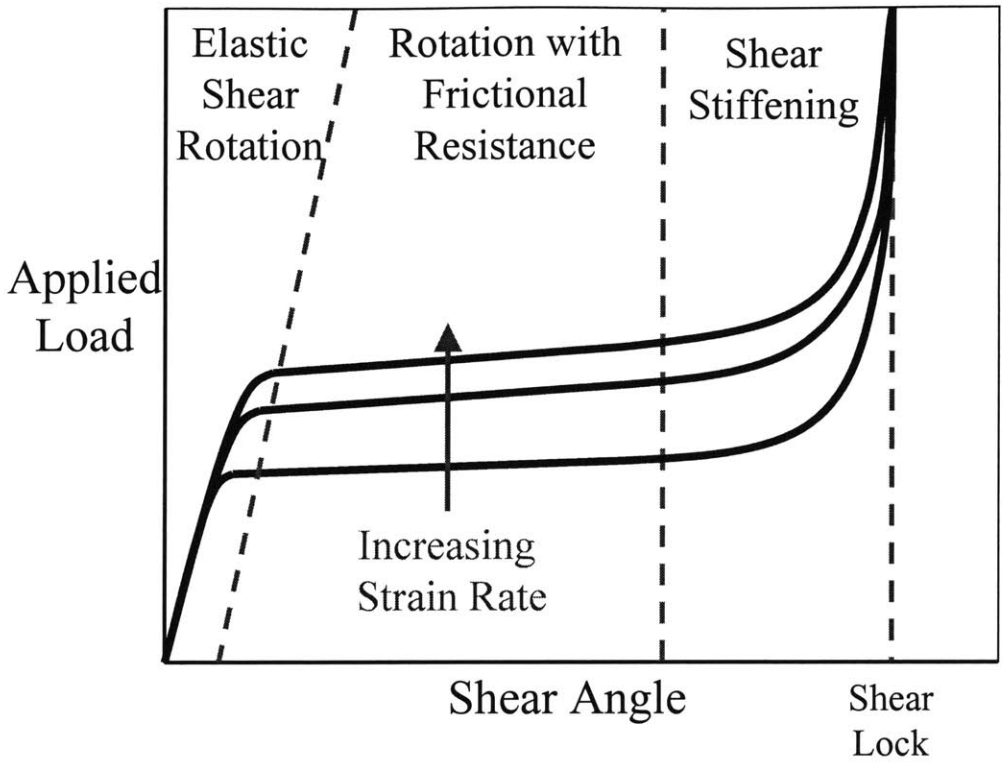
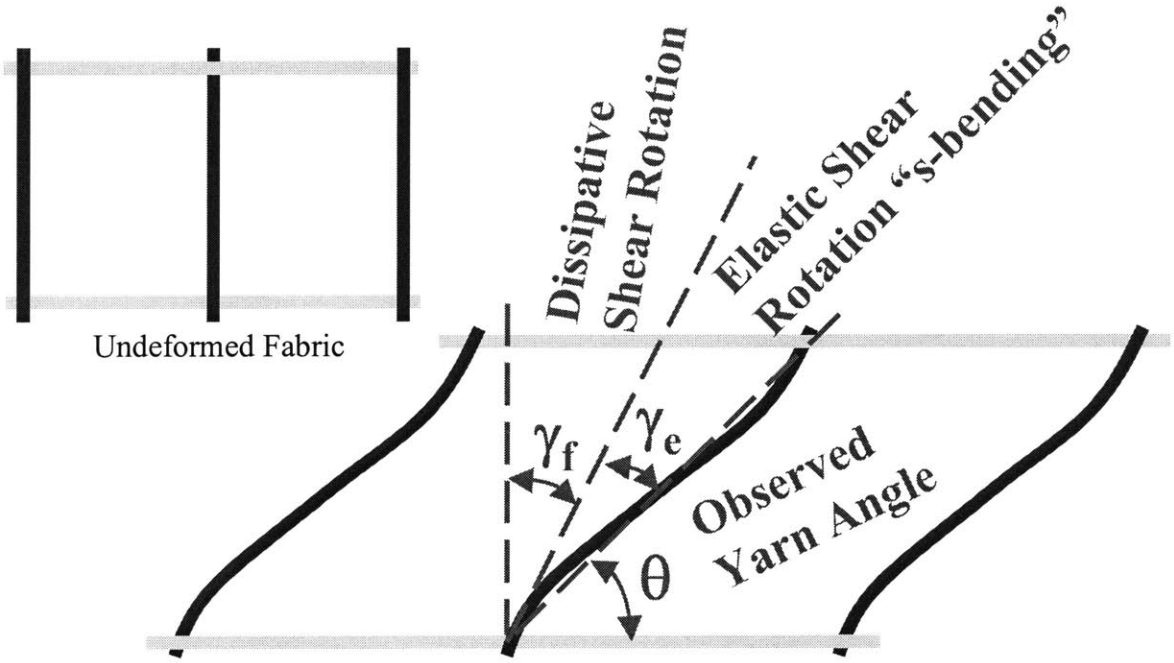


Figure 3-5 – Typical behavior of fabrics in shear



$$\gamma = \gamma_e + \gamma_f = \pi/2 - \theta$$

Figure 3-6 – Decomposition of shear angle into elastic and dissipative components (initially orthogonal)

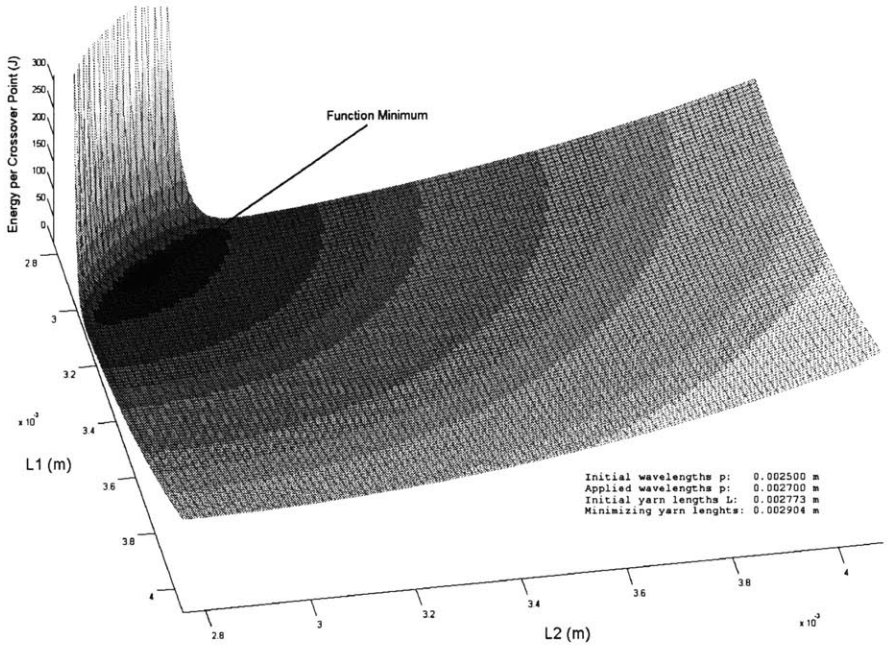


Figure 3-7 – Typical energy surface for fabric in even biaxial tension

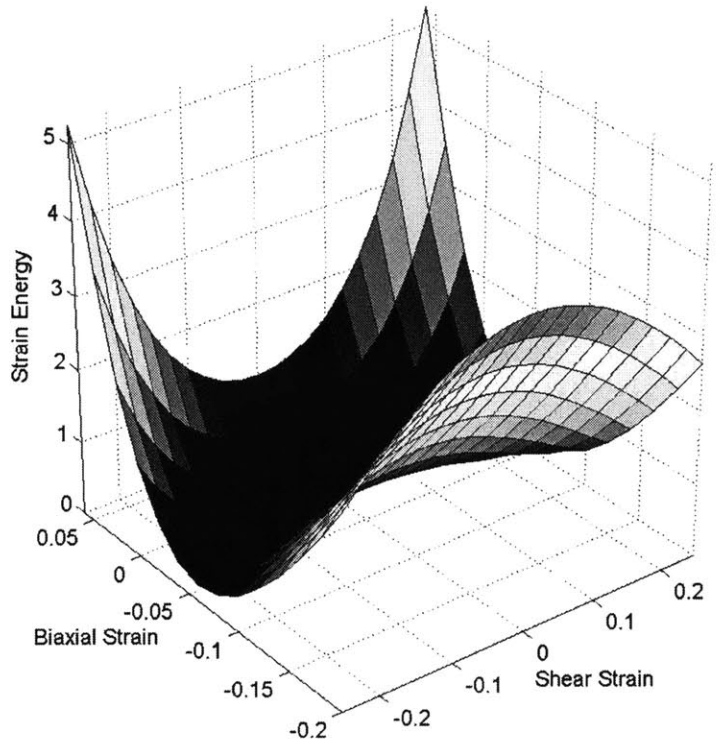
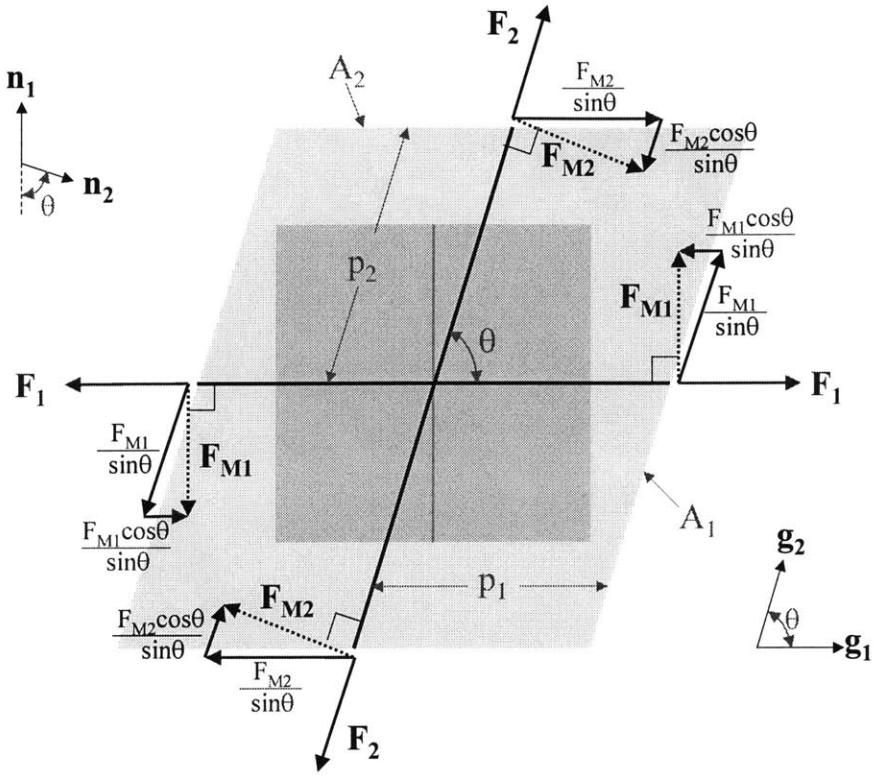


Figure 3-8 – Energy function for buckling fabric geometry, at different states of even biaxial tension and shear



Terms that compensate for the shear angle, keeping the shear load from the moment perpendicular to the yarns

Axial load carried by yarns

$$\boldsymbol{\sigma} = \left(\frac{F_1}{2p_2 \sin\theta} - \frac{M\cos\theta}{4p_1p_2\sin^2\theta} \right) \mathbf{g}_1 \otimes \mathbf{g}_1 + \left(\frac{F_2}{2p_1 \sin\theta} - \frac{M\cos\theta}{4p_1p_2\sin^2\theta} \right) \mathbf{g}_2 \otimes \mathbf{g}_2 + \frac{M}{4p_1p_2\sin^2\theta} \left(\mathbf{g}_1 \otimes \mathbf{g}_2 + \mathbf{g}_2 \otimes \mathbf{g}_1 \right)$$

Projection of moment load onto unit cell faces

Figure 3-9 – Forces on the unit cell resulting from the simplified model's stress tensor

Chapter 4

Numerical Implementation of the Fabric Model

4.1 Input and Output Requirements for the Finite Element Code

The ballistic fabric model described in the previous chapter has been implemented as a user-defined material into ABAQUS/Standard, an implicit, displacement based, finite element code. ABAQUS was selected because it allows easy implementation of user-defined material behavior. In future work we plan to implement the user material in an explicit version of the finite element code as was well, since explicit models are better suited for high-rate dynamic analysis.

In a typical nonlinear implicit analysis, an estimated incremental displacement field is generated using the principle of virtual work, which enforces equilibrium and boundary conditions in a weak form. The stresses and all other state variables are calculated from this displacement field at each integration point, and if these stresses do not satisfy equilibrium, the displacement field estimate is revised and new stress fields are calculated. This procedure is repeated until the equilibrium is satisfied within acceptable tolerances. A constitutive model for an implicit analysis must therefore provide a means of calculating the stresses and the updated values of any internal state variables that result from a known deformation history, and must also compute a Jacobian matrix that will be used in a Newton-Raphson iterative method to revise the estimated displacement field so as to better satisfy the principle of virtual work.

A user-defined material model is implemented into the implicit code ABAQUS/Standard through a FORTRAN user material subroutine, referred to as a "UMAT". For a given time increment beginning at some time t, the deformation gradient $\mathbf{F}(t)$ and the values of all internal state variables are known at each integration point. The length of the increment, Δt, and deformation gradient corresponding to the estimated displacement field at the end of the increment, $\mathbf{F}(t+\Delta t)$, are also known. Using this input data, the UMAT routine must calculate the Cauchy stress tensor at time $t+\Delta t$ corresponding to the estimated displacement field, and update any internal state variables. It must also compute the Jacobian matrix, which relates variational changes in the estimated incremental displacements to resulting variations in the predicted stress fields. This matrix is used in the global Newton-Raphson scheme to generate improved incremental displacement estimates. While accuracy of the Jacobian does not affect the accuracy of the solution, it does significantly affects the analysis convergence rate, and an inaccurate Jacobian may prevent the Newton-Raphson algorithm from converging.

4.2 Overview of Algorithm

The UMAT implements the ballistic fabric model using the following algorithm, shown schematically in **Figure 4-1**. First, the deformation gradient at the end of the increment $\mathbf{F}(t+\Delta t)$ is used to calculate all geometric parameters that can be determined directly. The other independent geometric parameters are then determined by minimizing the energy function while holding the known parameters constant. The energy per crossover point can be obtained for a given geometric configuration, using the component constitutive behaviors. After all the parameters that determine the fabric configuration have been calculated, the internal forces such as yarn tensions, locking forces, contact forces, yarn bending moments, etc. are evaluated using the component constitutive relations. The moment between yarns that resists rotation at the crossover points is calculated through an explicit integration scheme for the dissipative rotation. Next, inertial stabilization against unstable buckling modes is applied, and the geometric parameters that describe the fabric configuration and the stabilized internal forces are

used to calculate the stresses. The material Jacobian is computed numerically by perturbing the incremental displacement estimates. The following sections discuss specific challenges that were resolved during the implementation of this algorithm.

4.3 Integration of Dissipative Shear Rotation

At each time step, the total shear angle can be directly obtained from the deformation gradient. The magnitude of the dissipative shear angle and the rate of dissipative shear rotation are stored as state variables and their values at the beginning of the time increment, $\gamma_f(t)$ and $\dot{\gamma}_f(t)$, are therefore known. The dissipative shear angle is updated using an explicit integration scheme:

$$\gamma_f(t+\Delta t) = \gamma_f(t) + \dot{\gamma}_f(t)\Delta t \ . \tag{4.1}$$

The value of the dissipative angle is then used to determine the magnitude of the elastic shear angle at the end of the increment using **Equation 3.11.** The resulting moment between yarn families is then obtained using **Equation 3.10**, and the shear stresses are determined. The dissipative shear rotation rate, $\dot{\gamma}_f(t+\Delta t)$, is then updated using **Equation 3.12**.

The explicit integration scheme in **Equation 4.1** provides an acceptable approximation for the updated dissipative shear angle as long as the change in the dissipative rotation rate over the increment is small. In order to minimize the integration errors, the updated value of the dissipative shear rotation rate is compared to the value at the beginning of the increment whenever the explicit scheme is used. If the change is excessive, the current analysis step is aborted and reattempted with a smaller time increment size. This test is only performed when the dissipative rotation rates are larger than a small fraction of the estimated macroscopic strain rate, thus preventing the algorithm from enforcing needlessly small increment sizes.

4.4 Energy Minimization

Most fabric models require more parameters to define their configuration than the three parameters that can be determined directly from the deformation gradient, as discussed in **Section 3.4**. The remaining free independent parameters are determined through an energy minimization procedure. The energy of the unit cell is expressed as a function of all the independent parameters, and the function is minimized with respect to the free parameters while the three known parameters are held constant. The derivatives of the energy function for the ballistic fabric model include fourth order polynomials and trigonometric functions, and the set of equations corresponding to the minimum energy configuration has no closed-form solution. Therefore, the minimum energy configuration cannot be obtained from a closed-form analytical expression, and it must be determined numerically.

4.4.1 Newton's Method

The first implementation of the fabric model employed a two-dimensional Newton's Method to determine the two free parameters, the yarn lengths L_1 and L_2. The strain energy function was differentiated with respect to these two parameters to obtain the energy gradients. Newton's method requires derivatives of the functions to be zeroed, so each gradient function was differentiated again with respect to each length parameter, yielding four more equations. The Newton's method minimization subroutine evaluates the two gradient expressions at some guess of L_1 and L_2. If either expression is nonzero (relative to a numerical threshold), the four second derivatives (which are first derivatives of the gradients) are used to choose new L_1 and L_2 guesses closer to the minimum. This process is repeated until the two gradient expressions both evaluate to zero, within the numerical threshold. For more details on multidimensional Newton's methods, refer to a text on numerical minimization such as Press et. al [1992].

This approach was effective for an initial implementation of the model, which used simplified locking relations and no bending energy, but it exhibited several disadvantages. First, the strain energy function is bounded on two sides as shown in **Figure 4-2**, since the yarn lengths can never be shorter than the wavelengths. The function cannot be evaluated outside these bounds. However, Newton's method can sometimes predict a new guess that violates these bounds. This problem requires a modification to the algorithm that limits the length parameters and holds the algorithm's walk within the bound of the energy function. This can result, for certain initial guesses, in a path that follows the bound for some time before leaving the bound and moving towards the minimum, which adversely affects the algorithm's efficiency. This behavior is shown in **Figure 4-3**, where the worse initial guess results in a large number of steps that follow the bound for many iterations. The algorithm's performance is very sensitive to the initial guess.

Additionally, the energy function is typically poorly behaved near its lower bounds, as is also shown in **Figure 4-2**. Here the function reaches its minimum very close to the bounds and then rapidly approaches very large values. The greater the applied strains, the closer the minimum lies to the bounds and the more dramatically the gradients change. The large and rapidly changing slopes near the minimum sometimes cause convergence difficulties, especially when the deformations become large and the minimum moves very close to the bounds. At increasingly large applied strains the gradient expressions converge to values increasingly further from zero, which is a result of the large, rapidly changing gradients near the minimum. This condition requires an undesirable variable-convergence criterion that scales with the magnitude of deformation.

A third limitation is that, while this method is relatively efficient and easy to implement in cases where there are only two free parameters, it becomes less efficient and more difficult to implement in cases where there are more than two free parameters, as is the case with more complicated geometries. For example, models that capture ovalization of the yarn cross sections would require at least four free parameters. Modeling more

phenomena within the fabric's weave structure, such as yarn twist effects or yarn swelling, or modeling a more complicated weave geometry (such as a twill weave) would require more free parameters. Newton's method becomes increasingly less efficient and more difficult to implement as the number of free parameters increases.

One other shortcoming of Newton's method is the requirement for the evaluation of the energy function derivatives. Newton's method is a so-called "second order" minimization method, meaning that both first and second derivatives of the objective function are required. Calculating these derivatives can be difficult and computationally inefficient. Since the energy minimization routine will be called many times over the course of the analysis (at least four times for each increment of implicit analysis at each integration point in the finite element model), its speed will have a large effect on the efficiency of the overall model.

More sophisticated second order and first order (requiring only first derivatives) methods are available, such as the conjugate gradient method. However, a so-called "zeroth order method" that requires only the objective function and not the value of the derivatives is preferable to first or second order methods in this application. Such methods eliminate the need to calculate derivatives and make the model versatile and easy to modify. If changes to the component constitutive relations are made, only the objective energy function and the corresponding force relations need to be modified, eliminating the need to update derivative expressions as well.

Two effective zeroth order methods considered here are the downhill simplex method and the simulated annealing method. Advantages and disadvantages of each are discussed below. For the ballistic fabric model, which has only five independent configuration parameters and a single global minimum, the downhill simplex method is more efficient and is the method that has been implemented in the ballistic fabric model. The simulated annealing method is more effective for complex models that require larger numbers of free parameters or which contain internal instabilities that create local minima in the energy function.

4.4.2 The Downhill Simplex Method

A simplex is a polytope that exists in n-dimensions, where n is the dimensionality of the problem. It has $n+1$ vertices, each of which represents a "guess"—a point where the objective function is evaluated. The values of the free variables at each vertex can be thought of as "coordinates" in the function's domain space. For example, in a one-dimensional problem (a single free parameter) a simplex is a line segment. In two dimensions (as is the case for the ballistic fabric model) simplices are triangles; in three dimensions they are tetrahedrons. Higher order simplices are difficult to describe geometrically, but the simplex algorithm using higher order simplices is the same. The downhill simplex method, described by Press et. al. [1992] and by Grabitech Solutions AB, reflects and scales a simplex within the bounded variable space spanned by the objective function, following rules that ensure that each scaled reflection results in a new simplex whose vertices are closer to the function's minimum.

The most basic downhill simplex algorithm uses a simplex of constant size. First, an initial simplex is defined to lie close to the initial "guess" for the minimization procedure. The size of the simplex is a measure of the "step size" of the minimization algorithm. The objective function is evaluated at each of the simplex's $n+1$ vertices, and the vertices are ranked from "best" (designated B) to "worst" (designated W)—for minimization the best vertex corresponds to the smallest objective function value. The "coordinates" of the midpoint P of the "face" opposite the worst vertex W is determined by averaging the "coordinates" of all the vertices except the worst, and a vector WP pointing from the worst vertex to this midpoint is calculated. A new vertex R is determined by reflecting W over P so that $R = P + WP$, and point R replaces point W in the simplex. Hence the simplex is reflected so that its worst vertex is replaced by one that may be better, and the simplex moves away from a less favorable location. Two additional rules ensure the convergence of this method. First, a new point R at a given iteration is never permitted to become the worst vertex W in the next iteration—this prevents the simplex from oscillating between two points. Second, bounds are included by ensuring that the initial simplex lies completely within the function bounds and then by applying a very

unfavorable function estimate to any vertex that violates the bounds, rather than trying to evaluate the actual function at this point, to ensure that it will be subsequently replaced. This basic simplex algorithm is shown in **Figure 4-4** [Grabitech].

The basic downhill simplex method uses a fixed simplex size, and eventually begins to circulate around a function's minimum, since the fixed size prevents the algorithm from "converging" in a traditional sense. One solution to this problem is to test to see if the simplex has had the same best vertex for a large number of consecutive iterations, implying that the simplex has begun to circulate. When this occurs, the simplex size can be reduced and the process restarted from the vicinity of the best vertex. In this manner, increasingly small simplices will move to and then circulate around the function's optimum, which will allow the method to converge. The path that results from a "circulating simplex" method is shown in **Figure 4-5**.

The modified simplex method is another approach that varies the simplex size to increase the method's efficiency and to allow convergence. **Figure 4-6** [Grabitech] shows the algorithm for the modified simplex method. It differs from the basic simplex algorithm through the addition of the following new rules:

- When the new vertex R is determined, the objective function is immediately evaluated at R, and R is compared to the existing simplex vertices.
- If R is better than the best vertex B, it means that the direction of R is favorable and a new point E that expands the simplex is calculated by $E = P + \varepsilon WP$, where ε is an expansion factor greater than 1. The objective function is evaluated at E, and if E is also better than B, it is accepted and the simplex is expanded in the favorable direction.
- If E is not better than B, or if R was not better than B but was better than the next to worst simplex point N, then it means that the direction is not as favorable, so no scaling is applied and R is used.
- If R is worse than N but still better than W, it means that moving in the direction of R is only slightly favorable, so the simplex is contracted and the

vertex $C^+ = P + cWP$ is used instead of R, where c is a contraction factor less than 1.

- If, on the other hand, R is worse than W, it means that the direction of R is unfavorable so instead of being reflected the simplex is merely scaled away from its worst vertex, and W is replaced by $C^- = P - cWP$.

These rules cause the simplex size and shape to vary and allow the simplex to move very rapidly across unfavorable areas and then converge upon the function's minimum. Convergence can be defined to occur when the size of the simplex (measured by vector WP) shrinks below a tolerance limit, or when the distance between best vertices in successive steps remains below a tolerance limit for a certain number of consecutive steps. In either case the implication is that the simplex is small and close to the optimum, so that further iterations will not improve the algorithm result relative to the tolerable error. Both of these criteria are enforced in the ballistic fabric model. **Figure 4-7** shows the path taken by the modified downhill simplex method, for an energy surface corresponding to uneven biaxial tension.

The downhill simplex method has several advantages that make it an attractive approach. It is a zeroth order method requiring no derivatives. It does not require that the function be continuous or that it be defined outside its bounds; the only requirement is that it can be evaluated at all points in its domain. The modified version of the downhill simplex method converges rapidly with a computational cost comparable to Newton's method for the ballistic fabric model. Its behavior is not adversely affected by the fact that the function is bounded or by the large, rapidly changing gradients near the minimum.

One disadvantage of the downhill simplex method is that its behavior is not completely understood in a rigorous mathematical framework, and that there are certain, very specific, cases where it will fail to converge to the correct solution. One example of this phenomenon occurs when the energy function is perfectly symmetric with respect to the free variables, which would occur if a perfectly balanced fabric were subjected to even biaxial extension or compression. When the initial simplex is also symmetric and when

its axis of symmetry coincides with that of the energy function, the simplex algorithm sometimes does not converge. This problem can be avoided by ensuring that the initial simplex does not share an axis of symmetry with the energy surface.

Another disadvantage of the simplex method is that its memory and computational requirements become large as the problem dimensionality becomes large. For a problem with n free parameters, the algorithm requires that a simplex in n dimensions with $n+1$vertices be stored, along with the function's value at each vertex. This requires an $n+1$ by $n+1$ matrix. In each iteration of the simplex method, the rows of this matrix must be sorted. This makes the simplex method inefficient for problems with very large dimensionalities. Fortunately, minimization problems that arise in fabric analysis typically have significantly fewer than 100 free parameters, which means that the memory and computational requirements of the simplex method will not be excessive. A final shortcoming of the simplex method is that, like most optimization schemes, it can locate a local minimum but cannot escape from one to find the global minimum of a function with multiple minima. Such an energy function could arise in the case of a fabric model that includes multiple crossover points, such as a fabric model for a twill weave, and that has buckling instabilities that give rise to local energy minima. Physically, if the fabric were subjected to sufficient perturbation to prevent it from remaining in a quasi-stable state at a local minimum, it would tend to assume the configuration corresponding to the global minimum of the energy function. In this case, a minimization scheme that can escape from local extrema and locate a global extremum would be required.

4.4.3 Simulated Annealing

Simulated annealing [SA] is a zeroth order optimization algorithm that can escape local extrema. It has all the advantages of the downhill simplex method—it is a zeroth order method, it is unaffected by poorly behaved gradients, bounds are easily incorporated—but is typically less efficient than the downhill simplex method unless the problem's

dimensionality is large. In simulated annealing, an algorithm walks through a number of states that form a "Markov chain". The probability of transitioning to a more favorable state is unity (i.e. "downhill" moves are always accepted), while the probability of transitioning to a less favorable state is less than unity. This probability depends on the change in energy associated with the transition and also on an artificial "temperature" parameter, initially large to allow free movement about the function domain but reduced throughout the process. Consequently, the algorithm initially moves from state to state relatively freely and samples a large portion of the function domain, but, as time progresses, unfavorable transitions will become more and more infrequent until finally the algorithm will only accept moves towards a minimum. New states to be tested for acceptance are selected randomly according to rules governing the "neighborhood" around the current state—only states within that neighborhood can be selected (i.e., only states within a certain "radius" of the current state in the function's domain space). The neighborhood can be increased to allow large steps and fewer acceptances, or decreased for smaller steps and more acceptances, but eventually, when the function is near the minimum and the "temperature" is small enough, no new states will be accepted regardless of the neighborhood size, because all neighboring states will involve a move to a less favorable condition. The manner in which the "temperature" parameter is decreased is referred to as the "cooling schedule" and is has a significant effect on the algorithm's efficiency. **Figure 4-8** shows a simulated annealing algorithm's random walk for both fast and slow cooling schedules projected onto a fabric energy function that results from a state of uneven biaxial extension.

It has been rigorously proven that this algorithm will always converge to the global extremum provided that the temperature parameter converges to zero and an infinite number of steps at each temperature are permitted. Convergence in a finite number of steps is affected by the cooling schedule, the neighborhood control scheme, and the convergence criteria. A more aggressive cooling schedule will typically result in faster convergence but will explore less of the function domain and has a reduced likelihood of escaping from local extrema. Even with a very aggressive cooling schedule (or no cooling at all, when only downhill moves are accepted), SA is less efficient than the

downhill simplex method unless the dimensionality of the problem is large. For this reason, the downhill simplex method is preferred for the ballistic fabric model, though SA remains an attractive alternative for future models with larger dimensionalities or which might require global minimization in the presence of local minima.

4.5 Numerical Jacobian Matrix

For implicit analyses, the UMAT must calculate the material Jacobian matrix. ABAQUS uses a vector representation of the stress and incremental strain tensors, where $\{\sigma_1\ \sigma_2\ \sigma_3\ \sigma_4\ \sigma_5\ \sigma_6\}$ correspond to the components $\{\sigma_{11}\ \sigma_{22}\ \sigma_{33}\ \sigma_{12}\ \sigma_{13}\ \sigma_{23}\}$ of the Cauchy stress tensor, and $\{\Delta\varepsilon_1, \Delta\varepsilon_2, \Delta\varepsilon_3, \Delta\varepsilon_4, \Delta\varepsilon_5, \Delta\varepsilon_6\}$ correspond to the components $\{\varepsilon_{11}, \varepsilon_{22}, \varepsilon_{33}, 2\varepsilon_{12}, 2\varepsilon_{13}, 2\varepsilon_{23}\}$ of the relative strain $\boldsymbol{\varepsilon} \approx \ln(\mathbf{U}_t)$, where $\mathbf{U}_t$ is the relative stretch tensor between $\mathbf{F}(t)$ and $\mathbf{F}(t + \Delta t)$. The Jacobian is a 6x6 matrix whose *ij*-component gives the variation in the i^{th} stress component resulting from a perturbation of the j^{th} strain component of the incremental displacement estimate.

$$J_{ij} = \frac{\partial \sigma_i}{\partial(\Delta \varepsilon_j)} \tag{4.2}$$

While the Jacobian does not affect the stress or internal state variable values that the UMAT predicts corresponding to a particular deformation history, ABAQUS uses the Jacobian to estimate an improved incremental displacement field for the next iteration of the Newton-Raphson implicit procedure. Therefore, an accurate Jacobian is required for efficient convergence, while inaccurate calculation of the Jacobian matrix results in slow convergence or divergence of the iteration scheme.

Calculating the exact material Jacobian analytically is impossible for all but the simplest fabric models, as the numerical energy minimization procedure does not have a closed analytical form. Therefore the Jacobian must also be calculated numerically. For each

strain component, a perturbation of the incremental displacement estimate is calculated so that the strain variation is approximately an order of magnitude smaller than the strain increment for the current iteration. A variational deformation gradient that reflects this perturbation is generated. The variational deformation gradient is multiplied by the actual deformation gradient to yield a trial deformation gradient. A trial Cauchy stress tensor is calculated using the trial deformation gradient, and the variations of the stress components with respect to the variation of each strain component are evaluated. This process is repeated for all in-plane strain components. With this approach, a change to the material model does not necessitate a change to the scheme for determining the Jacobian.

4.6 Local Buckling and Inertial Stabilization

Fabrics are thin structures whose in-plane stiffness is much greater than their bending stiffness, so they tend to buckle out of plane when subjected to compressive in-plane loads. Therefore, structural fabrics are either subjected to tensile loads only, or are constrained to remain planar, typically by bonding the fabric to other materials in a multi-layer structure. However, even when the fabric is constrained to remain planar, the fabric yarns can buckle locally. The local buckling modes that a model can capture depend on the assumed geometry of that model. The geometry selected for the ballistic fabric model has the two in-plane buckling modes shown in **Figure 4-9**. One of these modes occurs when yarns in compression rotate out of plane, bending very sharply at the crossover points and greatly increasing their crimp angle. This mode is referred to as "yarn buckling" and is resisted in the ballistic fabric model by the yarns' bending stiffness and the interference's spring's stiffness in tension. The other buckling mode is a shearing mode where crossover points in alternating rows translate to the sides. This mode is referred to as referred to as "shear buckling" and is resisted in the ballistic fabric model by the rotational resistance at the crossover points. Because both the yarn bending stiffnesses and the interference spring's tensional stiffness tend to be very small or zero, the yarn buckling mode tends to be the lower energy mode.

Locking will tend to arrest both buckling modes after sufficient deformation. However, significant deformation is possible before this occurs, especially in loosely woven fabrics or in fabrics with small locking stiffnesses. Consequently, any section of the modeled fabric that is locally subjected to compression can experience a "snap-through" bifurcation where the loads overcome the resisting forces and the fabric structure attempts to rapidly snap to a buckled configuration. In a quasi-static implicit analysis, which does not include inertial terms, this snap-through causes numerical difficulties and can prevent convergence:

- In nonlinear analysis, small displacement increments are criteria for convergence as well as small force residuals.
- When a model buckles and undergoes a large change in displacement, the quasi-static implicit code keeps reducing the time increment in an unsuccessful effort to reduce the size of the displacement increments.
- However, the displacement increments required to reach equilibrium do not scale with the size of the time increment when buckling occurs, since the snap-through associated with the buckling occurs instantaneously.
- Therefore, if the displacement increments required to reach the equilibrium configuration are too large, the iteration scheme does not converge.

This problem does not occur in dynamic analyses, since the inertia of the material is included, and instantaneous motion is not possible. When a structure buckles, it moves to its new equilibrium configuration only as quickly as the forces acting on it can accelerate it. Small displacement increments are still required for accuracy, but now the displacement increments scale with the size of the time increment, so reducing the time increment does reduce the displacement increments.

A common solution to the local buckling problem in quasi-static analyses is the addition of inertial stabilization. Small, "artificial inertia" terms are added to the stiffness matrix to stabilize the model against buckling. The magnitude of these terms varies with the "rate" of deformation, which is proportional to the displacement increments divided by

the size of the load step. These terms tend to slow the snap-through, as real inertia limits the rate of motion in a dynamic analysis, and cause the magnitude of the displacement increment to scale with the size of the load step. The acceptable time increment becomes larger as more artificial inertia is added. The disadvantage of this approach is that it introduces error, as there is some energy loss associated with the stabilizing forces. Adding larger mass terms increases the stabilizing forces and allows larger time increments, at the cost of greater error due to more energy loss through stabilization. To reduce this energy loss, it is desirable to stabilize only the degrees of freedom that affect buckling.

Both of the ballistic fabric buckling modes involve yarn rotation, so artificial inertia is added only to the rotational degrees of freedom of the yarns in the unit cell geometry. This can be accomplished by adding moments that result from the rotational inertia of the yarns to the internal unit cell forces before the stress tensor is calculated. The inertial stabilization scheme is implemented in the following manner. The rotational inertias of the yarn segments are calculated from their lengths, radii, and densities, both for in-plane stabilization (against shear buckling) or out-of-plane stabilization (against yarn buckling). These inertias differ slightly since the yarns are inclined differently about the appropriate axes of rotation. For circular yarns with density ρ, radius r, quarter-wavelength length L, and wavelength p, the relevant rotational inertias II are given by **Equation 4.3**. The subscript i designates the yarn family and the superscripts *(c)* and *(s)* indicate whether the inertia is relevant to out-of-plane rotation and yarn buckling or in-plane rotation and shear buckling, respectively. Oval yarns require a slightly different relation that involves the major and minor radii.

$$II_i^{(c)} = \frac{1}{2}\rho_i \pi r_i^4 L_i + \frac{2}{3}\rho_i \pi r_i^2 L_i^3$$
$$II_i^{(s)} = \frac{\rho_i \pi r_i^4 L_i}{2\cos^2 \beta_i} + \frac{2\rho_i \pi r_i^2 p_i^2 L_i}{3} \tag{4.3}$$

The crimp angles (relevant to yarn buckling), the in-plane yarn angles (relevant to shear buckling), and the rates of change of these angles at each time step are stored as state variables. The average rotational accelerations of the yarns in each of the two directions over the time increments are obtained from these values. For shear buckling, only the rotation that contributes to shear deformation is considered. The shear angle is apportioned between the two yarn families according to their relative rotational inertias in order to preserve moment equilibrium. The product of the accelerations and the rotational inertias gives the stabilizing reaction moments to both out-of-plane and in-plane yarn rotation, as given by **Equation 4.4**. The out-of-plane moment is divided by the yarn amplitude to convert it to a reaction force F_{Si} that counteracts extension or compression of the yarn family i.

$$F_{si} = \frac{II_i^{(c)} \ddot{\beta}_i}{2A_i}$$
$$M_s = \frac{II_1^{(s)} II_2^{(s)} \ddot{\gamma}}{II_1^{(s)} + II_2^{(s)}} \tag{4.4}$$

Here the $\ddot{\beta}_i$ and $\ddot{\gamma}$ represent rotational accelerations of the crimp angles and the shear angle respectively. The forces F_{si} are added to the in-plane component of the axial yarn loads and the moment M_s is added to the moment between yarn families at the crossover points, before stresses are calculated. These inertial stabilization moments are shown acting in **Figure 4-9**.

Typically, the inertial terms are so small that many short time steps would be required for a stable analysis of a buckling transient. The yarn densities can be scaled to increase computational efficiency. As the scaling of the inertial terms is increased, the required time increment can be increased and the analysis can be performed more efficiently. An excessive increase of the mass scaling, however, will introduce errors due to large amounts of energy dissipated through stabilization. Tests on the ballistic fabric model indicate that some fabrics require no scaling, while other fabrics requires that the densities be scaled by several orders of magnitude. In all cases, acceptable time steps

were achieved while maintaining negligibly small inertial stabilization energy compared to the energy stored or dissipated through other deformation mechanisms.

It is important to note that because inertial stabilization has only been added to specific degrees of freedom, this method should allow larger inertia scaling and faster analysis with less error than "blanket" methods that add inertial terms to every degree of freedom (as in the optional automatic stabilization scheme built into ABAQUS). Also, the inertial terms added into the proposed model are physically motivated. Even in a dynamic analysis that does not suffer from buckling instabilities, these inertial terms should be included (but not scaled), as their effect would not otherwise be included in a continuum mass matrix. A continuum mass matrix describes the distribution of point masses in space, but contains no information about the orientation of rigid bodies below the continuum length scale. Therefore, a continuum mass matrix used in a dynamic analysis would include information about the distribution of the centers of mass of the yarns within the fabric plane, but no information about the yarn orientations. Because the rotational inertias of the yarns may be significant compared to the translational inertia of the fabric continuum, these terms need to be added in a dynamic analysis to obtain accurate results, even though a dynamic analysis has no need of stabilization against buckling.

4.7 Element Selection and Nonlinear Strain Gradients

Finite element solutions to boundary value problems are approximations of the actual solution—a finite element model cannot assume arbitrary deformed shapes, since the continuum is discretized into elements that can assume only shapes described by their shape functions. A finite element model must take on a deformed shape subject to these constraints and therefore tends to predict a stiffer response. The error of a finite element model depends on the mesh density and the element type. Element selection is of particular importance to the ballistic fabric model, especially in the low-stress regime of deformation. Because the interaction behavior between the two yarn families is highly

nonlinear, element types that enforce linear strain fields give incorrect results and can predict unrealistic, mesh-dependent oscillations in the predicted loads and stresses.

When the fabric is stretched along the longitudinal yarn direction without locking, there is a unique value of strain along the transverse yarn direction that allows both the interaction spring and the transverse yarns to be relaxed, so that forces and energy are minimized. If a different value of transverse strain is enforced, the interaction spring and consequently the yarns will be extended or compressed and a state of tension or compression will exist in both yarn families. The relationship between the optimal strains in the two directions is nonlinear, as shown in **Figure 4-10**, because of the nonlinear nature of the geometry.

Unfortunately, this characteristic of the fabric model behavior makes certain element types unsuitable in the presence of nonlinear strain gradients across the elements. Consider a case where a model is meshed with linear strain elements (e.g. 8-noded elements with quadratic displacement interpolation) that are subjected to non-uniform strains in one yarn direction and unconstrained in the other. The strain in the constrained direction will vary linearly across each element, since an element is capable only of linear strain variations. Because the other direction is unconstrained, the element will take on a strain field that minimizes the forces in that direction and the energy in the element. In order to truly minimize the forces and energy, a nonlinear strain variation in the unconstrained direction across the element would be necessary, since the relationship between optimal strains is nonlinear. However, the element is not capable of nonlinear strain variations. Therefore, it will adopt the linear strain variation that minimizes the energy. The mesh will be unable to truly minimize the energy and the resulting strains will lie above the optimal curve at some integration points and below it at others. This in turn means that both positive and negative transverse stresses will be present in the element. This effect is illustrated in **Figure 4-11**. Strips of 4-node and 8-node linear strain elements are subjected to a linearly varying strain field in the y-direction and left free to expand or contract in the x-direction. Even thought the strain fields are continuous and vary monotonically, the resulting stress fields display mesh-based

oscillations. **Figure 4-11** displays contour plots of the stress σ_{xx} along the unconstrained direction. The 4-node elements display a saw-tooth stress pattern, with regions of compression on the left of the elements and regions of tension on the right. The 8-node elements have undulating stress patterns, indicating regions of tension at the element edges and regions of compression at the element centers. This implies that the linear strain gradient in the x-direction lies on different sides of the optimal curve in these locations, as is shown in **Figure 4-10.** In other words, the inability of a linear strain element to capture nonlinear strain variations in at least one direction causes the element to predict stress oscillations in cases where non-uniform tensile strains are present and where the elements are not completely constrained in all directions.

Numerical studies have shown that some elements are more sensitive to this problem than others. **Figure 4-12** compares the external work required to deform the models shown in **Figure 4-11** for different element types. The models meshed with 4-noded elements have an increased mesh density to account for the lower order of the shape functions. **Figure 4-13** shows the stress patterns predicted by different element types for a tensile test. Fully integrated 4-node elements were found to be the most sensitive to this problem—the stresses take a saw-tooth pattern varying from negative to positive and they are artificially stiff. Fully integrated 8-node elements with comparable node densities behave better but still exhibited similar problems, showing undulating stress patterns that varies from positive to negative to positive at the three integration points across the element. The work required to deform these elements is greater than the estimated true work. Reduced integration elements fare better. Reduced integration 4-node elements suffer from unconstrained hour-glassing modes, but, when stabilized with hourglass stiffness control, they behave well. These elements have a single integration point and are essentially constant strain elements; therefore each element falls exactly on the optimal curve and correctly reports non-undulating, near zero transverse stresses. Unfortunately, these elements require a much finer mesh and also hourglass stiffness control. Hence these elements are excessively stiff when sufficient hourglass control is applied for stability. This is evident from **Figure 4-12**.

The 8-node reduced integration elements are the most compliant. This element type has four integration points and is a linear strain element, so it does exhibit stress undulations, in a saddle-type pattern for this load case. However, the magnitudes of these undulations tend to be smaller than those of the fully integrated elements, and the work required to deform these elements is the smallest. Note that the work needed to deform these elements is exactly the same as the work needed to deform the 4-node reduced integration elements after the work needed to overcome hourglass stiffness is subtracted. These results imply that the 8-noded reduced integration elements are the best elements to use in conjunction with the fabric model, while the 4-node reduced integration elements can be used (with a very fine mesh and with hourglass control) to investigate the stress contours in the low-stress regime.

It must be emphasized that this phenomenon is only significant at relatively small deformations and low stresses, when the fabric response is dominated by crimp interchange. At large deformations and high stresses, the effects of this phenomenon become insignificant and the different element types perform more consistently.

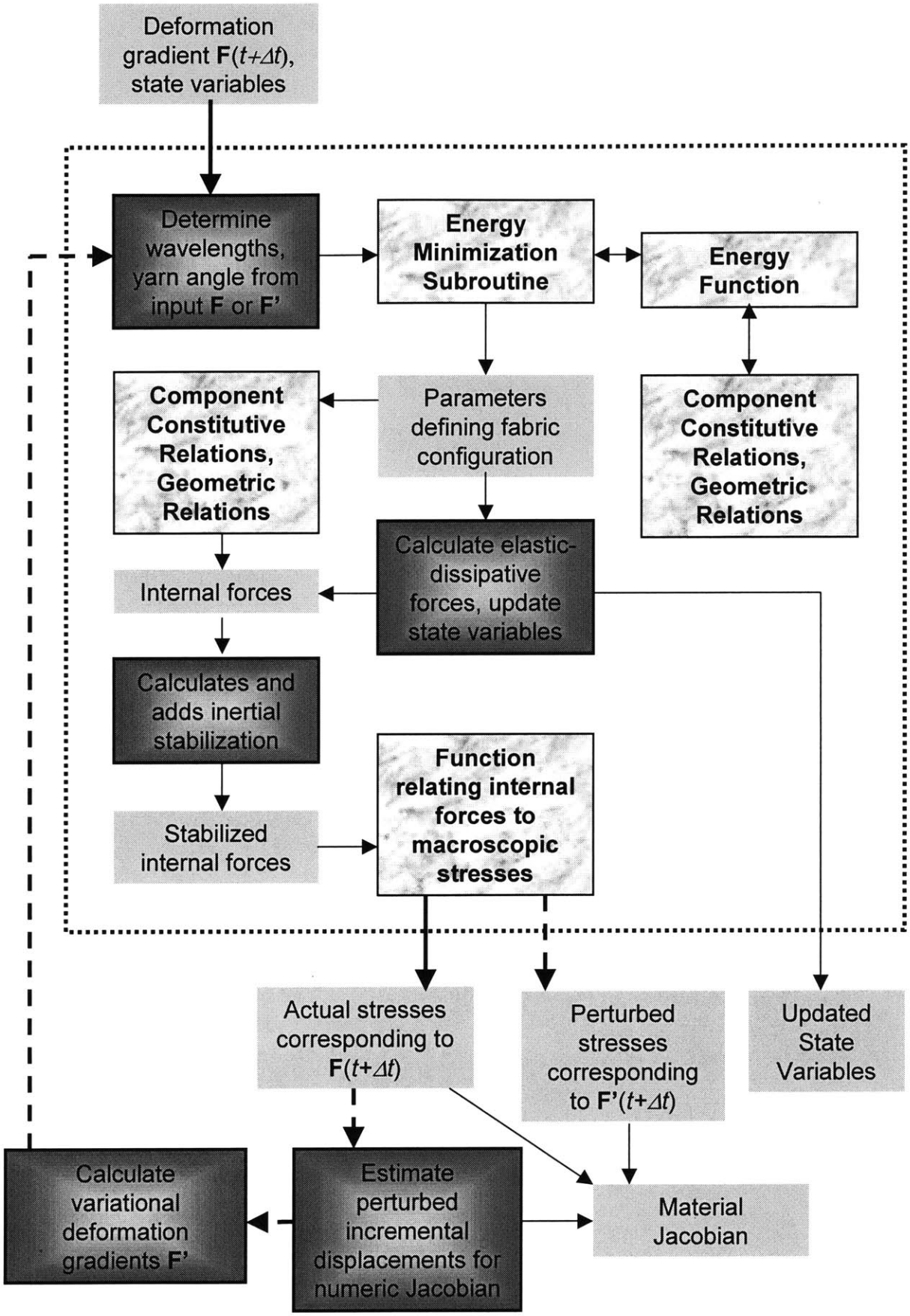


Figure 4-1 – UMAT Algorithm

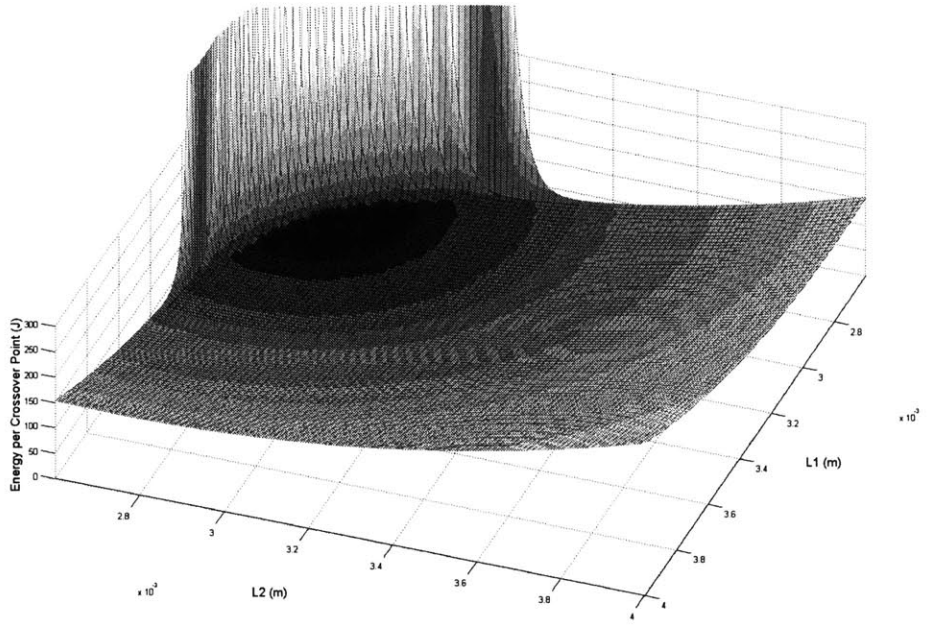


Figure 4-2 – Energy function in even biaxial extension

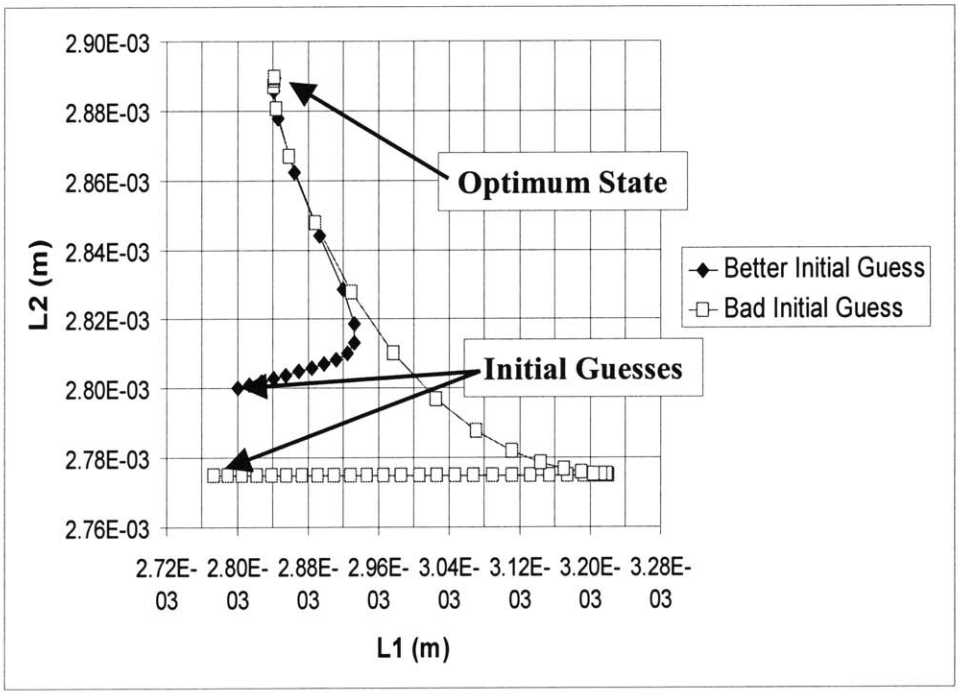


Figure 4-3 – Convergence of $\{L_1, L_2\}$ in Newton's method for different initial guesses

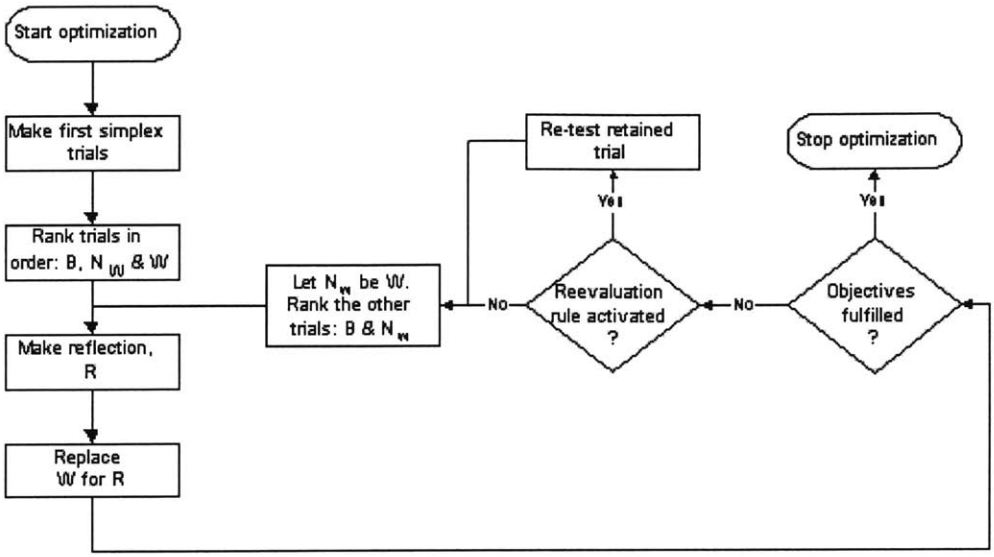


Figure 4-4 – Basic simplex algorithm (Grabitech Solutions AB)

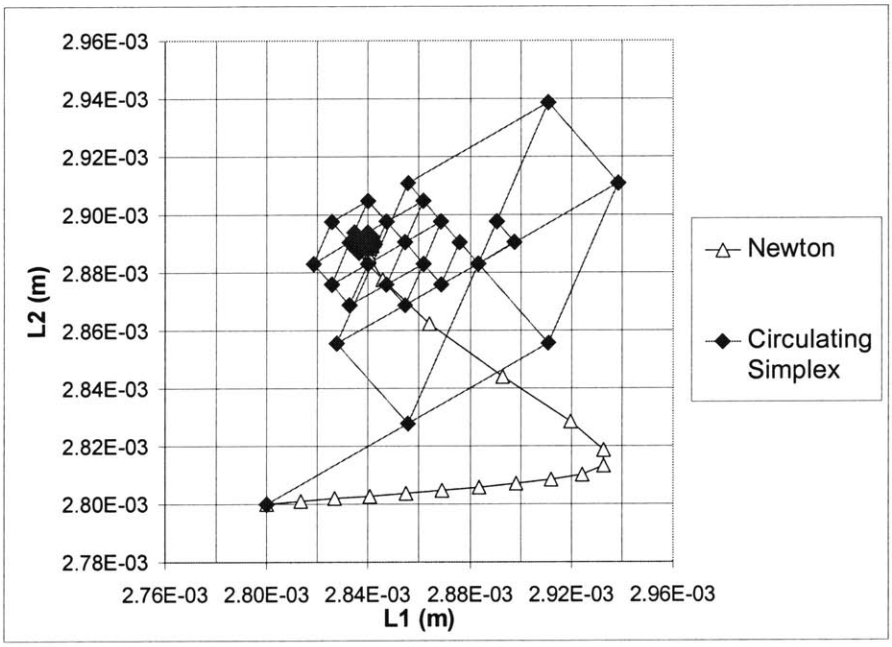


Figure 4-5 – Newton's method and circulating simplex algorithm paths for uneven biaxial extension

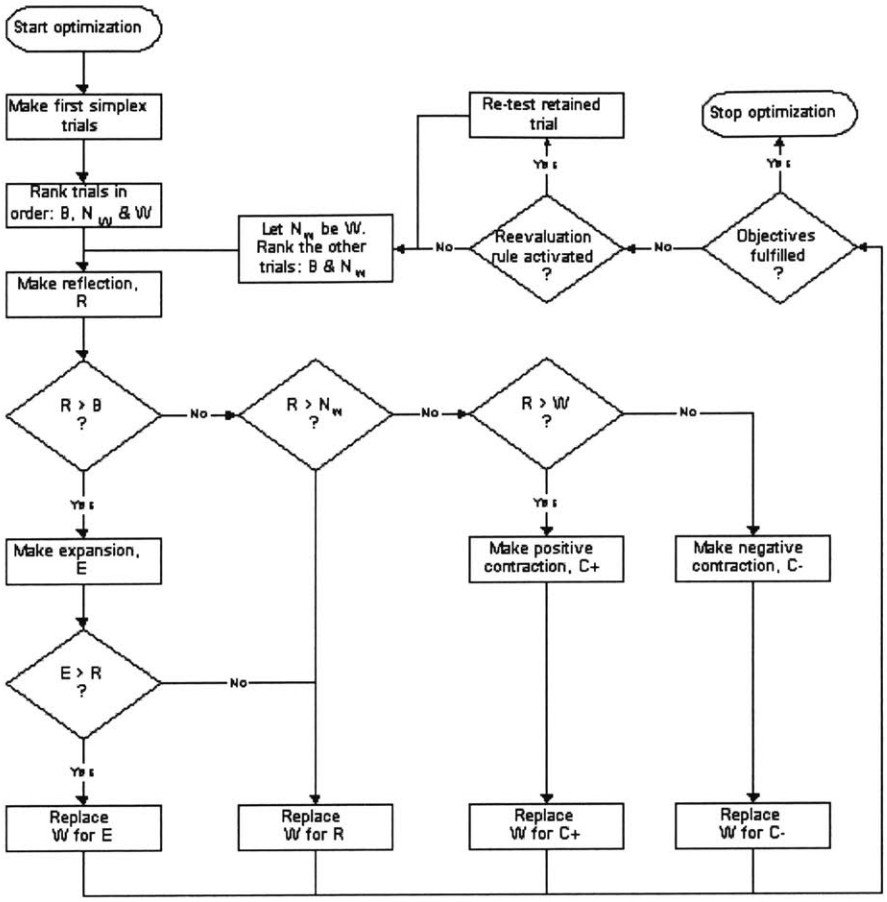


Figure 4-6 – Modified downhill simplex algorithm (Grabitech Solutions AB)

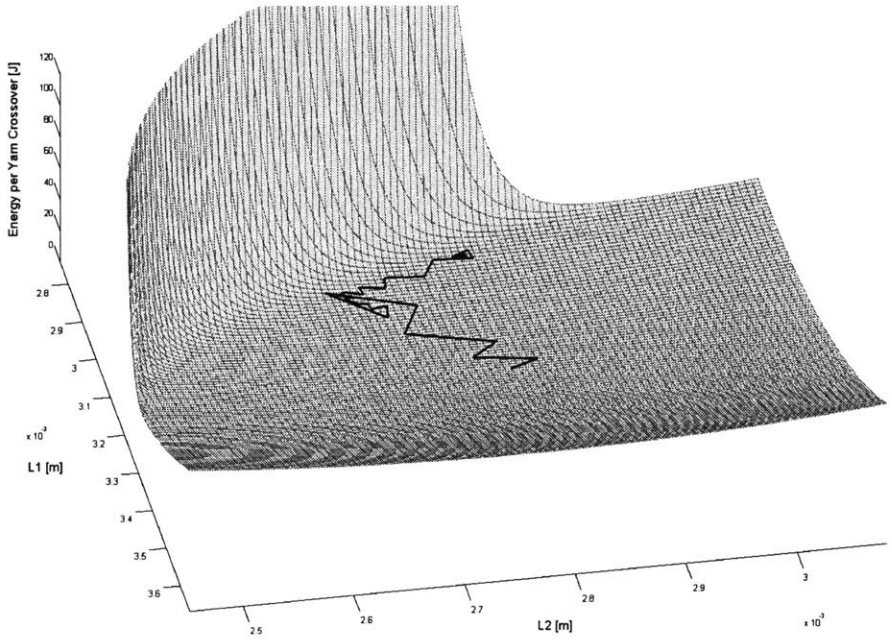
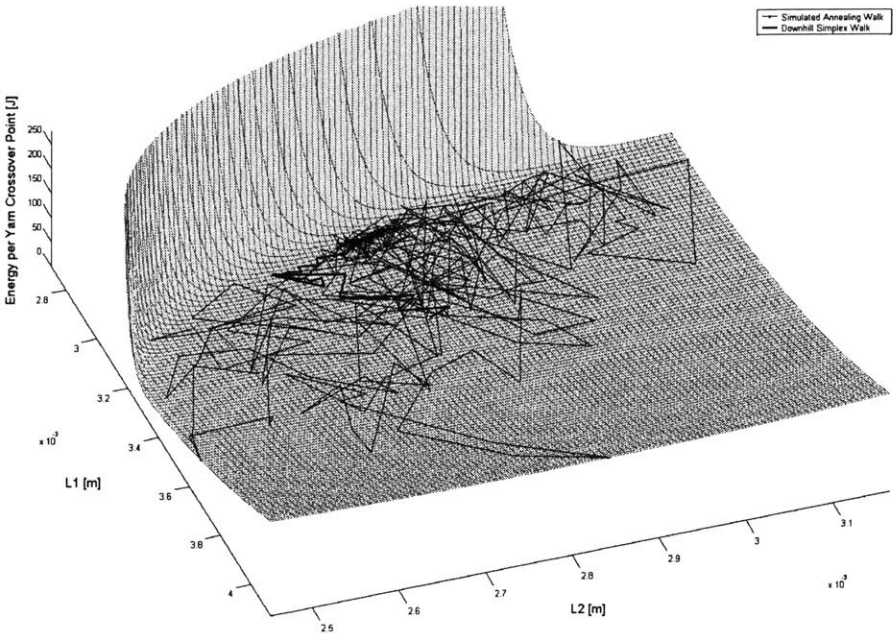
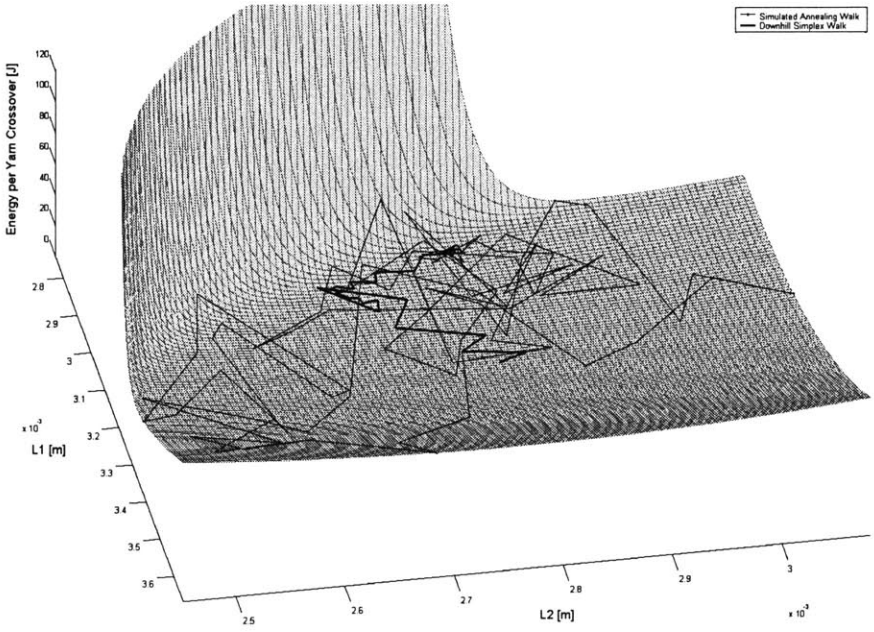


Figure 4-7 – Modified downhill simplex algorithm path for uneven biaxial extension



Slow Cooling Schedule



Fast Cooling Schedule

Figure 4-8 – Simulated annealing and modified downhill simplex algorithm paths for uneven biaxial extension

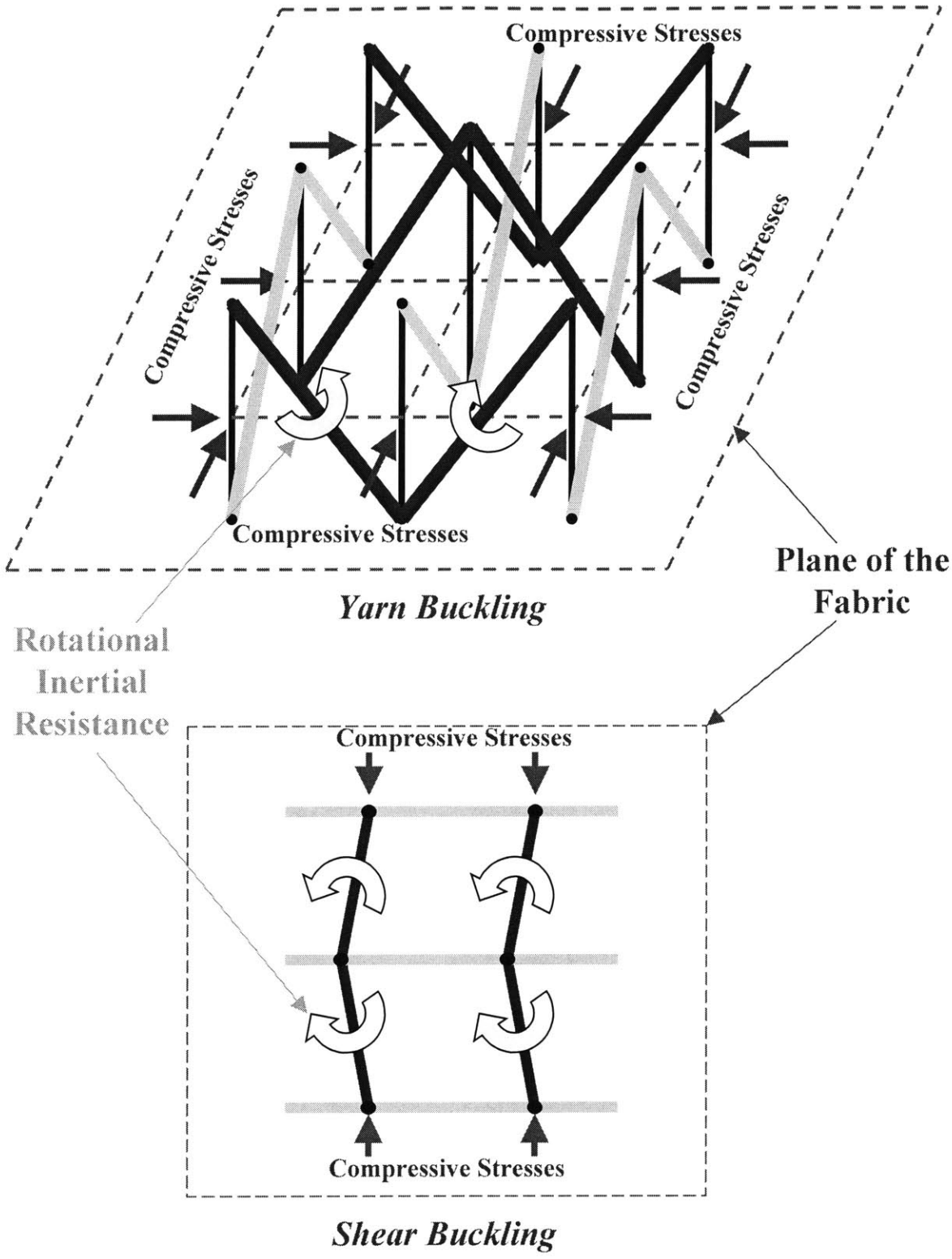


Figure 4-9 – Modes of local buckling for ballistic fabric geometry, with stabilizing inertia

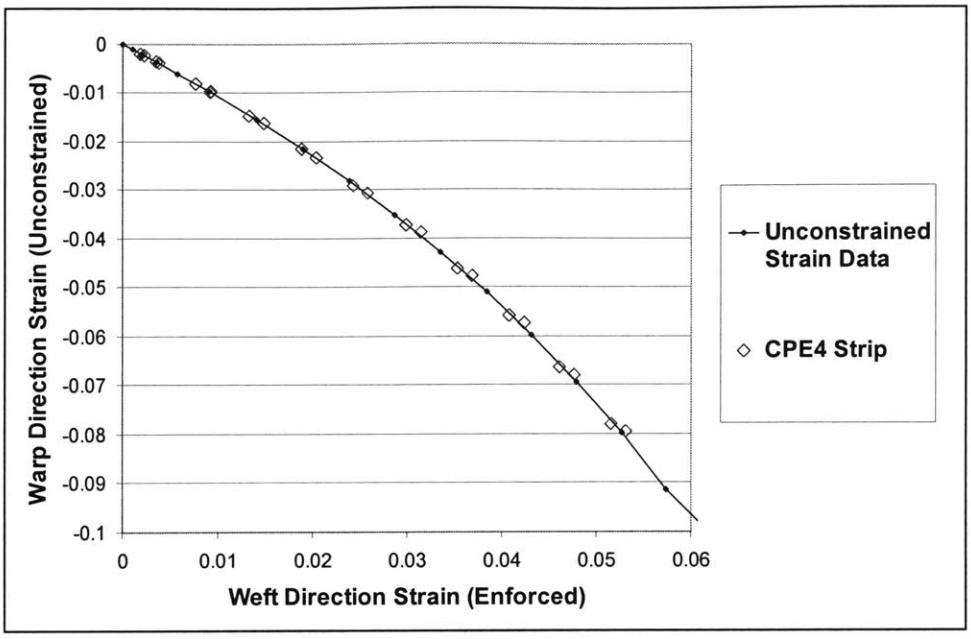


Figure 4-10 – Optimal warp strain for zero interference as a function of weft strain, with integration point strains of 4-node elements in element strip test

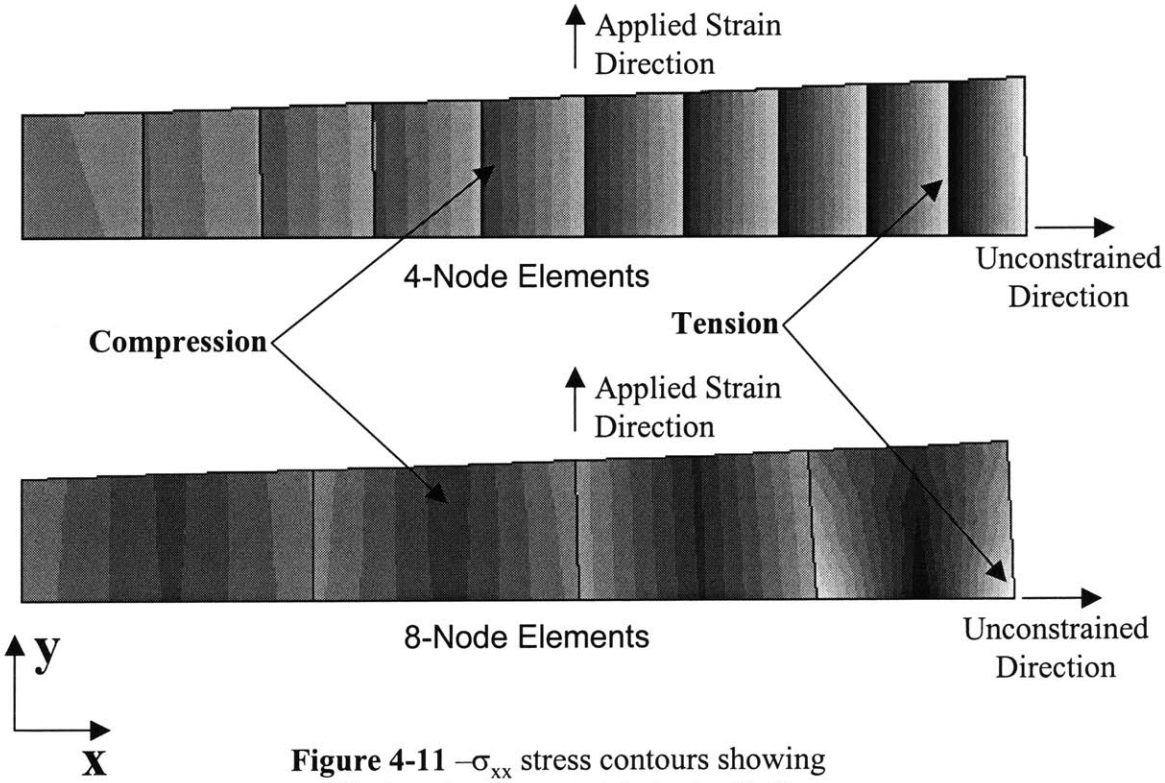


Figure 4-11 $-\sigma_{xx}$ stress contours showing oscillations in element strip test with linear strain elements

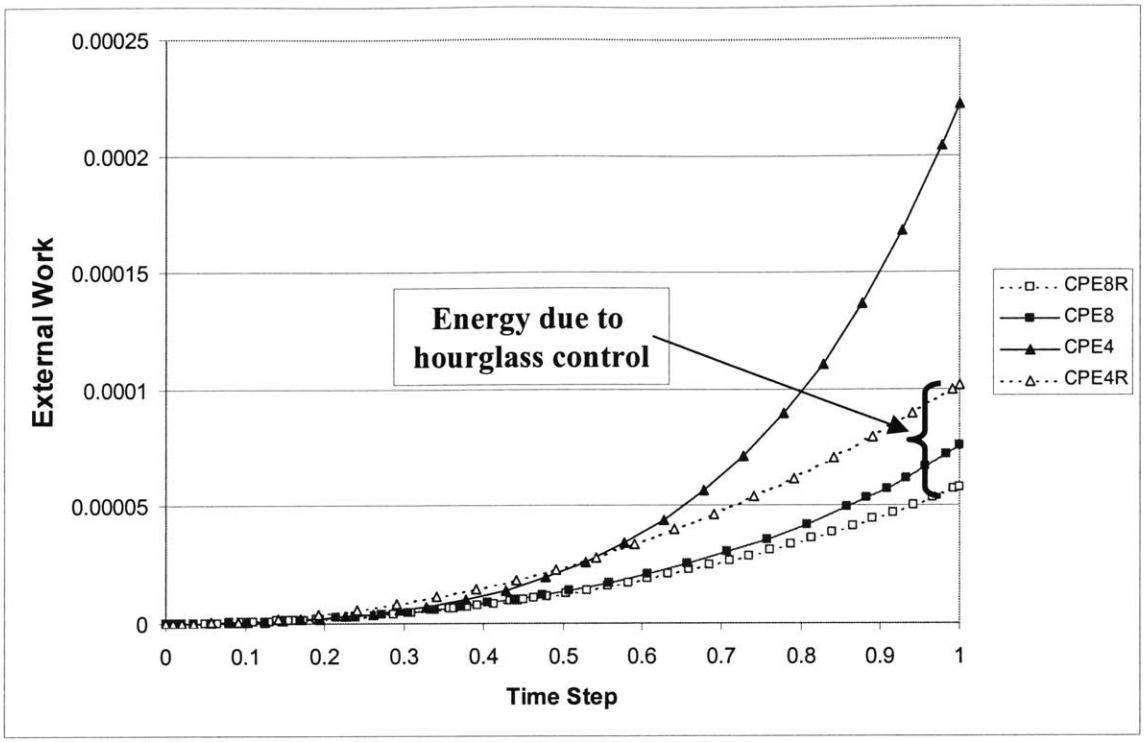


Figure 4-12 – Work required to deform element strips of different element types with equivalent meshes

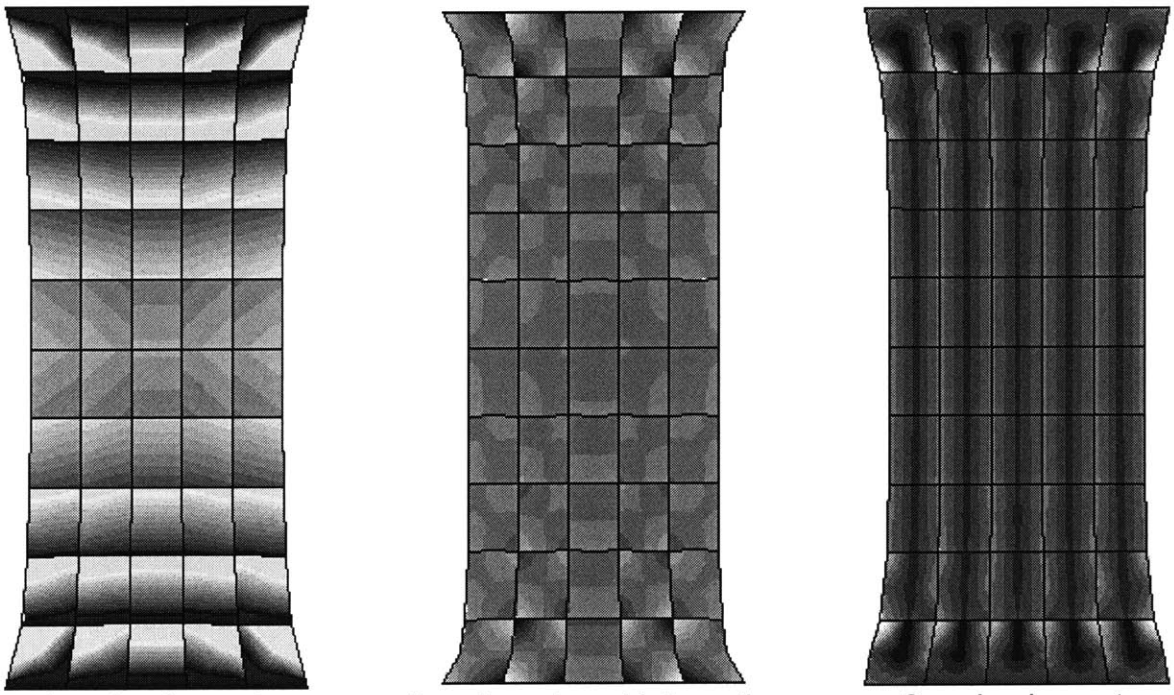


Figure 4-13 – Stress patterns in a tensile test model that appear for different element types

Chapter 5
Analysis of Boundary Value Problems

5.1 Testing the Behavior of the Model

As each different fabric behavior was implemented into the model, numerical tests were preformed to verify that the results predicted by the model were physically realistic. A real fabric typically does not exhibit mechanical responses where all the various fabric behaviors are clearly exhibited. For example, some fabrics may permit large degrees of crimp interchange and never lock, while others will lock almost immediately and permit only small amounts of crimp interchange. Testing all the different behaviors using real fabrics would require measuring the properties of a wide variety of fabrics whose responses are dominated by different behaviors. Instead, the model was initially tested using "dummy" fabric materials. These dummy materials had stiffnesses similar to ballistic fabrics, but their geometric parameters were chosen so that specific behaviors would dominate their response. Use of these dummy materials facilitated the development of the model, and demonstrated its ability to realistically capture each behavior, before the model was applied to the analysis of a real fabric.

Two different dummy fabrics were considered. Their properties are summarized in **Table 5:1**. Both of these materials were balanced, plain weave fabrics woven from yarns with circular cross sections. The yarn stiffnesses are roughly those of Kevlar yarns. However, the dimensions of the weave (wavelength, yarn radii, crimp amplitude, etc.) are one order of magnitude larger those that of real Kevlar fabric in order to amplify the effects of specific fabric behaviors, particularly locking and crimp interchange. One of the two fabrics, designated as "locking", represents a very tight weave that locks at very

low with levels of deformation with or without shear; its primary stiffening mechanism is locking. The other, designated as "non-locking", has a larger wavelength and represents a very loose weave that only locks at large shear angles; its primary stiffening mechanism is yarn stretching after the yarns straighten.

Figure 5-1 describes a numerical experiment designed to investigate the model's ability to realistically capture crimp interchange. A single element, composed of the non-locking fabric and oriented with the yarn families aligned with element axes, is subjected to uniform biaxial stress until the load reaches a preset limit. This load is then held constant on the weft yarns while the fabric is extended in the warp direction. The model predicts that the element contracts in the weft direction as it expands in the warp direction, exhibiting crimp interchange. The initial slope of the warp direction stress-strain curve is strongly dependent on the load maintained on the weft yarns, which is also evidence of crimp interchange. At larger weft loads the warp response is stiffer. This behavior is physically realistic and consistent with fabric behavior described in the literature. Regardless of the weft load, as the yarns straighten the slope of the warp stress-strain curve tends towards a constant value—the modulus of the yarns—and the model ceases to contract in the weft direction. This indicates that at this point the warp yarns have completely straightened and crimp interchange ceases to occur. This experiment demonstrates the model's ability to capture crimp interchange.

A similar experiment, shown in **Figure 5-2**, shows that the model can realistically capture locking. In this experiment, the tight weave material is used. In a first simulation, the routines that evaluate the contribution of locking to the fabric response are disabled. The resulting warp stress-strain curve is similar in shape to the curves in **Figure 5-1**—it is initially compliant as crimp interchange occurs but its slope approaches the yarn modulus as the yarns straighten and crimp interchange ceases. When the locking subroutines are enabled, the model behavior changes. Initially crimp interchange is allowed to occur and the behavior is not affected, but after the onset of locking, crimp interchange is arrested and the warp stress-strain curve turns up sharply and rapidly approaches a slope close to the value corresponding to the modulus of the yarns. The

results of this numerical experiment demonstrate that the model can effectively capture locking as well as crimp interchange

Additional single element trials were performed to examine the model shear response. These trials verified the ability of the model to track yarn directionality and capture rate-dependent shear behavior. **Section 5.3** discusses the model shear response in more detail by describing model predictions of a bias-extension test on a real ballistic fabric.

After the material model was verified under carefully controlled loading conditions on a single element, its response to more complex loading conditions in multi-element simulations was tested. A model was built to simulate a tensile-test of a fabric strip in the warp yarn direction, with clamped ends. The boundary conditions in this test result in non-homogeneous loading conditions with non-uniform tensile strains and stress gradients. The response of the fabric strip is affected by the yarn orientations, crimp interchange, locking, and the model shear behavior. **Figure 5-3** shows the stress contours predicted for the locking fabric. The deformed plot realistically agrees with typical patterns of fabric deformation, exhibiting contraction in the center of the strip that results from crimp interchange. The areas of highest stress are at the edges, where the yarns experience the largest elongations. The corresponding average macroscopic nominal stress-strain curve in **Figure 5-4** shows a very small increase in stress initially as crimp interchange permits large deformations. At the point where the fabric begins to lock the curve rapidly turns upwards and its slope approaches a value controlled by the tensile modulus of the yarns. This behavior qualitatively agrees with data trends measured from actual fabrics.

These tests establish that the model is capable of capturing yarn directionality, crimp interchange, rate-dependent shear, and locking in a physically realistic manner. They demonstrate that the model can be used for both carefully controlled single-element simulations and for more practical multi-element simulations that represent actual structures with realistic loading conditions.

5.2 Measuring the Fabric Properties

The ballistic fabric model is used to simulate the behavior of DuPont's S706 Kevlar™ ballistic fabric. The accuracy of the model is evaluated by comparing its predictions to tests performed on actual S706 samples. Both crimp interchange and locking affect the behavior of this fabric. Though its two yarn families are composed of the same material and have the same denier (cross sectional area), the weave parameters, specifically the crimp amplitudes, are different in the two directions. This implies that the mechanical response measured in each direction will be different and will involve different stiffening mechanisms—locking and yarn straightening—in different degrees. S706 is therefore an effective material for testing a wide variety of fabric behaviors.

5.2.1 List of Model Parameters

The linear ballistic fabric model requires twenty-three material parameters that describe the weave parameters of the fabric and the material constants of the component constitutive relations. These parameters, their dimensionalities, and the aspects of the model that they affect are summarized below.

- r_1, r_2 Minor (through-thickness) radii of the yarn families, which affect crimp interchange and locking [length]
- R_1, R_2 Major (in-plane) radii of the yarn families, which only affect locking [length]
- ρ_1, ρ_2 Mass densities of the yarns, used only for inertial stabilization [mass/length^3]
- ${}^0p_1, {}^0p_2$ Initial quarter-wavelengths of the yarn families, used to determine initial fabric configuration [length]
- θ_1, θ_2 Initial orientations of the yarn families relative to the model x-axis, which determine the initial yarn angle and initial orientation of the weave at a given location [radians]
- ${}^0L_1$ Initial yarn length per quarter wavelength in the warp direction, used to determine the initial configuration of the fabric [length]. This parameter, the two initial

wavelengths, and the minor radii completely determine the initial yarn length in the weft direction and both the initial crimp amplitudes and crimp angles, using the assumptions of zero initial interference and yarn stretch

- k_1, k_2 Axial yarn stiffnesses per unit length, which describe the extensile behavior of the yarns of each family [force]. Ideally these values should be equal to EA, the product of the moduli of the respective yarns and their cross sectional areas.
- K_I, a_I Parameters describing the exponential interference relationship between yarns at the crossover points [force, length^{-1}]
- K_L, a Parameters describing the power law locking interference relationship [force/length^a, dimensionless]
- k_{b1}, k_{b2} Stiffnesses of the torsional springs describing the bending behavior of the yarns at the crossover points [moment/radian]
- K_S Stiffness of the torsional spring describing the elastic resistance to yarn rotation at the crossover points [moment/radian]. This represents the response to elastic "s-bending" of the yarns between crossover points.
- $\dot{\gamma}_0$ M_0, b Parameters describing the rate-dependent power law that governs dissipative shear rotation [radians/time, moment, dimensionless]. M_0 is a strength parameter that determines the moment required to generate dissipative yarn rotations at rate $\dot{\gamma}_0$. b is a rate sensitivity exponent.

As many as possible of these twenty-three parameters were measured or estimated from tests on the S706 ballistic fabric and its yarns. The model's predictive capabilities are evaluated by comparing the fabric experimental responses to the model predictions for behaviors that are dominated by the measurable properties. Some of the properties, notably the locking and rate-dependent shear parameters, could not be measured directly as the necessary specialized equipment was not yet available at the time of this study. Consequently, the predictive capability of the model for behaviors influenced by these parameters cannot be evaluated at this time. However, the model's effectiveness as a simulation tool is evaluated by fitting the model predictions to measured fabric behavior.

The properties are of two types: geometric properties that can be measured directly from samples of the woven fabric, and component constitutive parameters that can be measured from mechanical tests on the fabric or its component yarns.

5.2.2 Geometric Parameters

The quarter wavelengths are easily measured directly from the fabric. The quarter wavelength of a yarn family is determined by counting the number of yarns that cross that family per unit length. This number is inverted to give the length per crossing yarn, and then divided by two, since one yarn crosses every half wavelength rather than every quarter-wavelength. S706 has 34 yarns per inch in both directions, which results in equal quarter wavelengths of 0.3735 mm.

The radii, initial crimp amplitudes, and initial yarn lengths, which have a significant effect on the crimp interchange and locking, are more difficult to measure. **Figure 5-5** shows micrographs of a cross section of the S706 weave, perpendicular to the warp and weft directions. These micrographs were created by embedding a fabric sample in epoxy, sectioning the sample, and imaging it in an optical microscope. It is tempting to measure the geometric parameters of the weave such as the major and minor yarn radii, the yarn amplitudes, the crimp angles, and yarn lengths directly from such micrographs. However, the exact plane at which the fabric is sectioned is difficult to control precisely, and the angle and position of the sectioning plane affects the appearance of the cross section. Only a section plane that cuts through the crossover points exactly orthogonal to both the plane of the fabric and the yarn directions will reflect the true crimp amplitudes and angles. Small inclinations of the sectioning plane will alter the appearance of both the amplitudes and minor yarn radii in the section images. The micrographs remain a valuable qualitative tool for selecting appropriate fabric geometries for the model, but cannot be used to measure the fabric geometric properties directly without precise control of the sectioning method.

The remaining geometric properties are determined as follows. The yarn lengths are estimated by marking off a distance on the fabric parallel to the yarn direction, then pulling the yarns from the fabric, straightening them, and measuring the new distance between marks. As long as the assumption of negligible wrapping is valid, the ratio of the two distances will equal the ratio of the yarn length L to the quarter wavelength p.

Once the yarn lengths and wavelengths are known, the amplitudes and crimp angles can be calculated using **Equation 3.1** and **3.2**. Geometric constraints require that the sum of the minor radii, less any interference (which is assumed to initially be zero) must equal the sum of the amplitudes of the two yarn families. The minor radii can therefore be calculated by assuming that they will be approximately equal for the two yarn families, since the two yarn families have equal deniers and similar weaves. Tthis is equivalent to assuming that the two yarn families have the same initial shape as well as the same cross sectional area. The data indicates that the warp crimp amplitude is initially smaller than the weft crimp amplitude, and therefore more crimp interchange and larger strains before stiffening are expected when the fabric is pulled in the weft direction. The difference in crimp amplitudes is also qualitatively suggested by the micrographs in **Figure 5-5**; the warp yarns appear to be straighter.

The major radii are difficult to measure without using the micrographs. Since the yarn denier (cross sectional area) is specified (as the sum of the deniers of the component fibers) and the minor radii are known, the major radii can theoretically be calculated if the cross sections are assumed to be elliptical. However, the micrographs shown in **Figure 5-5** indicate that the actual yarn cross section lies between elliptical and diamond-shaped. In other words, the yarn widths calculated assuming elliptical yarns would underestimate the actual yarn widths. The major radii affect only the locking behavior of the fabric, which is also controlled by the locking relation. Since the locking relation is also difficult to measure directly, the major radii are considered "fitting parameters", selected so as to match the experimental fabric behavior.

The mass densities ρ_i are used only for the inertial stabilization calculations. The density specified in literature for Kevlar, 1441 kg/m^3, is used.

The yarn family angles θ_i determine both the initial angle between yarn families and the initial orientation of the fabric. Note that angles differing by 180° are equivalent. S706, like many woven fabrics, has an orthogonal weave, so the angle between θ_1 and θ_2 is

$\pi/2$ (90°), meaning that $\theta_2 = \theta_1 + \pi/2$. θ_1 is prescribed at each location to reflect the appropriate initial orientation of the fabric in a given analysis.

5.2.3 Component Constitutive Parameters

The most important component constitutive parameters for a ballistic fabric model are the yarn stiffnesses, since the tensile behavior of the yarns dominates the high stress fabric response. Tensile tests were performed on single yarns [Jearanaisilawong, 2003], with the resulting stress-strain curves shown in **Figure 3-3**. The tests indicate an initially compliant response that tends towards a constant modulus under large loads, until failure begins. However, tests performed at different strain rates ($\dot{\varepsilon} = 0.001$ s^{-1} and $\dot{\varepsilon} = 0.01$ s^{-1}) produced different estimates for the yarn moduli, even though the literature data implies that, at these relatively low strain rates, the effect of rate dependence on the mechanical response of Kevlar should be negligibly small. One possible explanation is that rate-dependent slippage occurred at the grips in the single yarn tests; therefore, improved methods of gripping single yarns are being explored. These methods will allow more accurate measurements of the yarn stiffnesses. The current model uses the data measured from the low-rate ($\dot{\varepsilon} = 0.001$ s^{-1}) single-yarn tests, which indicate that the weft yarns are less stiff than the warp yarns. Data in the literature confirms that this is often the case, due to increased damage experienced by the weft yarns during the weaving process. However, given the uncertainties regarding the testing methods, especially the possibility of yarn slip, these stiffness values may underestimate the actual yarn stiffnesses.

The interference parameters are extremely difficult to measure, because they involve one-sided compressive interactions between yarns subjected to very specific boundary conditions. One simple test devised to investigate this phenomenon involves placing fabric coupons between rigid plates and performing a compression test, as discussed in **Section 3.3.3**. The results of such a test are shown in **Figure 3-4**. Experimental data is reduced to give the force per crossover point as a function of the compressive

displacement at each crossover point. Since interference is a compressive phenomenon, the response measured through this macroscopic compression test and the actual interference response should have a similar forms. Of course, in this test the yarns are subjected to compressive loads from both sides, so the boundary conditions do no precisely reproduce the yarn interference configuration. Therefore, the results of this test will not give a quantitatively accurate interference relation. More accurate test might be performed with the use of a biaxial tensile testing machine.

When an exponential fit to the data in **Figure 3-4** is performed to determine K_I and a_I, the response predicted by the model is too compliant to match the fabric behavior under tensile loading. The excessive compliance determined by the compressive test is probably due to the many alternative modes of deformation available to a fabric woven from multi-fiber yarns to accommodate out-of-plane compression. Therefore, a much stiffer response, achieved by increasing the value of the interference exponent a_I by an order of magnitude, is used in the model. This larger value of a_I might overestimate rather than underestimate the compressive stiffness at the crossover points, and consequently predict smaller out-of-plane displacements of the crossover points. However, since the yarns in S706 have a fairly small minor radius relative to other structural dimensions such as wavelength and yarn length, and since the yarns are already significantly compacted in the undeformed state, their response to compression at the crossover points is very stiff, and out-of-plane displacements due to that compression tend to be negligibly small compared to the in-plane deformations. Therefore, an artificially stiff interference model will predict the macroscopic deformation behavior of the fabric more accurately than one that is too compliant.

The compressive data from **Figure 3-4** may be more appropriate to predicting the locking constitutive relation. Locking is a compressive phenomenon as well, and tends to be more compliant than interference at the crossover points, as the multifiber yarns tend to deform and compact as their fibers are forced to fill the available space. Since locking is also a difficult phenomenon to measure at the structural level, and since accuracy will be lost due to geometric assumptions of ellipticity, the locking parameters K_L and a are

estimated from the data from the sandwich compression test. Here a piecewise power law-linear relation is assumed, which fits the measured trend better than an exponential relation.

The bending stiffnesses can be determined from the low-stress portion of the single yarn tests, as the yarns straighten before they begin to stretch. The amplitude and crimp angle of the crimped yarns can be calculated knowing the current wavelength (from the extension) and the yarn length. If both the amplitude and the total force on the yarn are known, the moment at the peaks and troughs can be determined. Therefore, a moment-crimp angle plot can be generated and the effective bending stiffnesses of the yarns can be measured. Because of the current uncertainties regarding the single yarn tests, this calculation has not been performed. Yarn bending has a very small effect on the in-plane deformation of the fabric in the high stress regime of interest for ballistic analysis and is included primarily for stability. If bending stiffnesses are chosen to be too small, then small deformations of the fabric in the low stress regime would have negligibly small strain energies associated with them, since resistance to deformation in this regime is dominated by yarn bending during crimp interchange. This results in a numerically unstable model. The minimum bending stiffnesses that provide adequate stability are therefore used. If the low stress behavior is important for a specific analysis, more exact values for the yarn bending stiffnesses can be determined using the procedure outlined above.

The remaining parameters are those that control the shear response of the fabric prior to locking. These parameters can be measured through a series of carefully controlled shear-frame experiments at different strain rates. Currently no shear frame data is available, so the models capacity to predict fabric shear response from measured shear properties has not yet been tested. The shear properties are therefore "fitting parameters" in the model, chosen so as to fit the measured response of a fabric tested in bias-extension, since this test configuration involves large yarn rotations.

The material parameters for the S706 Kevlar model are summarized in **Table 5:2**. Properties that were accurately measured directly from the fabric or from experiments performed on the yarns are listed with white backgrounds. "Fitting parameters"—properties that were difficult to measure directly, but were instead chosen to fit the fabric simulation responses to experimental data—are listed with grey backgrounds.

5.3 Experimental Comparison of Macroscopic Behavior

S706 fabric was tested in three different modes of deformation—uniaxial extension with clamped ends in both the warp and weft direction, and bias extension at a 45° offset. These tests were simulated using the ballistic fabric model implemented into ABAQUS and the simulation results were compared to the experimental results.

The tensile tests in the direction of the warp and weft yarns were performed with a specimen aspect ratio of approximately 10:1, to minimize the effect of the clamped boundary conditions. The results of these tests are shown in **Figures 5-6** through **5-8**. **Figure 5-6** shows photographs of a warp direction tensile sample under no load and in the high stress regime just prior to failure at 4% nominal axial strain. These photographs show the contraction of the fabric due to crimp interchange. **Figure 5-6** also shows plots of the deformed configuration predicted by the model, with contours showing the warp and weft direction stresses. The model prediction of transverse contraction due to crimp interchange is in good agreement with the experimental measurements. The model predicts that, at 4% axial strain, the strip will undergo a 4.5% contraction in the transverse direction at the center of the strip, as compared with a 4.0% contraction observed in experiments. This slight difference may be due to the excessive stiffness of the relation describing compression at the crossover points. The model predicts large stress gradients and a region of transverse tension at the clamped ends, where contraction is constrained. In the center of the strip transverse stress is negligibly small and axial stresses are large and fairly uniform. The largest stresses are at the edges of the strip. These predictions qualitatively agree with the observed experimental behavior, where

yarn failure initiates at the outer edge of the strip. In this case, where little locking or yarn rotation occurs and bending stresses are negligibly small, the yarn tensions are almost directly proportional to the warp and weft-direction stresses.

Plots of the weft direction tests are not shown, as they are very similar in character to those of the warp direction tests. The chief difference is that the strip tested in the weft direction undergoes greater contraction due to crimp interchange, because the weft yarns have larger initial crimp amplitudes and are therefore capable of more crimp interchange before the yarns straighten or lock. The model predicts that the weft direction yarn strip will undergo a 5.8% contraction at 4% axial strain, while a 5.9% contraction was observed in experiments. The quantitative contractions of both the warp and weft strips are therefore well predicted by the model.

Figure 5-7 shows the load-extension curves from warp-direction tensile tests, compared with the model prediction. There is good correlation between the experimental results and the simulation prediction up until failure, which is not included in the model. However, the model can be used to predict failure if the failure loads for the yarns are known, as discussed in **Section 5.4**. The model indicates that, because the warp amplitude is initially so small, very little locking occurs before the yarns straighten and the response is dominated first by crimp interchange, and then by the yarn compliance after the yarns straighten. The parameters that affect these behaviors—initial wavelengths, amplitudes, and yarn stiffness—were all directly measured. The fact that the predicted curve agrees so closely with the experimental curves indicates that the model can effectively predict the behavior of a fabric in cases where the response is dominated by these effects.

Figure 5-8 compares the load-displacement curve predicted by the simulation to the experimental curves for the weft direction pull. The agreement here is less satisfactory—the curve turns up at the correct displacement, but does so at too slow a rate and approaches a different final slope. The difference in the rate at which the curves turn is due to inaccuracies in the manner the model captures the locking phenomenon. Because

the initial weft amplitude is larger than the initial warp amplitude, more crimp interchange occurs in the weft-direction tensile test, and larger strains are possible before stiffening. This is exhibited by both the experimental and the simulation data. However, in the weft-direction test, the weft yarns actually begin to lock before they completely straighten, while in the warp-direction test the warp yarns straighten almost immediately. Hence, in the weft-direction test, locking rather than yarn straightening controls when and how the curve turns upwards. The macroscopic response is not precisely predicted in the area where locking dominates, because the locking relation in the model is somewhat simplified, and the locking parameters cannot be chosen to precisely fit both the bias-extension test data and the weft-direction test data. The discrepancy between the slopes of the experimental and simulation curves at high elongation is a consequence of the constitutive parameters selected for the stiffness of the weft yarns, which may be inaccurate due to uncertainties concerning the single yarn tests, as discussed in **Section 5.2.** Additional tests need to be conducted on the yarns to determine more accurate material properties to use in the model.

The third test was a bias-extension strip tensile test. A strip of fabric was cut so that the warp and weft yarns were oriented at 45° angles to the loading direction. The strip, which had a considerably smaller aspect ratio (about 3:1), was then subjected to a tensile test, which induced large amounts of yarn rotation as the yarns attempted to realign with the direction of load. The strip was constrained to remain planar by sandwiching it between transparent plates. This test was intended to investigate the shear behavior of the fabric model, since the bias-extension process is dominated by yarn rotation. This shear behavior could not be measured prior to the experiment without specialized equipment, so these experiments were used to verify that the model could serve as simulation tool and that the model predictions could be fit to the experimental data. Though the shear behavior may be rate dependent, these tests were only performed at a single rate—0.01 s^{-1}—and rate-dependence effects were not investigated.

Figure 5-9 shows photographs of the bias extension strip both undeformed and at 17% nominal axial strain, and compares it to the deformation predicted by the model at the

same extension. Two samples are shown—one has been marked with lines corresponding to a rectangular mesh aligned with the loading direction, while the other has been marked with lines showing the yarn orientations. Note that all plots are at the same scale. The deformed shape and amount of yarn rotation predicted by the model are shown both with a fringe plot and with a vector plot that shows the orientations of the yarns in the deformed configuration. Again, there is very good qualitative and quantitative agreement between the model and the experiments. The model predicts deformation patterns that are nearly identical to those observed experimentally, including triangular areas at each end of the strip where the stress, strain, and yarn rotation are all very small, bounded by areas of higher stress and large strain gradients. These triangles are flanked by triangles of intermediate stress and strain, and beyond these triangles the center of the strip undergoes approximately uniform strain, with stresses largest near the sides of the strip. The points where the largest stresses and most dramatic strain gradients appear are the vertices of the end triangles. The amount of contraction at various points along the strip is also well predicted by the model. The model predicts the physical response, which indicates that it correctly captures effects of yarn directionality and stress transfer.

Figure 5-10 shows the load-extension curves from the bias-extension tests, compared to the best fit of the model data, in both the low stress and the high stress regime. Here again there is reasonably good agreement between the simulation predictions and the experimental data, though fitting the model parameters facilitates this agreement. The lack of experimental data isolating the locking and shear behavior of the yarns prevents direct evaluation of the model's predictive capacity for this complex history of deformation. In the low stress regime, the load response can be matched by varying the reference shear strain rate or the reference moment (the "strength parameter"). Stiffening in this region is dominated by the elastic shear stiffness. Some stiffening also occurs because yarn rotation becomes less efficient in permitting bias extension as the shear angle increases; this stiffening is well captured by the model. The axial load dramatically increases when the fabric begins to lock. By adjusting the major radius of the yarns, the shear strain at which the modeled fabric locks can be matched to the strain at which the

actual fabric locks, though the behavior during the onset of locking varies because of approximations in the locking relation. The major radii that resulted from this fit are about 85% of the quarter wavelengths, greater than the radii calculated from the elliptical yarn assumption, but less than those calculated from the diamond-shaped yarn assumption, which is in good agreement with the micrograph in **Figure 5-5** where the actual yarn cross section lies between these two shapes. The apparent major radii in **Figure 5-5** are also approximately 85% of the quarter wavelengths. Therefore, the major radii required to fit the experimental behaviors are within reasonable bounds.

The ultimate stiffness is dominated by two factors—the yarn stiffnesses, which can be precisely measured and should not be adjusted, and the locking stiffness relation, which is a function of shear angle. Adjusting the parameters affecting locking allows this final stiffness to be well matched to the experimental stiffness, though matching both the strain at which the model begins to lock and the final stiffness is difficult, again due to simplifications in the locking model. This experimental data implies that a better locking model is necessary in order to accurately capture large-strain shear behavior.

The results of these tests show that, while the model still requires some refinement, it can capture the experimentally measured low-rate behavior of a ballistic fabric with good agreement. The model qualitatively predicts all the responses exhibited by the fabric during the experiments, capturing key behaviors such as yarn directionality and crimp interchange. When fabric parameters can be accurately measured, the model quantitatively predicts fabric behavior that depends on these parameters very well. Behaviors that are influenced by parameters that cannot be accurately measured can still be well simulated by fitting the model parameters to experimental data, indicating that the model is an effective simulation tool. The discrepancies between the experimental data and the model predictions were largest for behaviors affected by locking, and suggest the need for a more accurate description of locking within the model, especially in shear. This improvement can be implemented in future versions of the model. The good agreement between model and experiment validates both this specific model and the

modeling approach that was used to develop it as a continuum tool for capturing the macroscopic behavior of a woven fabric.

5.4 Predicting the Response of the Fabric Structure

The objective of this work is to provide a method for developing continuum models that can both simulate the macroscopic response of a fabric to applied loads and predict the response of the fabric structure to macroscopic deformation, tracking the behavior of the yarns at the structural level. **Section 5.3** demonstrates that the ballistic fabric model can effectively simulate macroscopic fabric behavior. This section will discuss the model's capabilities for tracking the fabric structural response and how these structural responses can be used to predict failure.

There are a wide variety of structural-level variables that may be of interest in an engineering analysis. These variables are of two types. The first type of variables relates to the configuration of the fabric geometry. Examples include yarn wavelength and yarn angle, which together determine the areal density and the size and shape of the gaps between yarns in the deformed configuration. These factors may be relevant if the fabric is being used to contain a fluid or protect against contaminants. Crimp angle and yarn extension both relate to the manner in which the yarns are being deformed, and the magnitude of that deformation. These variables may be of interest in cases where micro-components, such as microelectronics or microfluidic devices, are woven into the yarns, or even embedded within the yarn fibers. The second type of variable contains information regarding the loads carried by yarns and the forces acting between yarns at the structural level. Examples include the yarn tensions, which are required to predict yarn failure. Other examples include the contact forces between the yarns, both at the crossover points and where the yarns jam against one another during locking. These contact forces will affect the friction forces between yarns and therefore are relevant to failure modes that involve yarn pullout. They also may cause failure of micro-components that can only be subjected to limited transverse loads.

All of these variables are either directly tracked by the model (if they are required for the calculation of the stresses) or can be readily calculated from the model parameters. **Figure 5-11** shows contour plots of contact forces between yarns at the crossover points for two different modes of loading—warp direction pull and bias extension. In the warp pull test the only areas where contact forces are large lies near the grips, since lateral contraction is constrained here. In the center of the strip, unconstrained lateral contraction results in small transverse stresses, which correspond to small contact forces at the crossover points. The stress contours are very different in the bias extension test. Here the contact forces are largest at tip of the constrained triangular region at the grips, where the yarns jam tightly against each other and stresses are large. At these points of high contact forces, yarn pullout would be most difficult. Also, these would be the locations where interwoven micro-components would be most likely to fail do to large transverse forces.

By using the failure load indicated by the single yarn tests in **Figure 3-3**, the model's ability to determine yarn loads can be used to predict the macroscopically applied load at which the fabric will fail (due to breakage of the yarns). **Figure 5-12** shows contours of warp yarn tension in the warp-direction tensile test. Like axial stresses, yarn tensions are distributed nearly uniformly across the fabric strip, with the largest values in the yarns closest to the edges. Hence the model implies that failure will begin at the edges and propagate inwards, which is consistent with experimental observations. The macroscopic load at which the yarn tensions exceed the failure load from **Figure 3-3** is the load at which the fabric strip will fail. The revised load-extension plot in **Figure 5-12** compares this model-predicted failure point to experimental observations. The model predicts the load at which the fabric fails very accurately. These examples demonstrate that the model is capable of tracking fabric structural parameters, and that these parameters can be used to accurately predict the onset of failure.

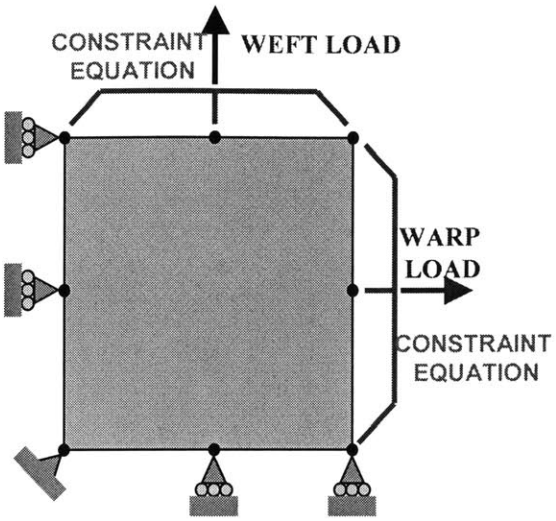
Table 5:1 - Dummy material propeties used to test model behavior

Property[1]	Dummy Material #1 "Locking"	Dummy Material #2 "Non-locking"	Property[1]	Dummy Material #1 "Locking"	Dummy Material #2 "Non-locking"
Warp Radius r_1	0.0012	0.0012	Warp Bending Stiffness k_{b1}	1×10^{-2}	1×10^{-2}
Weft Radius r_2	0.0012	0.0012	Weft Bending Stiffness k_{b2}	1×10^{-2}	1×10^{-2}
Warp Yarn Density[2] ρ_1	1.44×10^6	1.44×10^6	Interference Stiffness K_I	50	50
Weft Yarn Density[2] ρ_2	1.44×10^6	1.44×10^6	Interference exponent a_I	2×10^4	2×10^4
Initial Warp Quarter-wavelength p_1	0.0025	0.0035	Shear Stiffness[4] K_s	1×10^{-4}	1×10^{-4}
Initial Weft Quarter-wavelength p_2	0.0025	0.0035	Reference Shear Rotation Rate[4] $d\gamma_0/dt$	0.02	0.02
Initial Warp Yarn Length L_1	0.002773085	0.0037	Reference Shear Rotation Strength[4] M_0	2.5×10^{-4}	2.5×10^{-4}
Warp Yarn Stiffness[3] k_1	1×10^8	1×10^8	Shear Rate Sensitivity[4] b	1	1
Weft Yarn Stiffness[3] k_2	1×10^8	1×10^8			

[1]Dummy materials used with earlier model version that had circular yarns and used interference relation to also describe locking
[2]Yarn densities scaled to increase inertial stabilization
[3]In this model, yarn stiffnesses are absolute, not per unit length
[4]Typical shear properties, various other shear properties used to test rate-dependent behavior

Table 5:2 - Material data for S706 Kevlar

Property	S706	Property	S706
Warp Minor Radius r_1 [m]	0.000075	Warp Bending Stiffness k_{b1} [N-m/rad]	1×10^{-3}
Warp Major Radius R [m]	0.000320	Weft Bending Stiffness k_{b2} [N-m/rad]	1×10^{-3}
Weft Minor Radius r_2 [m]	0.000075	Interference Stiffness K_I [N]	3.094×10^{-3}
Weft Major Radius R_2 [m]	0.000320	Interference exponent a_I [m^{-1}]	1×10^5
Warp Yarn Density ρ_1 [kg/m^3]	1440	Locking Stiffness K_L [N/m^a]	3.2504×10^{15}
Weft Yarn Density ρ_2 [kg/m^3]	1440	Locking Exponent a	3.6978
Initial Warp Quarter-wavelength p_1 [m]	0.0003735	Locking Transition Force F_T [N]	0.25
Initial Weft Quarter-wavelength p_2 [m]	0.0003735	Shear Stiffness K_s [N-m/rad]	1×10^{-3}
Initial Warp Yarn Length L_1 [m]	0.00037828858	Reference Shear Rotation Rate $d\gamma_0/dt$ [rad/s]	0.5
Warp Yarn Stiffness k_1 [N]	3649.57	Reference Shear Rotation Strength M_0	3×10^{-5}
Weft Yarn Stiffness k_2 [N]	3293.67	Shear Rate Sensitivity b	1
Data measured from fabric and experiments			
Data chosen so that simulation predictions fit experimental results			



Loads and boundary conditions
in single element biaxial test

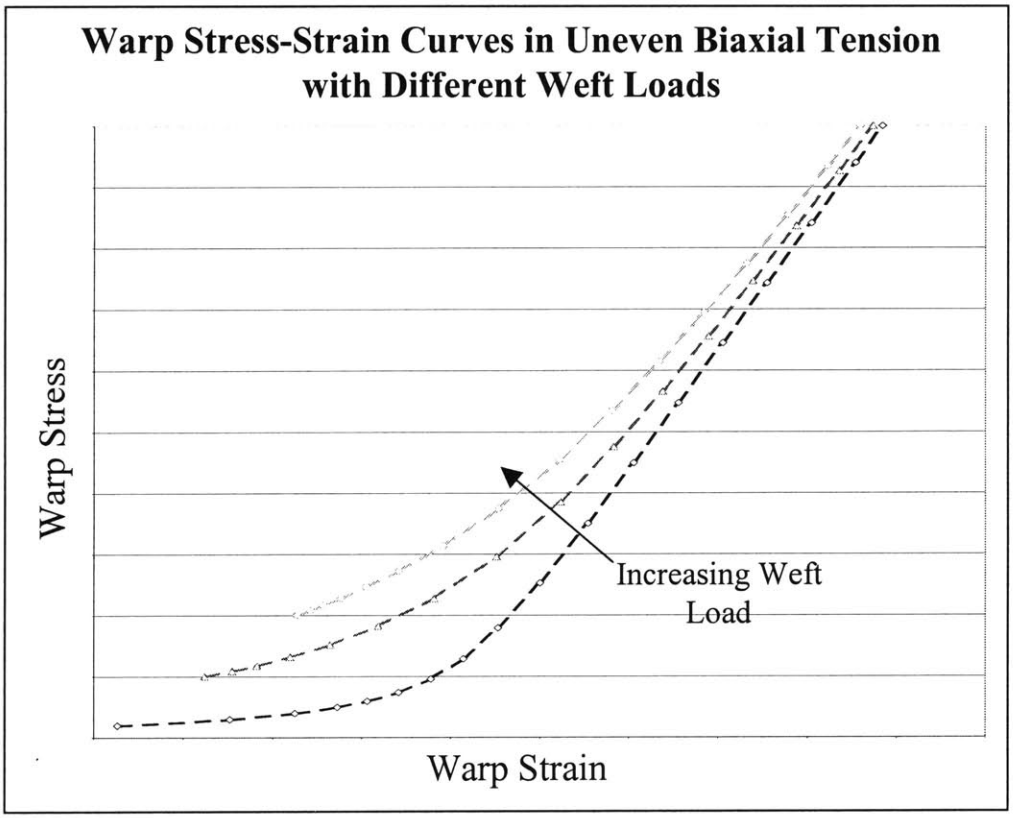
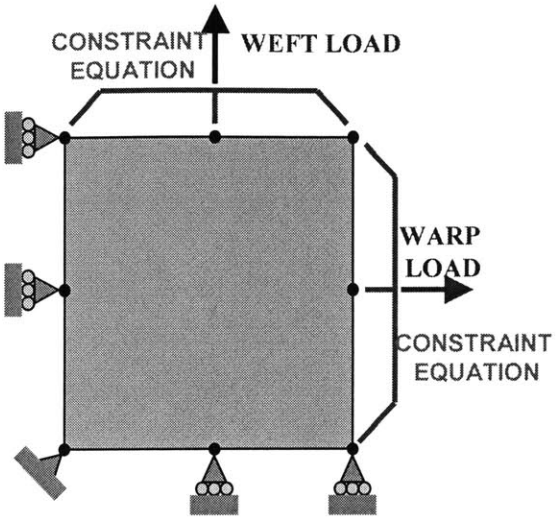


Figure 5-1 – Single element results showing crimp interchange capabilities of model



Loads and boundary conditions
in single element biaxial test

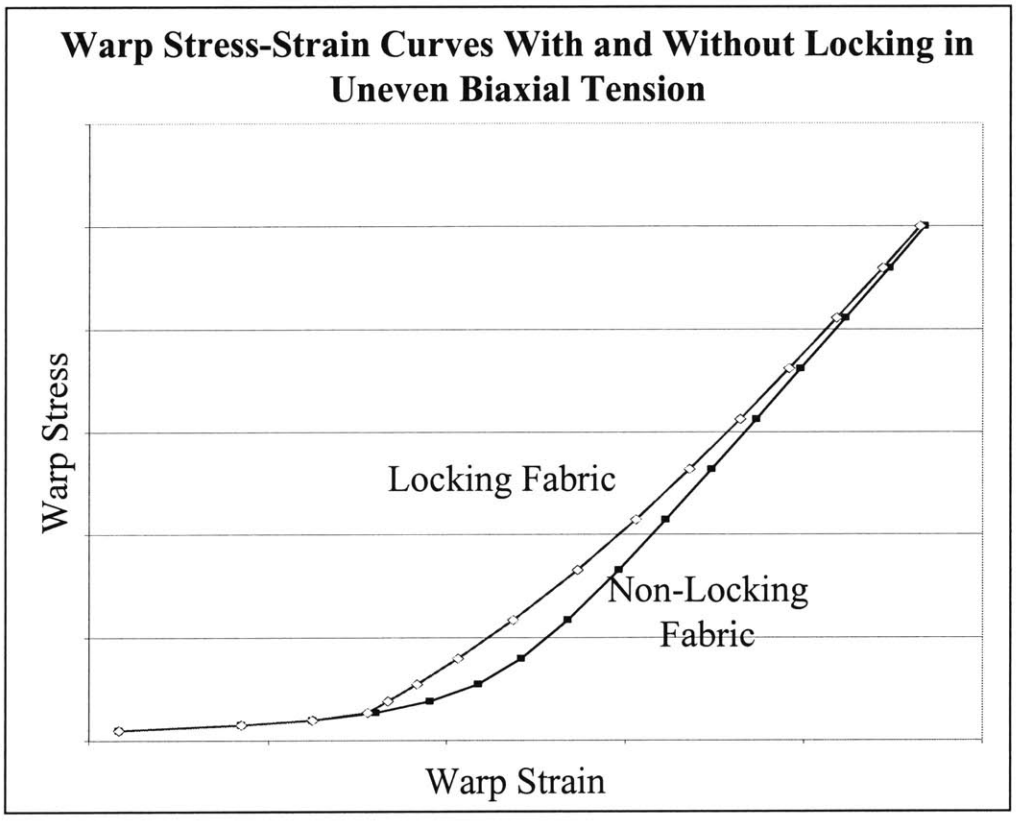


Figure 5-2 – Single element results
showing locking capabilities of model

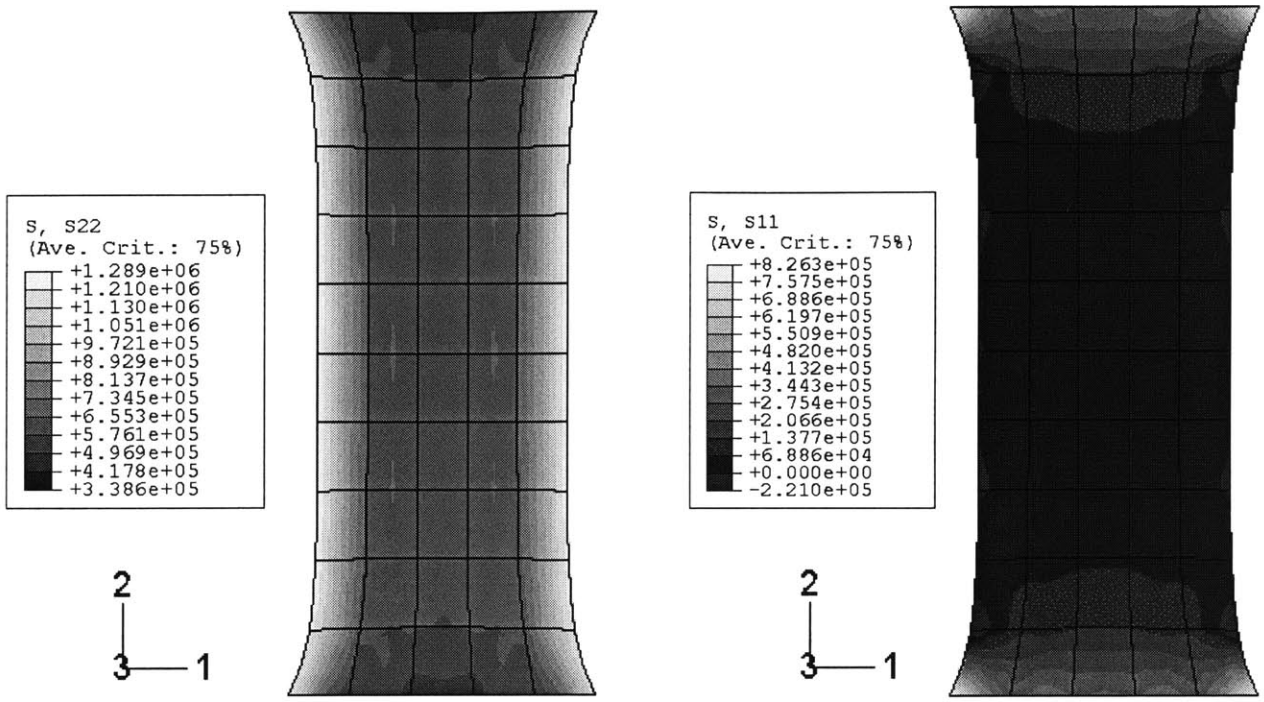


Figure 5-3 – Stress contours in simulated tensile test using locking dummy material

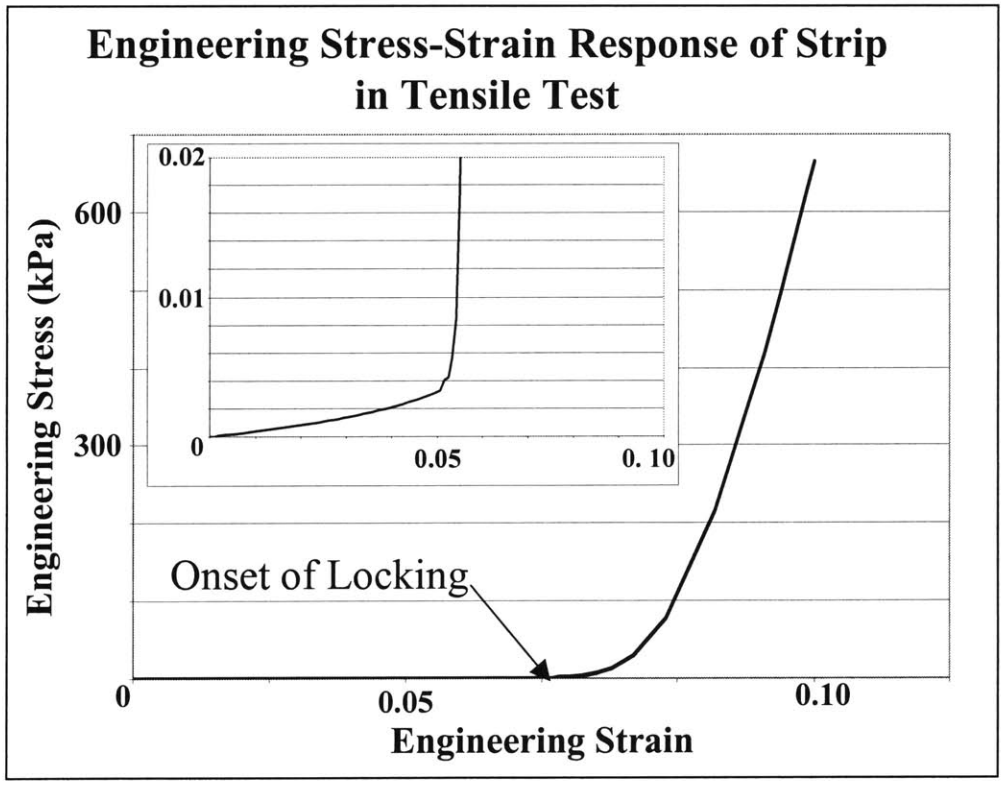


Figure 5-4 – Stress-strain curve in simulated tensile test using locking dummy material

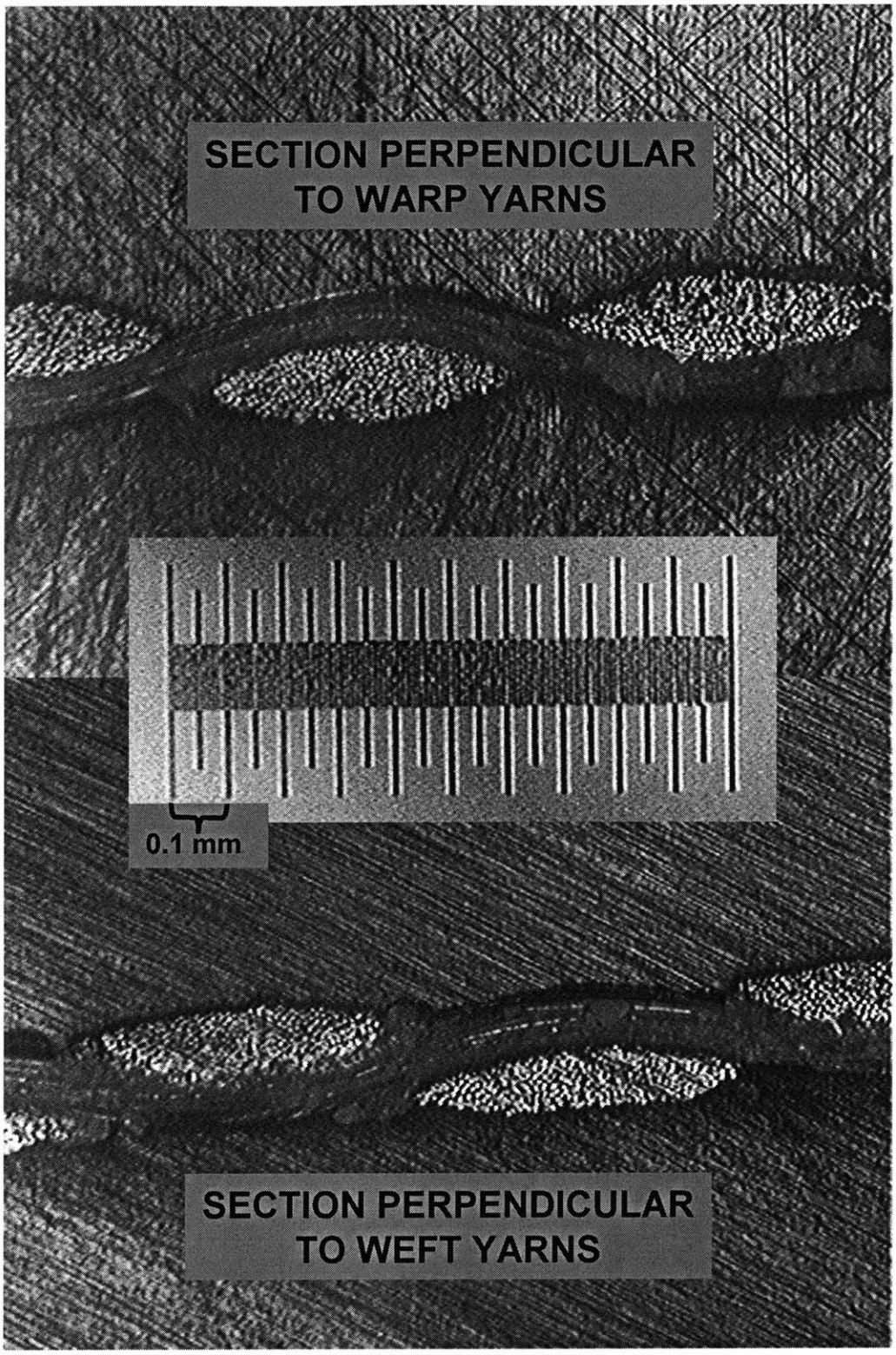
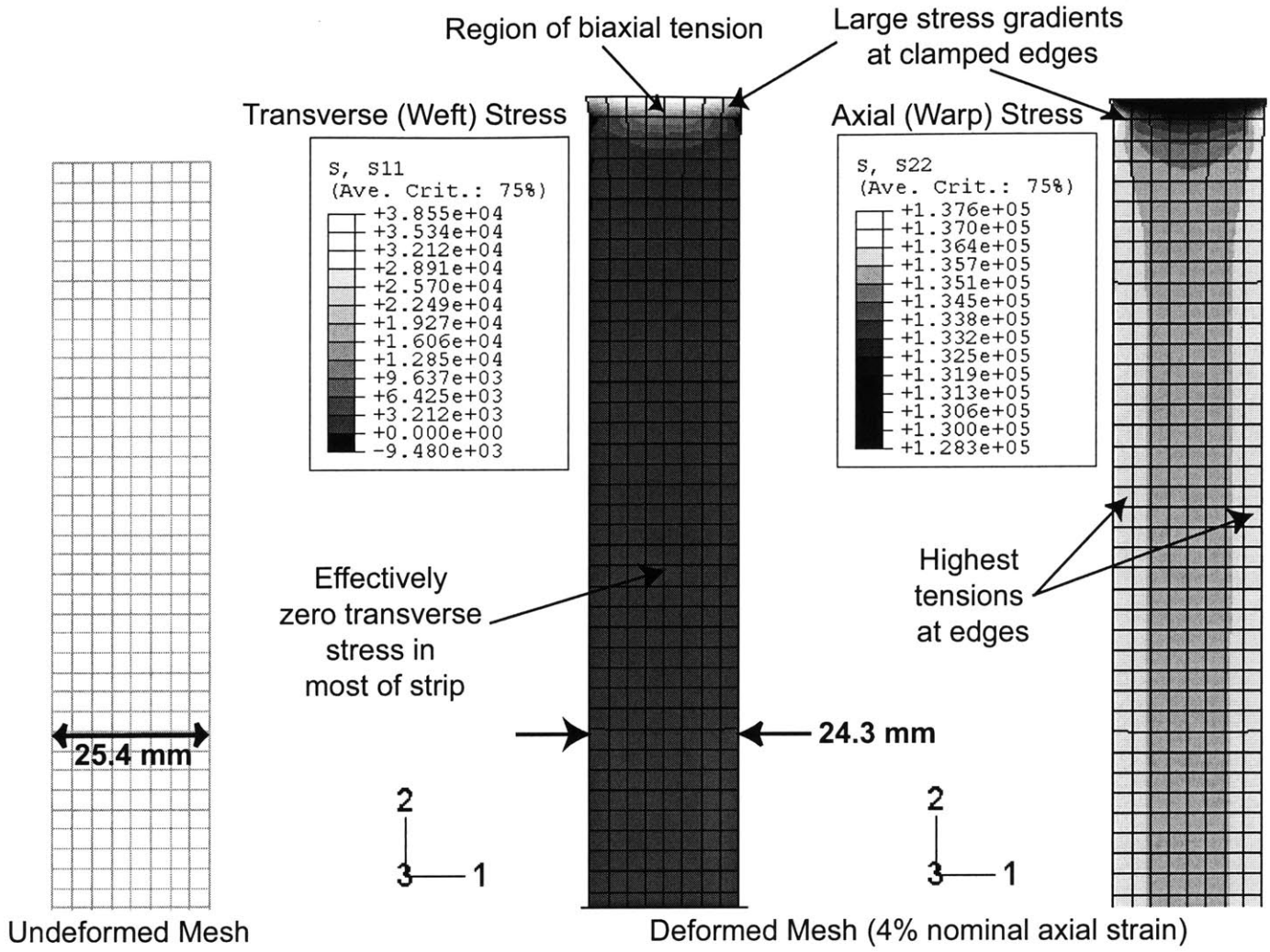


Figure 5-5 – Fabric cross sections showing microstructure (Jearanaisilawong, 2003)



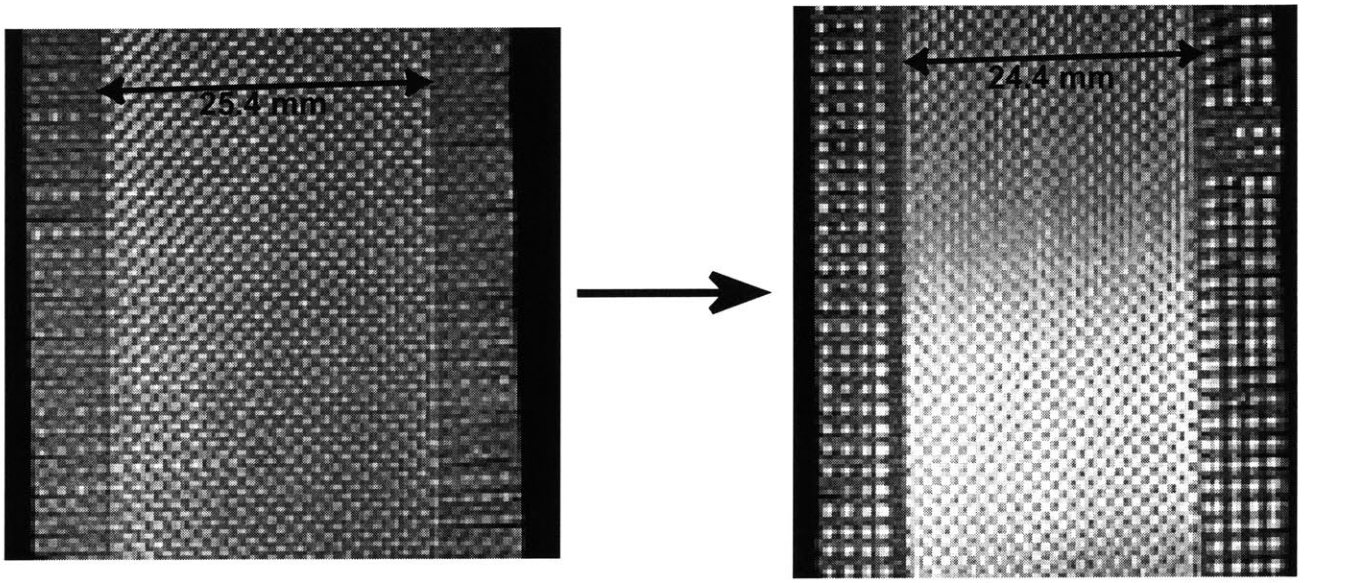


Figure 5-6 - Deformation and stresses in warp direction tensile test
(Photographs from Jearanaisilawong, 2003)

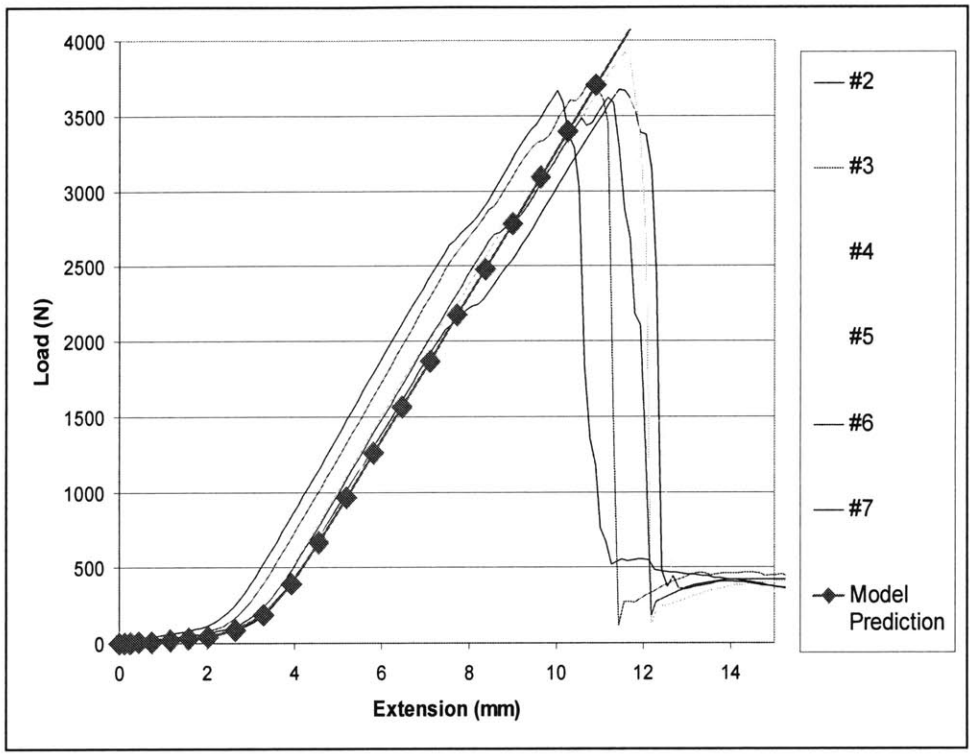


Figure 5-7 – Warp direction tensile test load-extension curves compared to model prediction (Experimental data from Jearanaisilawong, 2003)

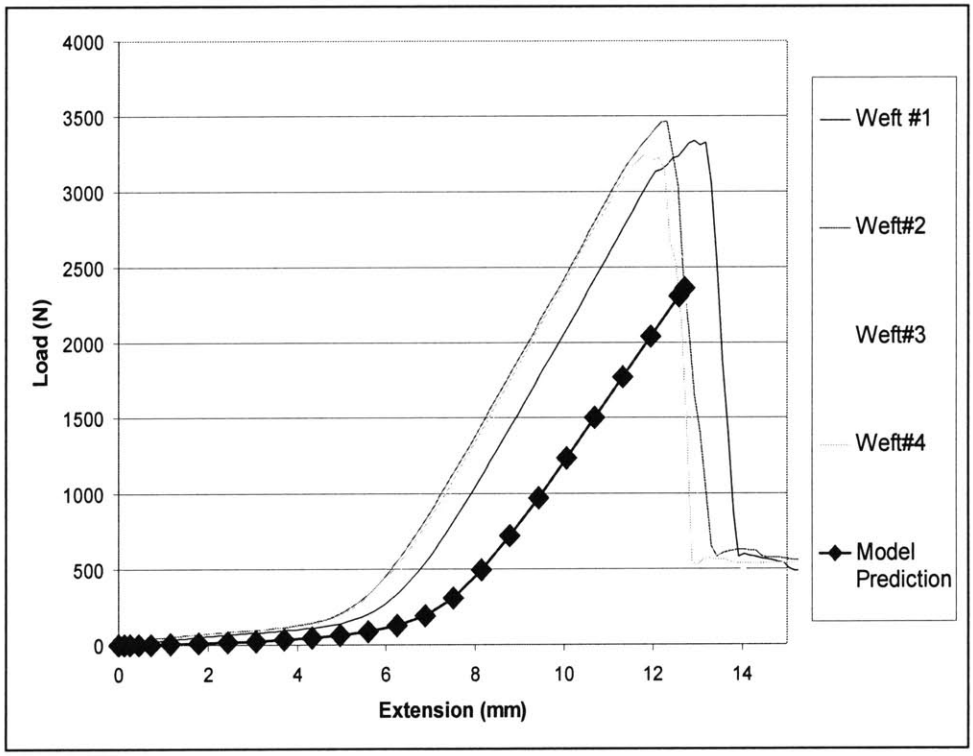
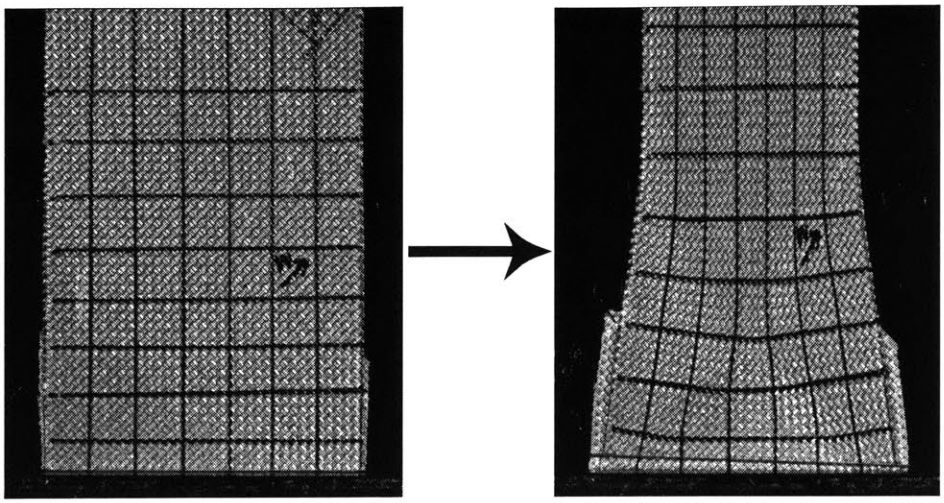
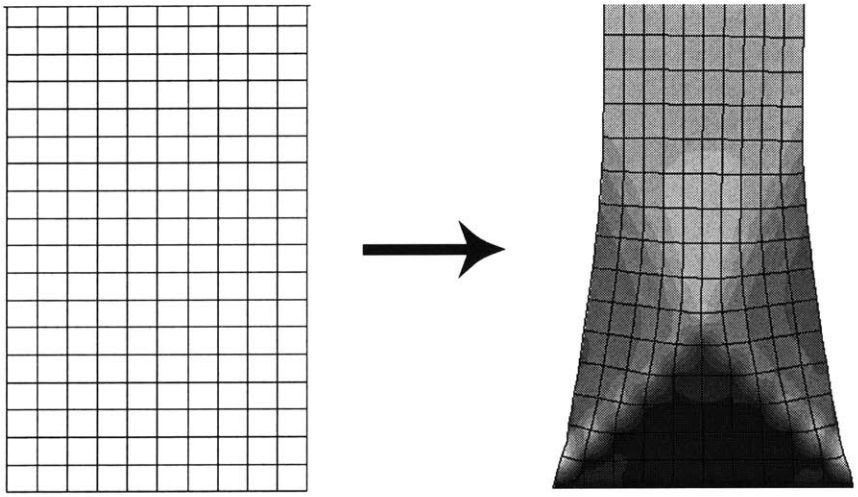


Figure 5-8 – Weft direction tensile test load-extension curves compared to model prediction (Experimental data from Jearanaisilawong, 2003)



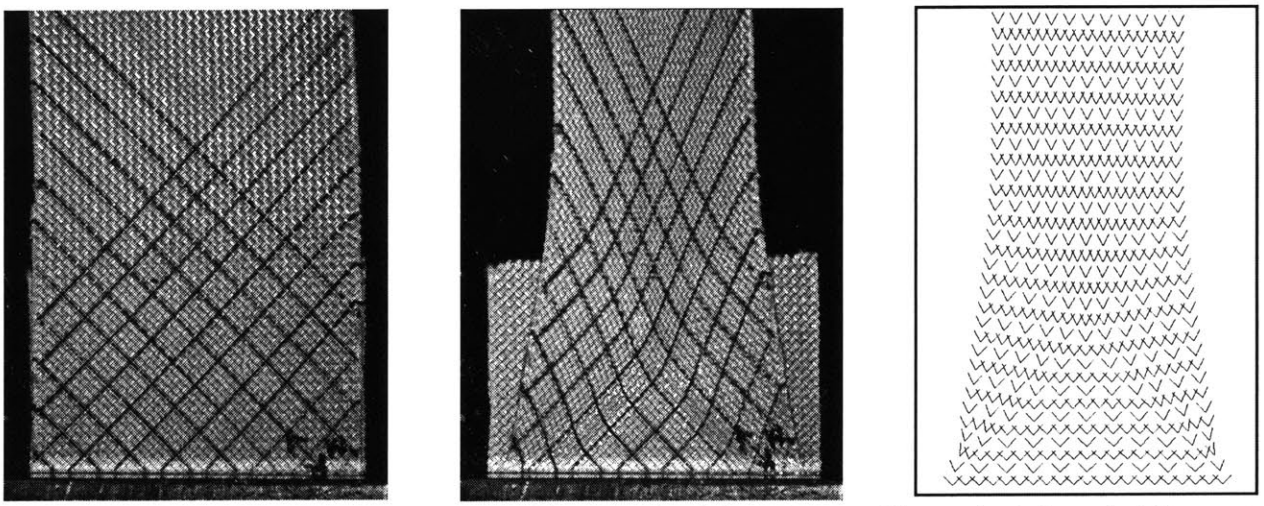
Undeformed fabric

17% nominal axial strain



Undeformed mesh

Shear rotation at 17% nominal axial strain predicted by model



Undeformed fabric with grid lines showing yarn directions

17% nominal axial strain

Yarn orientation at 17% nominal axial strain predicted by model

Figure 5-9 - Deformation of fabric strip in bias extension test
(Photographs from Jearanaisilawong, 2003)

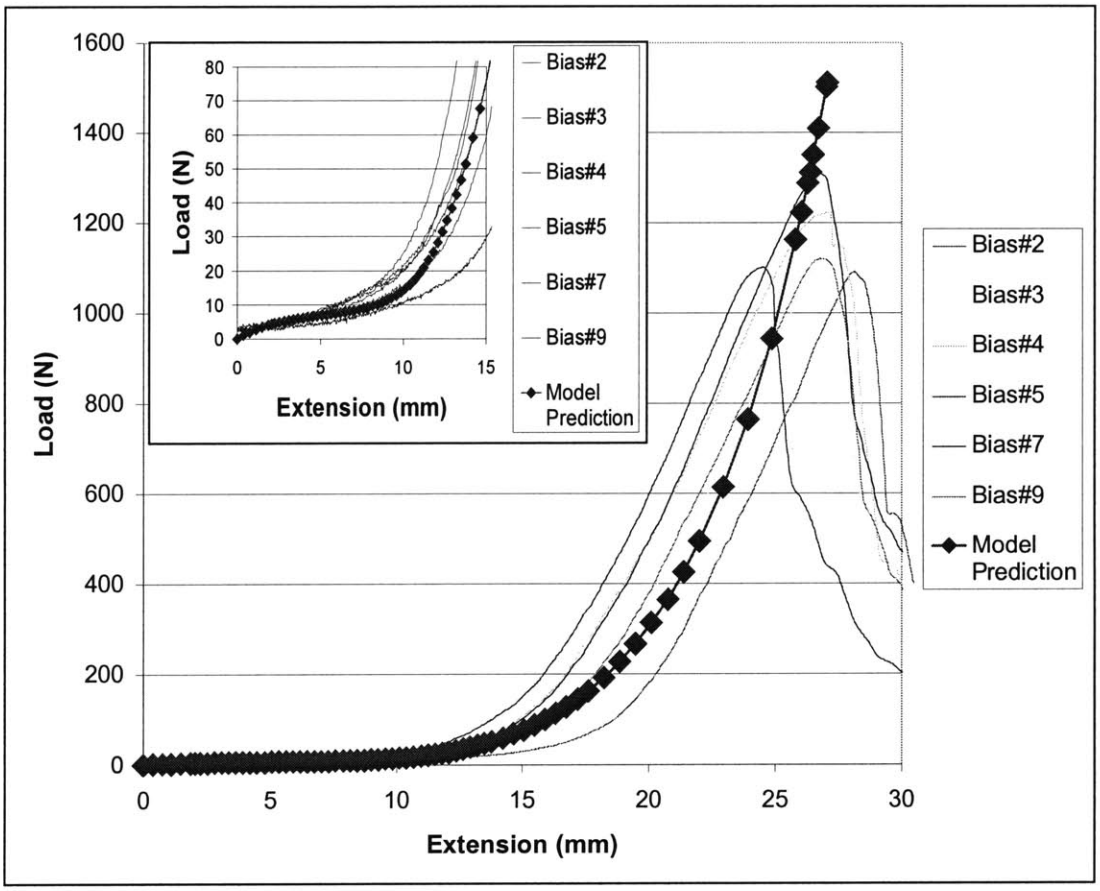


Figure 5-10 – Bias-extension load-extension curves compared to model prediction (Experimental data from Jearanaisilawong, 2003)

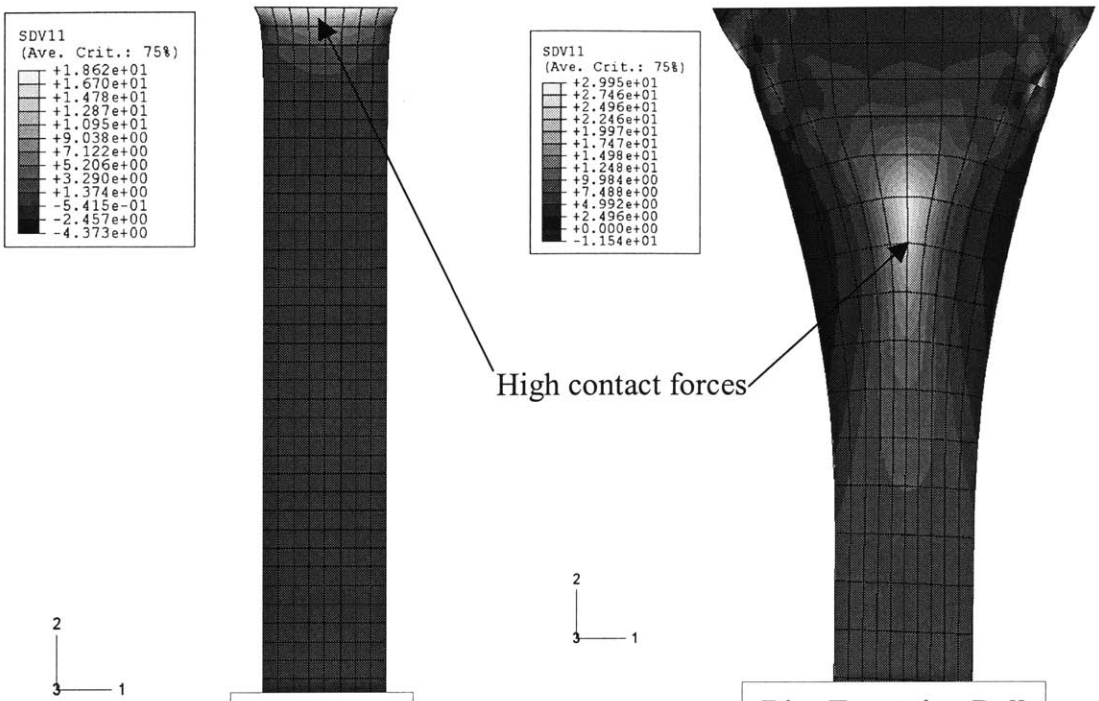


Figure 5-11 – Contours of contact force between yarns

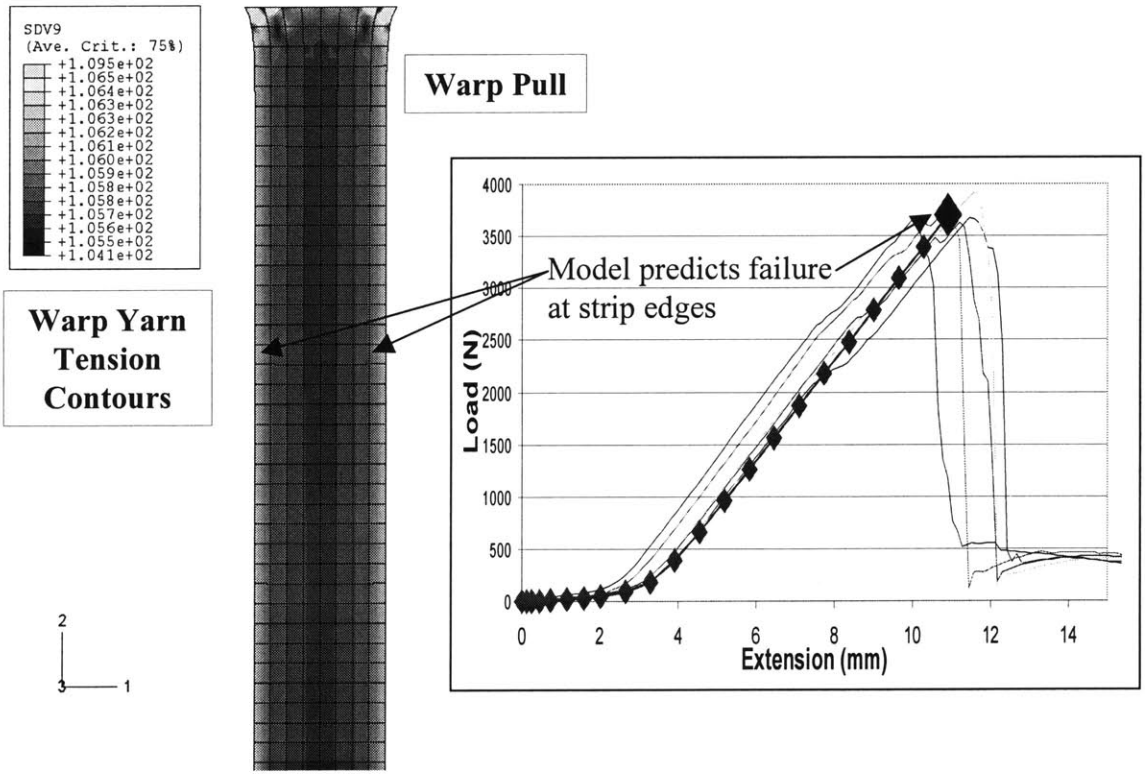


Figure 5-12 – Predicting fabric failure through yarn tensions

Chapter 6
Conclusions and Future Work

6.1 Conclusions

We propose a general approach for developing mechanical models of woven fabrics that can be used in a wide variety of fabric applications. The approach is physically motivated and is capable of accurately simulating the macroscopic continuum response of woven fabrics while capturing the behavior of the component yarns at a structural level. Woven fabrics exhibit a number of unique mechanical behaviors that can be captured using this approach. While a wide range of models have been proposed in the literature for various industrial applications, which effectively capture certain behaviors of specific fabrics, few of these models satisfy the requirements that our approach is intended to meet. Models must serve as accurate simulation tools, effective predictive tools, and must be practical and efficient to use.

The model discussed in this paper allows simulation of the in-plane behavior of woven fabrics prior to yarn failure or pullout. Five steps comprise the modeling approach. First, the fabric's geometry is idealized, a unit cell is defined, and relations between geometric parameters are derived. Next, component constitutive relations that describe the response of the component yarns under various modes of deformation are established. These first two steps determine the complexity of the model, and hence how accurately the model captures complicated fabric behaviors at the cost of computational efficiency. The third step is to establish a method of determining the configuration of the fabric structure from the deformation history. For simple models with three or fewer independent parameters describing the unit cell configuration, the fabric state is directly determined by the

deformation gradient. Additional free parameters in more complicated models are determined by an energy minimization argument. Once the fabric state is determined, the loads carried by the yarns within the unit cell are calculated from the geometric relations and component constitutive relationships. The fifth step is to transform these internal loads into macroscopic stresses. For simple models, the macroscopic stresses are directly calculated from the strain energy function; stresses in more complicated models can be related to the internal loads and the state of the unit cell through an equilibrium argument.

This procedure has been used to develop a model for a plain weave ballistic fabric (Kevlar S706). A simplified fabric lattice geometry similar to that proposed by Kawabata is assumed, including linear elastic yarn extension, exponential elastic yarn interference at the crossover points, power-law locking relations, and linear elastic bending relations. The model also includes power-law rate dependent yarn rotation effects, but it does not include wrapping or yarn twisting effects. The model has five independent configuration parameters, and an exact analytical expression for the minimum energy configuration does not exist, so the fabric configuration is determined using a numerical energy minimization process. The stresses are determined through an equilibrium argument.

A number of challenges arose when this model was implemented into ABAQUS Standard for quasi-static analyses. Various energy minimization algorithms were investigated, including Newton's method, a modified downhill simplex method, and a simulated annealing technique. The bounds on the energy function and the large, rapidly changing gradients near the minimum posed difficulties for Newton's method. Zeroth order methods such as simplex methods or simulated annealing are more attractive methods because of their versatility. For the current model, a modified downhill simplex algorithm proved the most effective.

The lattice geometry is subject to local yarn buckling, even when the fabric is constrained to remain planar. Multi-element analyses subjected to complex load conditions could not be performed without stabilizing the model against bifurcation. User-defined inertial stabilization terms were introduced that add inertia only to the rotational degrees of

freedom of the yarns, which allows effective stabilization with low energy loss. Though these terms are intended to stabilize against buckling in quasi-static analyses, they are also required in dynamic analyses.

Because fabrics display nonlinear relations between the strains in the two yarn directions, most finite element formulations, which are capable of capturing only linear strain distributions, exhibited difficulties in the low-stress regime. Elements that cannot capture the true strain fields required to minimize stress and energy respond in an artificially stiff manner, and assume displacements that result in mesh-dependent stress oscillations. Fully integrated elements suffer the most from this problem, while 8-node reduced integration elements suffer the least, with oscillations of smaller amplitudes and lower artificial stiffening effects. In the high stress regime, the differences in stiffness are negligible and the true stress fields dominate over the non-physical oscillating stress fields.

The ballistic fabric model was validated through various stages of testing. First, the model was tested under various loading conditions using "dummy" materials with properties similar to those of Kevlar but chosen specifically to highlight specific fabric behaviors. These tests indicated that the model was capable of capturing all of the relevant fabric behaviors. Next, real properties of a plain weave Kevlar fabric were measured through experimental tests. Many of the model parameters were determined from these tests, so that the predictive capability of the model for behaviors dominated by these parameters could be evaluated. Some properties could not be directly measured with the available equipment, especially properties relating to yarn interaction (interference and locking) and shear. The finite element code ABAQUS was used to simulate mechanical experiments on the fabric and the simulation predictions were compared to the experimental results. The experimental measurements qualitatively agree with the simulation predictions for every test, which indicates that the model is capable of capturing the dominant mechanisms of fabric deformation. Good quantitative agreement indicated that the model could accurately predict fabric behaviors dominated by properties that can be directly measured, and that the remaining properties could be

determined by fitting the model predictions to experimental results. The largest discrepancies between the simulations and the experiments involved behaviors dominated by locking, which implies that a more accurate locking relationship needs to be implemented. However, the generally good agreement between model and experiment serves to validate this model and the approach that was used to develop it. It was also demonstrated that the model could track variables describing behavior at the fabric structural level, such as yarn loads and contact forces, and that these variables could be used to accurately predict the onset of failure. Therefore, the approach we have proposed satisfies our intended objectives.

6.2 Future Work

A number of steps can be taken to improve and expand both the ballistic fabric model and the general fabric modeling approach. The first step is to address the discrepancies between the experimental data and the simulations and the need to determine material properties through curve fitting. Methods of measuring the material properties that were not accurately determined will be explored. No reliable method exists for measuring the interference relation where the yarns cross; a method using a biaxial tensile testing machine may be effective. Similarly, no reliable method exists for measuring the locking relations. Most of the discrepancies between the model predictions and the experimental results appear in behaviors dominated by locking, which implies that a more accurate locking relation should be implemented into the model. A detailed mechanical analysis of the fabric structure that includes the individual yarn fibers might reveal the nature of the locking relation that should be used, and may even be able to predict the appropriate material properties.

The ultimate goal of this study is to develop a model capable of capturing the effects of advanced fabric technologies on ballistic armor. The current model has been implemented only for two-dimensional, quasi-static, implicit analysis. Ballistic analysis is by definition dynamic, involves three-dimensional phenomena, and is usually

performed explicitly. Therefore, the current model needs to be expanded to thin, three-dimensional structures (membranes or shells), and implemented into an explicit code for dynamic analysis. At the same time, the material behaviors for the yarns, which were measured quasi-statically, should be re-evaluated in the high strain-rate regime. Finally, this model was developed specifically for ballistic analysis, but the general modeling approach should prove effective for a variety of different fabric applications to which it could be applied.

Bibliography

[1] Bassett, R.J. and Postle, R., 1999, "Experimental Methods for Measuring Fabric Mechanical Properties," *Textile Research Journal*, **69(11)**, pp. 866-875.

[2] Breen, D.E., House, D.H., and Wozny, M.J., 1994, "A Particle-Based Model for Simulating the Draping Behavior of Woven Cloth", *Textile Research Journal,* **64**, pp. 663-685.

[3] *Computational Science Education Project*, 1996, "Simulated Annealing," http://csep1.phy.ornl.gov/CSEP/MO/NODE28.html

[4] Cunniff, P.M., 1992, "An Analysis of the System Effects in Woven Fabrics Under Ballistic Impact", *Textile Research Journal*, **62(9)**, pp. 495-509.

[5] Cunniff, P.M., 1996, "A Semiempirical Model for the Ballistic Impact Performance of Textile-Based Personnel Armor", *Textile Research Journal,* **66(1)**, pp. 45-59.

[6] Duque-Anton, M., 1997, "Constructing Efficient Simulated Annealing Algorithms", *Discreet Applied Mathematics*, **77**, pp. 139-159

[7] Grabitech Solutions AB, "The Simplex Optimization Methods: The Basic Simplex Method", http://www.grabitech.com/simplex_b.htm

[8] Grabitech Solutions AB, "The Simplex Optimization Methods: The Modified Simplex Method", http://www.grabitech.com/simplex_m.htm

[9] Hearle, J.W.S., Grosberg, P., and Backer, S., 1969, *Structural Mechanics of Fibers, Yarns, and Fabrics,* John Wiley and Sons, New York, NY, pp. 323-354.

[10] Holzapfel, G.A., 2000, *Nonlinear Solid Mechanics*, John Wiley and Sons, New York, NY, pp. 265-277.

[11] Jearanisailiwong, P., 2003, "Experiments on Ballistic Kevlar" (manuscript in preparation), Master's Thesis, Massachusetts Institute of Technology, Boston, MA.

[12] Kato, S., Yoshino, T., Minami, H., 1999, "Formulation of Constitutive Equations for Fabric Membranes Based on the Concept of Fabric Lattice Model", *Engineering Structures*, **21**, pp. 691-708.

[13] Kawabata, S. and Niwa, M. , and Kawai, H., 1973, "The Finite-Deformation Theory of Plain Weave Fabrics Part I: The Biaxial-Deformation Theory," *J. Text. Inst.,* **64,** pp. 21.

[14] Luke, B.T., "Simulated Annealing," http://members.aol.com/btluke/simann1.htm

[15] Mohammed, U., Lekakou, C., Dong, L., and Bader, M. G., 2000, "Shear Deformation and Micromechanics of Woven Fabric," *Composites*, **31A**, pp. 299-308.

[16] Morey, C., Scales, J., and Van Vleck, E.S., 1998, "A Feedback Algorithm for Determining Search Parameters for Monte Carlo Optimization," *Journal of Computational Physics* **146** (1998), pp. 263-281

[17] Ng. S., Tse, P., Lau, K., 1998, "Numerical and Experimental Determination of In-Plane Elastic Properties of 2/2 Twill Weave Fabric Composites," *Composites,* **29B**, pp. 735-744.

[18] Pan, N. and Zeronian, S. H., 1993, "An Alternative Approach to the Objective Measurement of Fabrics", *Textile Research Journal*, **63(1)**, pp. 33-43.

[19] Parga-Landa, B. and Hernandez-Olivares, F., 1995, "An Analytical Model to Predict Impact Behavior of Soft Armours", *International Journal of Impact Engineering*, **16(3)**, pp. 455-466.

[20] Press, W.H., Teukolsky, S.A., Vetterling, W.T., Flannery, B.P., 1992, *Numerical Recipes in FORTRAN: The Art of Scientific Computing,* 2nd ed., Cambridge University Press, Cambridge, pp. 372-375, 402-406, 436-448/

[21] Realff, M.L., 1992, "Mechanical Properties of Fabrics Woven from Yarns Produced by Different Spinning Technologies," Ph.D. thesis, Massachusetts Institute of Technology, Boston, MA.

[22] Roylance, D., Chammas, P., Ting, J., Chi, H., and Scott, B., 1995, "Numerical Modeling of Fabric Impact," *Procedings of the National Meeting of the ASME*, San Francisco, CA.

[23] Ruan, X. and Chou, T., 1996, "Experimental and Theoretical Studies of the Elastic Behavior of Knitted-Fabric Composites," *Composites Science and Technology,* **56**, pp. 1391-1403.

[24] Shim, V.P.W., Tan, V.B.C., and Tay, T.E., 1995, "Modelling [sic] Deformation and Damage Characteristics of Woven Fabric Under Small Projectile Impact," *International Journal of Impact Engineering*, **16(4)**, pp. 585-605.

[25] Shim, V.P.W., Lim, C.T., and Foo, K.J., 2001, "Dynamic Mechanical Properties of Fabric Armour", *International Journal of Impact Engineering*, **25**, pp. 1-15.

[26] Spencer, A.J.M., 1971, "Theory of Invariants", in: A.C. Eringen, ed., *Continuum Physics,* Volume I, Academic Press, New York.

[27] Wang, J., Page, J.R., and Paton, R., 1998, "Experimental Investigation of the Draping Properties of Reinforcement Fabrics," *Composites Science and Technology*, **58**, pp. 229-237.

Appendix
Model Source Code

This is a user-material model, or "UMAT", for the plain-weave ballistic fabric model, written in FORTRAN and intended for use with ABAQUS Standard. It includes a number of subroutines and functions in addition to the UMAT subroutine and employs several "common" blocks. This code has been tested using DIGITAL Visual Fortran Developer Studio Standard Edition ver. 6.0.A and ABAQUS Implicit ver 6.3-1.

```
C     Plain Weave Linear Fabric Material Model with Elliptical Yarns
C     Developed by Michael J. King, May 2003
C     Massachusetts Institute of Technology
C
C     Includes:
C     - Crimp Interchange
C     - Yarn Elongation
C     - Yarn Bending
C     - Cross Sectional Stiffness
C     - Rate-Dependent Shear
C     - Crosslocking and shear locking
C     - Inertial stabilization against in-plane buckling
C     Does not include:
C     - Wrapping
C     - Yarn torsion
C     - Fiber slip
C     - Failure
C
C     Based on Kawabata Geometry
C     Linear elastic yarn extension and bending
C     Exponential elastic crossover point interference
C     Power-law elastic locking relation
C     Linear elastic shear rotation with rate-dependent
C           power-law shear dissipation
C
C     Common Blocks
C     -------------
C     Geometric parameters
C     COMMON /GEOM_INIT/ P1_INIT, A1_INIT, EL1_INIT,
C     1     P2_INIT, A2_INIT, EL2_INIT, THETA_INIT
C     Stiffness parameters
C     COMMON /STIFFNESS/ ENTERF_K, ENTERF_A, STIFF1, STIFF2, CROSS_K,
C     1     CROSS_A, SHEAR_K, BEND_K1, BEND_K2
C     Dissipative parameters
C     COMMON /SHEAR_DISS/ GAMMAF_DOT, EMM0
C     Yarn Radii
C     COMMON /RADII/ R1,R2, RR1, RR2
C     Machine variable
C     COMMON /MACHINE/ UNDFLOW
```

```
C
C
C     Material Properties (24)
C     ------------------------
C     PROPS(1)     minor warp radius R1 [length]
C     PROPS(2)     major warp radius RR1 [length]
C     PROPS(3)     minor weft radius R2 [length]
C     PROPS(4)     major weft radius RR2 [length]
C     PROPS(5)     mass density of warp yarns RHO1 [mass/length^3]
C     PROPS(6)     mass density of weft yarns RHO2 [mass/length^3]
C     PROPS(7)     initial warp quarter-wavelength P1_INIT [length]
C     PROPS(8)     initial weft quarter-wavelength P2_INIT [length]
C     PROPS(9)     initial warp yarn orientation [radians]
C     PROPS(10)    initial weft yarn orientation [radians]
C     PROPS(11)    initial warp yarn length (per quarter-wavelength)
C                        [length]
C     PROPS(12)    warp yarn stiffness per unit length [force]
C     PROPS(13)    weft yarn stiffness per unit length [force]
C     PROPS(14)    stiffness parameter for exponential
C                        interfernce relation ENTERF_K [force]
C     PROPS(15)    exponent for exponential interference
C                        relation ENTERF_A [1/length]
C     PROPS(16)    stiffness parameter for power-law locking
C                        relation CROSS_K [force/length^CROSS_A]
C     PROPS(17)    exponent for power-law locking relation CROSS_A
C                        [unitless]
C     PROPS(18)    warp yarn bending stiffness BEND_K1 [force-
C                        length/radian]
C     PROPS(19)    weft yarn bending stiffness BEND_K2
C                        [force-length/radian]
C     PROPS(20)    elastic shear stiffness SHEAR_K [force-length/radian]
C     PROPS(21)    reference rotation rate for power-law
C                        shear rotation [radians/time]
C     PROPS(22)    reference rotation strength for power-law
C                        shear rotation [force-length/radian]
C     PROPS(23)    exponent for power-law shear rotation [unitless]
C     PROPS(24)    reference macroscopic shear rate [radians/time]
C
C     State Variables (20)
C     --------------------
C     (the first 11 state variables are for output purposes only)
C     STATEV(1)    Warp half-wavelength p1 [length]
C     STATEV(2)    Weft half-wavelength p2 [length]
C     STATEV(3)    Warp yarn angle theta1 [radians]
C     STATEV(4)    Weft yarn angle theta2 [radians]
C     STATEV(5)    Warp Locking Energy [energy]
C     STATEV(6)    Weft Locking Energy [energy]
C     STATEV(7)    Warp half-yarn length L1 [length]
C     STATEV(8)    Weft half-yarn length L2 [length]
C     STATEV(9)    Warp yarn tension T1 [force]
C     STATEV(10)   Weft yarn tension T2 [force]
C     STATEV(11)   Contact force at crossover points [force]
C     STATEV(12)   Moment at crossover points [moment]
C     (the last six state variables are required by the solution
C                        process)
C     STATEV(13)   Warp crimp angle beta1 from previous time step
C                        [radians]
```

```
C     STATEV(14)  Warp crimp angle rate of change d(beta1)/dt from
C                       previous time step [radians/time]
C     STATEV(15)  Weft crimp angle beta2 from previous time step
C                       [radians]
C     STATEV(16)  Weft crimp angle rate of change d(beta2)/dt from
C                       previous time step [radians/time]
C     STATEV(17)  Dissipative shear angle gamma_f [radians]
C     STATEV(18)  Rate of change of dissipative shear angle
C                       d(gamma_f)/dt [radians/time]
C     STATEV(19)  Total shear angle gamma from the previous increment
C                       [radians]
C     STATEV(20)  Rate of change of total shear angle d(gamma)/dt
C                       from the previous increment [radians/time]
C
C ***************************************************
C THE FOLLOWING FUNCTIONS ARE USED TO CALCULATE
C GEOMETRIC PARAMETERS OF THE SYSTEM FROM OTHERS
C ***************************************************
C     Fucntion to return A when given L and p
      DOUBLE PRECISION FUNCTION AMPLITUDE(P,EL)
      INCLUDE 'ABA_PARAM.INC'
      IF (P .GE. EL) THEN
            WRITE(7,*) 'INADMISSIBLE WAVELENGTH INPUT IN AMP CALC'
            WRITE(7,*) 'P = ', P, '     L = ', EL
            CALL XIT
      END IF
      AMPLITUDE = DSQRT(EL**2 - P**2)
      RETURN
      END
C
C     Function to determine Beta when given L and p
      DOUBLE PRECISION FUNCTION BETA(P,EL)
      INCLUDE 'ABA_PARAM.INC'
      IF (P .GE. EL) THEN
            WRITE(7,*) 'INADMISSIBLE WAVELENGTH INPUT IN BETA CALC'
            CALL XIT
      END IF
      BETA = DACOS(P/EL)
      RETURN
      END
C
C     Function to determine L from A and p
      DOUBLE PRECISION FUNCTION EL_CLC(P,A)
      INCLUDE 'ABA_PARAM.INC'
      EL_CLC = DSQRT(A**2 + P**2)
      RETURN
      END
C
C     Function to determine interference
C     I = 0A1 + 0A2 - A1 - A2
      DOUBLE PRECISION FUNCTION ENTERF(P1,EL1,P2,EL2)
      INCLUDE 'ABA_PARAM.INC'
      COMMON /GEOM_INIT/ P1_INIT, A1_INIT, EL1_INIT,
     1      P2_INIT, A2_INIT, EL2_INIT, THETA_INIT
      ENTERF = A1_INIT + A2_INIT - AMPLITUDE(P1,EL1) -
     1      AMPLITUDE(P2,EL2)
      RETURN
```

```
      END
C
C ***********************************************************
C THE FOLLOWING FUNCTIONS AND SUBROUTINES ARE USED CHECKING
C FOR CROSSLOCKING AND EVALUATING CROSSLOCKING PENALTY ENERGY
C ***********************************************************
C     Function to determine correction factor xi
      DOUBLE PRECISION FUNCTION XI(PI,PJ,THETA)
      INCLUDE 'ABA_PARAM.INC'
      HORZ = DABS(PI*DCOS(THETA))
      DO WHILE (HORZ .GT. 2.D0*PJ)
            HORZ = HORZ - 2.D0*PJ
      END DO
      XI = DABS(1.D0 - HORZ/PJ)
      RETURN
      END
C
C     Subroutine to evaluate locking geometry
      SUBROUTINE LOCKING(I,P1,EL1,P2,EL2,THETA,DISTANCE,ALPHA,ENTERF_L)
      INCLUDE 'ABA_PARAM.INC'
      COMMON /RADII/ R1,R2, RR1, RR2
      IF (I .EQ. 1) THEN
            PI=P1
            PJ=P2
            ELJ=EL2
            RI = R1
            RJ = R2
            RRJ = RR2
      ELSE IF (I .EQ. 2) THEN
            PI = P2
            PJ = P1
            ELJ = EL1
            RI = R2
            RJ = R1
            RRJ =RR1
      ELSE
            WRITE(7,*) 'INVALID DIRECTION SELECTOR'
            CALL XIT
      END IF
      XI_I = XI(PI,PJ,THETA)
      AJE = XI_I*AMPLITUDE(PJ,ELJ)
      DISTANCE = DSQRT((PI*DSIN(THETA))**2 + AJE**2)
      ALPHA = DATAN(AJE/(PI*DSIN(THETA)))
      RJE = DSQRT((RRJ*DCOS(ALPHA))**2+(RJ*DSIN(ALPHA))**2)
      ENTERF_L = RI + RJE - DISTANCE
      RETURN
      END
C
C     Function to determine locking energy in i-direction
      DOUBLE PRECISION FUNCTION PHI_D(ENTERF_L)
      INCLUDE 'ABA_PARAM.INC'
      COMMON /STIFFNESS/ ENTERF_K, ENTERF_A, STIFF1, STIFF2, CROSS_K,
     1      CROSS_A, SHEAR_K, BEND_K1, BEND_K2
C     TRANSITION FORCE = 0.25 N     Force as which relation transitions
C                                        from power-law to linear
      ENTERF_L_TRANS = (0.25D0/CROSS_K)**(1.D0/CROSS_A)
```

```
C
      IF (ENTERF_L .LT. 0.D0) THEN  ! No locking energy in tension
            PHI_D = 0.D0
      ELSE IF (ENTERF_L .LT. ENTERF_L_TRANS) THEN           ! Power Law
            PHI_D = 2.D0*(CROSS_K/(CROSS_A+1.D0))*
     1            ENTERF_L**(CROSS_A+1.D0)
      ELSE  ! Linear
            EM = CROSS_A*CROSS_K*ENTERF_L_TRANS**(CROSS_A-1.D0)
            B = CROSS_K*ENTERF_L_TRANS**CROSS_A - EM*ENTERF_L_TRANS
            PHI_D1 = (CROSS_K/(CROSS_A+1.D0))
     1            *ENTERF_L_TRANS**(CROSS_A+1.D0)
            PHI_D2 = 0.5D0*EM*(ENTERF_L**2 - ENTERF_L_TRANS**2)
     1            + B*(ENTERF_L - ENTERF_L_TRANS)
            PHI_D = 2.D0*(PHI_D1 + PHI_D2)
      END IF
      RETURN
      END
C
C     Locking Force Function
      DOUBLE PRECISION FUNCTION T_L(ENTERF_L)
      INCLUDE 'ABA_PARAM.INC'
      COMMON /STIFFNESS/ ENTERF_K, ENTERF_A, STIFF1, STIFF2, CROSS_K,
     1      CROSS_A, SHEAR_K, BEND_K1, BEND_K2
      COMMON /RADII/ R1,R2, RR1, RR2
C     TRANSITION FORCE = 0.25 N
      ENTERF_L_TRANS = (0.25D0/CROSS_K)**(1.D0/CROSS_A)
      IF (ENTERF_L .LT. 0.D0) THEN  ! No force in tension
            T_L = 0.D0
      ELSE IF (ENTERF_L .LT. ENTERF_L_TRANS) THEN           ! Power Law
            T_L = CROSS_K*ENTERF_L**CROSS_A
      ELSE  ! Linear
            EM = CROSS_A*CROSS_K*ENTERF_L_TRANS**(CROSS_A-1.D0)
            B = CROSS_K*ENTERF_L_TRANS**CROSS_A - EM*ENTERF_L_TRANS
            T_L = EM*ENTERF_L + B
      END IF
      RETURN
      END
C
C ***********************************************************
C THE FOLLOWING FUNCTIONS AND SUBROUTINES ARE USED TO FIND
C THE FABRIC STATE THAT CORRESPONDS TO THE MINIMUM ENERGY
C AT A GIVEN DEFORMATION GRADIENT (FIXED P1, P2, THETA)
C ***********************************************************
C     Conditional Energy Function
      DOUBLE PRECISION FUNCTION PHI(P1,EL1,P2,EL2,THETA)
      INCLUDE 'ABA_PARAM.INC'
      COMMON /GEOM_INIT/ P1_INIT, A1_INIT, EL1_INIT,
     1      P2_INIT, A2_INIT, EL2_INIT, THETA_INIT
      COMMON /STIFFNESS/ ENTERF_K, ENTERF_A, STIFF1, STIFF2, CROSS_K,
     1      CROSS_A, SHEAR_K, BEND_K1, BEND_K2
      COMMON /RADII/ R1,R2, RR1, RR2
      COMMON /MACHINE/ UNDFLOW
C
      ENTERF_I = ENTERF(P1,EL1,P2,EL2)
      BETA1 = BETA(P1,EL1)
      BETA2 = BETA(P2,EL2)
      BETA1_INIT = BETA(P1_INIT,EL1_INIT)
```

```
      BETA2_INIT = BETA(P2_INIT,EL2_INIT)
C
      PHI_K1 = STIFF1*(EL1-EL1_INIT)**2
      PHI_K2 = STIFF2*(EL2-EL2_INIT)**2
      PHI_I  = (ENTERF_K/ENTERF_A)*(DEXP(ENTERF_A*ENTERF_I)
     1       - ENTERF_A*ENTERF_I - 1.D0)
      PHI_B1 = 0.5D0*BEND_K1*(BETA1 - BETA1_INIT)**2
      PHI_B2 = 0.5D0*BEND_K2*(BETA2 - BETA2_INIT)**2
      CALL LOCKING(1,P1,EL1,P2,EL2,THETA,DISTANCE,ALPHA,ENTERF_L1)
      CALL LOCKING(2,P1,EL1,P2,EL2,THETA,DISTANCE,ALPHA,ENTERF_L2)
      PHI_L1 = PHI_D(ENTERF_L1)
      PHI_L2 = PHI_D(ENTERF_L2)
C
      PHI = PHI_K1 + PHI_K2 + PHI_I + PHI_B1 + PHI_B2
     1      + PHI_L1 + PHI_L2
      RETURN
      END
C
C     Subrotine to minimize the energy function with
C     respect to (L1,L2) for given values of (p1,p2,theta)
      SUBROUTINE MINIMIZE_PHI(P1,EL1,P2,EL2,THETA,M_ERRCHK)
      INCLUDE 'ABA_PARAM.INC'
      COMMON /GEOM_INIT/ P1_INIT, A1_INIT, EL1_INIT,
     1      P2_INIT, A2_INIT, EL2_INIT, THETA_INIT
      COMMON /STIFFNESS/ ENTERF_K, ENTERF_A, STIFF1, STIFF2, CROSS_K,
     1      CROSS_A, SHEAR_K, BEND_K1, BEND_K2
      DIMENSION SIMPLEX(3,3),SWAP(3),P(2),VECTOR(2),R(3),E(3),C(3)
C
C     Terminate immediately if at zero energy state
      IF ((P1 .EQ. P1_INIT) .AND. (P2 .EQ. P2_INIT) .AND.
     1      (THETA .EQ. THETA_INIT)) THEN
            EL1 = EL1_INIT
            EL2 = EL2_INIT
            RETURN
      END IF
C     Calculate lower bounds on energy function
      BETA_MIN = 0.001D0      ! Smallest crimp angle allowed [radians]
      EL1_FLAT = P1/DCOS(BETA_MIN)
      EL2_FLAT = P2/DCOS(BETA_MIN)
C     Initializes L1 and L2 guesses to be 1% larger than "flat" values
      IF (EL1 .LE. EL1_FLAT) THEN
            EL1 = 1.01D0*EL1_FLAT
      END IF
      IF (EL2 .LE. EL2_FLAT) THEN
            EL2 = 1.01D0*EL2_FLAT
      END IF
      EL1_GUESS = EL1
      EL2_GUESS = EL2
C     Modified Simplex Minimization
C     Initial Simplex Size Parameter - Chooses size equal to a
C           percentage of the initial yarn length. Percentage is the
C           max strain in the yarn direction, but has a maximum value
C           of 1%
      SIZE = DABS(DMIN1(0.01D0,
     1      DMAX1(DLOG(P1/P1_INIT),DLOG(P2/P2_INIT))))
C     Scale Factors
      SCALE_E = 1.5D0
```

```
      SCALE_C = 0.5D0
C     Maximum tension error permitted [force units]
      T_ERROR = 1.D-6
C     Adjust initial guess to avoid symmetry problems
      IF ((P1 .EQ. P2) .AND. (EL1_GUESS .EQ. EL2_GUESS)) THEN
            EL1_GUESS = EL1_GUESS*1.0001D0
      END IF
C     Calculates initial unsorted simplex
C     simplex(simplex element,component[L1,L2,Phi])
      SIMPLEX(1,1) = EL1_GUESS
      SIMPLEX(1,2) = EL2_GUESS
      SIMPLEX(1,3) = PHI(P1,EL1_GUESS,P2,EL2_GUESS,THETA)
      SIMPLEX(2,1) = EL1_GUESS + 2.D0*SIZE*EL1_INIT
      SIMPLEX(2,2) = EL2_GUESS +      SIZE*EL2_INIT
      SIMPLEX(2,3) = PHI(P1,SIMPLEX(2,1),P2,SIMPLEX(2,2),THETA)
      SIMPLEX(3,1) = EL1_GUESS +      SIZE*EL1_INIT
      SIMPLEX(3,2) = EL2_GUESS + 2.D0*SIZE*EL2_INIT
      SIMPLEX(3,3) = PHI(P1,SIMPLEX(3,1),P2,SIMPLEX(3,2),THETA)
C     Sorts the simplex in order of decending energies (W=1, N=2, B=3)
      DO K = 1,2
            DO L = K+1,3
                  IF (SIMPLEX(K,3) .LT. SIMPLEX(L,3)) THEN
                        SWAP(1) = SIMPLEX(K,1)
                        SWAP(2) = SIMPLEX(K,2)
                        SWAP(3) = SIMPLEX(K,3)
                        SIMPLEX(K,1) = SIMPLEX(L,1)
                        SIMPLEX(K,2) = SIMPLEX(L,2)
                        SIMPLEX(K,3) = SIMPLEX(L,3)
                        SIMPLEX(L,1) = SWAP(1)
                        SIMPLEX(L,2) = SWAP(2)
                        SIMPLEX(L,3) = SWAP(3)
                  END IF
            END DO
      END DO
C     Stores best values
      PHI_BEST = SIMPLEX(3,3)
      EL1_BEST = SIMPLEX(3,1)
      EL2_BEST = SIMPLEX(3,2)
      N_IMPROVE = 0
C     Begin Simplex Loop
      DO J = 1,1000
C           Calculate midpoint of reflection place
            P(1) = (SIMPLEX(2,1)+SIMPLEX(3,1))/2.D0
            P(2) = (SIMPLEX(2,2)+SIMPLEX(3,2))/2.D0
C           Calculate reflection vector
            VECTOR(1) = P(1) - SIMPLEX(1,1)
            VECTOR(2) = P(2) - SIMPLEX(1,2)
C           Evaluate Reflection Point R
            R(1) = P(1)+VECTOR(1)
            R(2) = P(2)+VECTOR(2)
            IF ((R(1) .GT. EL1_FLAT) .AND. (R(2) .GT. EL2_FLAT)) THEN
                  R(3) = PHI(P1,R(1),P2,R(2),THETA)
            ELSE
                  R(3) = 1.D20
            END IF
```

```
C           Scale reflection vector according to Phi_R
C           If R is better than B, evaluate extension E
            IF (R(3) .LT. SIMPLEX(3,3)) THEN
                  VECTOR(1) = VECTOR(1)*SCALE_E
                  VECTOR(2) = VECTOR(2)*SCALE_E
                  E(1) = P(1)+VECTOR(1)
                  E(2) = P(2)+VECTOR(2)
                  IF ((E(1).GT.EL1_FLAT).AND.(E(2).GT.EL2_FLAT)) THEN
                        E(3) = PHI(P1,E(1),P2,E(2),THETA)
                  ELSE
                        E(3) = 1.D20
                  END IF
C                 If E is better than R, use E, otherwise, use R
                  IF (E(3) .LT. R(3)) THEN
                        SIMPLEX(1,1) = E(1)
                        SIMPLEX(1,2) = E(2)
                        SIMPLEX(1,3) = E(3)
                  ELSE
                        SIMPLEX(1,1) = R(1)
                        SIMPLEX(1,2) = R(2)
                        SIMPLEX(1,3) = R(3)
                  END IF
C           If R is worse than B, but better than N, use R
            ELSE IF (R(3) .LT. SIMPLEX(2,3)) THEN
                  SIMPLEX(1,1) = R(1)
                  SIMPLEX(1,2) = R(2)
                  SIMPLEX(1,3) = R(3)
C           If R is worse than B and N, but better than W, use C+
            ELSE IF (R(3) .LT. SIMPLEX(1,3)) THEN
                  VECTOR(1) = VECTOR(1)*SCALE_C
                  VECTOR(2) = VECTOR(2)*SCALE_C
                  C(1) = P(1)+VECTOR(1)
                  C(2) = P(2)+VECTOR(2)
                  IF ((C(1).GT.EL1_FLAT).AND.(C(2).GT.EL2_FLAT)) THEN
                        C(3) = PHI(P1,C(1),P2,C(2),THETA)
                  ELSE
                        C(3) = 1.D20
                  END IF
                  SIMPLEX(1,1) = C(1)
                  SIMPLEX(1,2) = C(2)
                  SIMPLEX(1,3) = C(3)
C           If R worse than all of the previous simplex values, use C-
            ELSE
                  VECTOR(1) = VECTOR(1)*SCALE_C
                  VECTOR(2) = VECTOR(2)*SCALE_C
                  C(1) = P(1)-VECTOR(1)
                  C(2) = P(2)-VECTOR(2)
                  IF ((C(1).GT.EL1_FLAT).AND.(C(2).GT.EL2_FLAT)) THEN
                        C(3) = PHI(P1,C(1),P2,C(2),THETA)
                  ELSE
                        C(3) = 1.D20
                  END IF
                  SIMPLEX(1,1) = C(1)
                  SIMPLEX(1,2) = C(2)
                  SIMPLEX(1,3) = C(3)
            END IF
```

```
C           Modified Simplex sort to ensure that new point is not W
            SWAP(1) = SIMPLEX(1,1)
            SWAP(2) = SIMPLEX(1,2)
            SWAP(3) = SIMPLEX(1,3)
            SIMPLEX(1,1) = SIMPLEX(2,1)
            SIMPLEX(1,2) = SIMPLEX(2,2)
            SIMPLEX(1,3) = SIMPLEX(2,3)
            SIMPLEX(2,1) = SWAP(1)
            SIMPLEX(2,2) = SWAP(2)
            SIMPLEX(2,3) = SWAP(3)
            IF (SIMPLEX(2,3) .LT. SIMPLEX(3,3)) THEN
                  SWAP(1) = SIMPLEX(2,1)
                  SWAP(2) = SIMPLEX(2,2)
                  SWAP(3) = SIMPLEX(2,3)
                  SIMPLEX(2,1) = SIMPLEX(3,1)
                  SIMPLEX(2,2) = SIMPLEX(3,2)
                  SIMPLEX(2,3) = SIMPLEX(3,3)
                  SIMPLEX(3,1) = SWAP(1)
                  SIMPLEX(3,2) = SWAP(2)
                  SIMPLEX(3,3) = SWAP(3)
            END IF
C           Calculates max change in tension
            IF (SIMPLEX(3,3) .GT. PHI_BEST) THEN
                  WRITE(7,*) 'WARNING: SIMPLEX STEP INCREASING ENERGY'
            END IF
            DEL_T1 = DABS(SIMPLEX(3,1) - EL1_BEST)*STIFF1
            DEL_T2 = DABS(SIMPLEX(3,2) - EL2_BEST)*STIFF2
            DEL_TV1 = DABS(VECTOR(1))*STIFF1
            DEL_TV2 = DABS(VECTOR(2))*STIFF2
C           Increments non-improvement counter if there is no
C           significant improvement, resets it if there is
            IF (DMAX1(DEL_T1,DEL_T2,DEL_TV1,DEL_TV2) .LT. T_ERROR) THEN
                  N_IMPROVE = N_IMPROVE + 1
            ELSE
                  N_IMPROVE = 0
            END IF
C           Updates best guess
            PHI_BEST = SIMPLEX(3,3)
            EL1_BEST = SIMPLEX(3,1)
            EL2_BEST = SIMPLEX(3,2)
C           Termination Condition - Terminates when best tensions have
C                 not changed (more than the max error) for more than
C                 six steps
            IF ((N_IMPROVE .GT. 6) .AND. (J .GT. 15)) THEN
                  EXIT
            END IF
      END DO
      IF (J .GT. 1000) THEN
            WRITE(7,*) 'WARNING: SIMPLEX METHOD DID NOT CONVERGE'
            M_ERRCHK = 1
      END IF
      EL1 = EL1_BEST
      EL2 = EL2_BEST
      RETURN
      END
C
C ***************************************************************
```

```
C THE FOLLOWING FUNCTION DETERMINES STRESS IF INPUT FORCE SCALARS AND
C FABRIC STATE ARE KNOWN
C ***************************************************************
      FUNCTION STRESS_CLC(I,J,P1,EL1,D1,BETA1,ALPHA1,G1,F1,EMB1,TL1,
     1
      P2,EL2,D2,BETA2,ALPHA2,G2,F2,EMB2,TL2,
     3                                        THETA,EM)
      INCLUDE 'ABA_PARAM.INC'
      DIMENSION G1(3), G2(3)
C     11-DIRECTION TERMS
C      Yarn Tension
       TERM1 = F1
C      Force from Yarn Bending
       TERM2 = EMB1*DSIN(BETA1)/EL1
C      Force from in-plane yarn moment
       TERM3 = EM*DCOS(THETA)/(2.D0*P1*DSIN(THETA))
C      Force from warp locking
       TERM4 = TL1*P1/D1
C      Force from weft locking
       TERM5 = TL2*(P2**2)*(DCOS(THETA))**2/(P1*D2)
       TERM5B = TL2*DSIN(ALPHA2)*P2*DABS(DCOS(THETA))*DSIN(BETA1)/EL1
C     22-DIRECTION TERMS
C      Yarn Tension
       TERM6 = F2
C      Force from Yarn Bending
       TERM7 = EMB2*DSIN(BETA2)/EL2
C      Force from in-plane yarn moment
       TERM8 = EM*DCOS(THETA)/(2.D0*P2*DSIN(THETA))
C      Force from warp locking
       TERM9 = TL2*P2/D2
C      Force from weft locking
       TERM10 = TL1*(P1**2)*(DCOS(THETA))**2/(P2*D1)
       TERM10B = TL1*DSIN(ALPHA1)*P1*DABS(DCOS(THETA))*DSIN(BETA2)/EL2
C     12-DIRECTION TERMS (SYMMETRIC)
C      In-plane yarn moment
       TERM11 = EM/(4.D0*P1*P2*(DSIN(THETA))**2)
C      Warp locking
       TERM12 = TL1*P1*DCOS(THETA)/(2.D0*P2*D1*DSIN(THETA))
C      Weft locking
       TERM13 = TL2*P2*DCOS(THETA)/(2.D0*P1*D2*DSIN(THETA))
C
       STRESS_CLC = (1.D0/(2.D0*P2*DSIN(THETA)))*
     1             (TERM1-TERM2-TERM3-TERM4-TERM5-TERM5B)*G1(I)*G1(J)
     2             + (1.D0/(2.D0*P1*DSIN(THETA)))*
     3             (TERM6-TERM7-TERM8-TERM9-TERM10-TERM10B)*G2(I)*G2(J)
     4             +(TERM11 + TERM12 + TERM13)*(G1(I)*G2(J)+G2(I)*G1(J))
       RETURN
       END
C
C ***************************************************************
C ***************************************************************
C                              UMAT SUBROUTINE
C ***************************************************************
C ***************************************************************
      SUBROUTINE UMAT(STRESS,STATEV,DDSDDE,SSE,SPD,SCD,
     1 RPL,DDSDDT,DRPLDE,DRPLDT,
     2 STRAN,DSTRAN,TIME,DTIME,TEMP,DTEMP,PREDEF,DPRED,CMNAME,
```

```
     3 NDI,NSHR,NTENS,NSTATV,PROPS,NPROPS,COORDS,DROT,PNEWDT,
     4 CELENT,DFGRD0,DFGRD1,NOEL,NPT,LAYER,KSPT,KSTEP,KINC)
      INCLUDE 'ABA_PARAM.INC'
      CHARACTER*80 CMNAME
      DIMENSION STRESS(NTENS),STATEV(NSTATV),
     1 DDSDDE(NTENS,NTENS),DDSDDT(NTENS),DRPLDE(NTENS),
     2 STRAN(NTENS),DSTRAN(NTENS),TIME(2),PREDEF(1),DPRED(1),
     3 PROPS(NPROPS),COORDS(3),DROT(3,3),DFGRD0(3,3),DFGRD1(3,3)
C     Internal variables to be defined
      DIMENSION E1(3), G1_INIT(3), G2_INIT(3), G1(3), G2(3),
     1 STRAN1(NTENS),
     2 VAR_G1(3), VAR_G2(3), VAR_DFGRD(3,3), TRIAL_DFGRD(3,3),
     3 VAR_STRESS(NTENS)
C     E1: Reference vector pointing in the 1-direction
C     Gi: unit vectors indicating orientation of warp and weft yarns
C     STRAN1: Array of strains at the end of the increments
C     VAR_Gi: warp and weft direction vectors used in numeric variation
C           for calculating the numeric Jacobean
C     VAR_DFGRD, TRIAL_DFGRD: Deformation gradients used in numeric
C           variation for calculating the numeric Jacobean
C     VAR_STRESS: Storage for stresses resulting from strain variations
C           for calculating the numeric Jacobean
C
C ************************************************
C Common variables used by multiple subroutines
C ************************************************
C     Geometric parameters
      COMMON /GEOM_INIT/ P1_INIT, A1_INIT, EL1_INIT,
     1      P2_INIT, A2_INIT, EL2_INIT, THETA_INIT
C     Stiffness parameters
      COMMON /STIFFNESS/ ENTERF_K, ENTERF_A, STIFF1, STIFF2, CROSS_K,
     1      CROSS_A, SHEAR_K, BEND_K1, BEND_K2
C     Dissipative parameters
      COMMON /SHEAR_DISS/ GAMMAF_DOT, EMM0
C     Yarn Radii
      COMMON /RADII/ R1,R2, RR1, RR2
C     Machine variable
      COMMON /MACHINE/ UNDFLOW
C
C ******************
C Variable Assignment
C ******************
C     Array of strains at the end of the increment
      DO I=1,NTENS
            STRAN1(I) = STRAN(I) + DSTRAN(I)
      ENDDO
C
      UNDFLOW = 1.0E-10
      PI = 2.D0*DASIN(1.D0)
C
C     Material Properties
C     Yarn Radii and density
      R1 = PROPS(1)
      RR1 = PROPS(2)
      R2 = PROPS(3)
      RR2 = PROPS(4)
      DENS1 = PROPS(5)
```

```
      DENS2 = PROPS(6)
C     Initial half-wavelengths
      P1_INIT = PROPS(7)
      P2_INIT = PROPS(8)
C     Initial Yarn orientations
      G1_INIT(1) = DCOS(PROPS(9))
      G1_INIT(2) = DSIN(PROPS(9))
      G1_INIT(3) = 0.D0
      G2_INIT(1) = DCOS(PROPS(10))
      G2_INIT(2) = DSIN(PROPS(10))
      G2_INIT(3) = 0.D0
      THETA_INIT = DABS(PROPS(10)-PROPS(9))
C     Initial yarn lengths and crimp amplitudes
C     NOTE: A1_INIT, A2_INIT, and L2_INIT are determined from radii,
C     initial wavelengths, and L1 to ensure a consistent, zero-stress
C     initial state.
      EL1_INIT = PROPS(11)
      A1_INIT = AMPLITUDE(P1_INIT, EL1_INIT)
      A2_INIT = (R1+R2) - A1_INIT
      EL2_INIT = EL_CLC(P2_INIT,A2_INIT)
C     Yarn axial stiffnesses - Input in terms of EA and must be divided
C     by yarn length to get k=EA/L
      STIFF1 = PROPS(12)/EL1_INIT
      STIFF2 = PROPS(13)/EL2_INIT
C     Yarn cross-sectinal stiffness properties
      ENTERF_K = PROPS(14)
      ENTERF_A = PROPS(15)
C     Crosslocking stiffness
      CROSS_K = PROPS(16)
      CROSS_A = PROPS(17)
C     Yarn bending stiffnesses
      BEND_K1 = PROPS(18)
      BEND_K2 = PROPS(19)
C     Elastic rotational stiffness
      SHEAR_K = PROPS(20)
C     Rotational dissipation properties
      GAMMA_F0 = PROPS(21)
      EM0 = PROPS(22)
      B = PROPS(23)
C     Macroscopic strain rate estimate
      GAMMA_DOT_TEST = PROPS(24)
C     Reference vector in 1-direction
      E1(1) = 1.D0
      E1(2) = 0.D0
      E1(3) = 0.D0
C     State Variables--initially have have zero value
      IF (TIME(2) .EQ. 0.D0) THEN
C           Wavelenghts from previous step
            OLD_P1 = P1_INIT
            OLD_P2 = P2_INIT
C           Dissipative rotation
            GAMMA_F = 0.D0
C           Dissipative rotation rate
            GAMMA_F_DOT = 0.D0
C           Total rotation from previous step
            OLD_GAMMA = 0.D0
```

```
C           Total Rotational velocity from previous step
            OLD_GAMMA_DOT = 0.D0
C           Crimp angles from previous step
            OLD_BETA1 = DATAN(A1_INIT/P1_INIT)
            OLD_BETA2 = DATAN(A2_INIT/P2_INIT)
C           Crimp angle rates from previous step
            OLD_BETA1_DOT = 0.D0
            OLD_BETA2_DOT = 0.D0
      ELSE
            OLD_P1 = STATEV(1)
            OLD_P2 = STATEV(2)
            OLD_BETA1 = STATEV(13)
            OLD_BETA1_DOT = STATEV(14)
            OLD_BETA2 = STATEV(15)
            OLD_BETA2_DOT = STATEV(16)
            GAMMA_F = STATEV(17)
            GAMMA_F_DOT = STATEV(18)
            OLD_GAMMA = STATEV(19)
            OLD_GAMMA_DOT = STATEV(20)
      ENDIF
C     Check to ensure initial fabric geometry is valid
      IF (A2_INIT .LT. 0.D0) THEN
            WRITE(7,*) 'INVALID INPUT PROPERTIES, NEGATIVE AMPLITUDE'
            CALL XIT
      END IF
C
C     Parameter to determine fraction of macroscopic strain rate
C           estimate that local dissipative strain rates must exceed
C           before explicit stability is checked
      RATE_CHECK_FACTOR = 0.01D0
C     Allowed percentage change of dissipative strain rate over time
C           step
      RATE_CHANGE_FACTOR = 0.15D0
C     Reduction factor if dissipative strain rate change is too great
      TIME_RED_FACTOR = 0.35D0
C     Parameter to enable inertial stabilization:
      STABILIZATION_FACTOR = 1.0D0
C
C ************************************
C Determination of geometric parameters
C ************************************
C     Initialize guess values of length for minimization function
      EL1 = EL1_INIT
      EL2 = EL2_INIT
C     Apply deformation gradient to get p1, p2, g1, g2, theta
      G1 = MATMUL(DFGRD1,G1_INIT)
      G2 = MATMUL(DFGRD1,G2_INIT)
      STRETCH1 = DSQRT(DOT_PRODUCT(G1,G1))
      STRETCH2 = DSQRT(DOT_PRODUCT(G2,G2))
      P1 = STRETCH1 * P1_INIT
      P2 = STRETCH2 * P2_INIT
      G1 = G1 / STRETCH1
      G2 = G2 / STRETCH2
      THETA = DACOS(DOT_PRODUCT(G1,G2))
      THETA1 = DACOS(DOT_PRODUCT(G1,E1))
      THETA2 = DACOS(DOT_PRODUCT(G2,E1))
C     Finds the L1 and L2 that correspond to the minimum energy state
```

```
C     associated with the applied p1, p2, and theta
      M_ERRCHK = 0
      CALL MINIMIZE_PHI(P1,EL1,P2,EL2,THETA,M_ERRCHK)
C     If minimization algorithm failed, attempt smaller time step
      IF (M_ERRCHK .EQ. 1) THEN
            PNEWDT = 0.5
            RETURN
      END IF
C     Determines cross section interference corresponding to pi and Li
      ENTERF_I = ENTERF(P1,EL1,P2,EL2)
C     Determines A and beta to correspond to p
      A1 = AMPLITUDE(P1,EL1)
      BETA1 = BETA(P1,EL1)
      A2 = AMPLITUDE(P2,EL2)
      BETA2 = BETA(P2,EL2)
C *********************************************
C Determination of rate-independent internal loads
C *********************************************
C     Fiber tension from elongations
      T1 = STIFF1*(EL1 - EL1_INIT)
      T2 = STIFF2*(EL2 - EL2_INIT)
C     Bending Moments
      EMB1 = BEND_K1*(BETA1 - BETA(P1_INIT,EL1_INIT))
      EMB2 = BEND_K2*(BETA2 - BETA(P2_INIT,EL2_INIT))
C     Locking forces (compressive)
      CALL LOCKING(1,P1,EL1,P2,EL2,THETA,D1,ALPHA1,ENTERF_L1)
      CALL LOCKING(2,P1,EL1,P2,EL2,THETA,D2,ALPHA2,ENTERF_L2)
      TL1 = T_L(ENTERF_L1)
      TL2 = T_L(ENTERF_L2)
C     Contact force between yarns
      CFORCE = ENTERF_K*(DEXP(ENTERF_A*ENTERF_I) - 1.D0)
C     Calculates effective in-plane forces in each direction
      F1 = T1*DCOS(BETA1)
      F2 = T2*DCOS(BETA2)
C
C ********************************************************************
C Determination of rate-dependent loads and update of rate-dependent
C state variables
C ********************************************************************
C     Determine total rotation angle
      GAMMA = THETA_INIT - THETA
C     Determine dissipative portion of rotation explicitly
      GAMMA_F_NEW = GAMMA_F + GAMMA_F_DOT*DTIME
C     Calculate elastic portion of rotation
      GAMMA_E = GAMMA - GAMMA_F_NEW
C     Calculate moment resulting from elastic rotation
      EM = SHEAR_K*GAMMA_E
C     Calculate new dissipative rotation rate from the moment
      GAMMA_F_DOT_NEW = GAMMA_F0*(EM/EM0)**B
C     Check to ensure that time step is small enough for explicit
C           determination of gamma_f
C     Only check if dissipation rate from previous time step is greater
C           than a percentage of the macroscopic strain rate estimate
      IF (DABS(GAMMA_F_DOT) .GE. RATE_CHECK_FACTOR*GAMMA_DOT_TEST) THEN
C     Check to ensure that the change in dissipative strain rate does
C           not exceed some percentage of the old dissipative strain
C           rate
```

```
      IF (DABS(GAMMA_F_DOT_NEW - GAMMA_F_DOT) .GT.
     1                  RATE_CHANGE_FACTOR*DABS(GAMMA_F_DOT)) THEN
            WRITE(7,*) 'WARNING, LARGE CHANGE IN DISSIPATIVE SHEAR
     1      STRAIN RATE'
            WRITE(7,*) 'GAMMA_F_DOT=',GAMMA_F_DOT,' GAMMA_F_DOT_NEW=',
     1 GAMMA_F_DOT_NEW
            WRITE(7,*) 'RATE_FACTOR =', RATE_CHECK_FACTOR,
     1            ' GAMMA_DOT_TEST =', GAMMA_DOT_TEST
            WRITE(7,*) 'REDUCING TIME STEP'
            PNEWDT = TIME_RED_FACTOR
            RETURN
      END IF
      END IF
C
C ************************************************************
C Stabilization
C     Below are code blocks for dynamic (inertial) stabilization
C     (based on the rotational inertia of the yarns).  Another
C     option is to employ ABAQUS's automatic stabilization
C     routine, which is a more general case of inertial
C     stabilization but will affect all DOF's.
C ************************************************************
C     Stabilization in Axial Compression
C     Determine the rotational inertias of the yarns in compressive
C           buckling
      COMP_I1 = 0.5D0*DENS1*PI*(R1**4)*EL1 +
     1      2.D0*DENS1*PI*(R1**2)*(EL1**3)/3.D0
      COMP_I2 = 0.5D0*DENS2*PI*(R2**4)*EL2 +
     1      2.D0*DENS2*PI*(R2**2)*(EL2**3)/3.D0
C     Caclucate the crimp angle rate
      BETA1_DOT = (BETA1 - OLD_BETA1)/DTIME
      BETA2_DOT = (BETA2 - OLD_BETA2)/DTIME
C     Calculate the crimp angle acceleration
      BETA1_DOTDOT = (BETA1_DOT - OLD_BETA1_DOT)/DTIME
      BETA2_DOTDOT = (BETA2_DOT - OLD_BETA2_DOT)/DTIME
C     Calculate the stabilizing forces
      FS1 = STABILIZATION_FACTOR*COMP_I1*BETA1_DOTDOT/(2.D0*A1)
      FS2 = STABILIZATION_FACTOR*COMP_I2*BETA2_DOTDOT/(2.D0*A2)
C     Determine total stabilized force
      F1 = F1 - FS1
      F2 = F2 - FS2
C
C     Stabilization in Shear
C     Determine the rotational inertias of the yarns in shear buckling
      ROT_I1 = DENS1*PI*(R1**4)*EL1/(2.D0*(DCOS(BETA1))**2) +
     1      (2.D0/3.D0)*DENS1*PI*(R1**2)*(P1**2)*EL1
      ROT_I2 = DENS2*PI*(R2**4)*EL2/(2.D0*(DCOS(BETA2))**2) +
     1      (2.D0/3.D0)*DENS2*PI*(R2**2)*(P2**2)*EL2
C     Calculate Rotation Rate
      GAMMA_DOT = (GAMMA - OLD_GAMMA)/DTIME
C     Calculate Rotational acceleration
      GAMMA_DOTDOT = (GAMMA_DOT - OLD_GAMMA_DOT)/DTIME
C     Calculate stabilizing moment
      EM_S = STABILIZATION_FACTOR *
     1      ROT_I1*ROT_I2*GAMMA_DOTDOT/(ROT_I1 + ROT_I2)
C     Total moment = physical moment + stabilization moment
      EM = EM + EM_S
```

```
C
C ***************************
C Calculate Stress Components
C ***************************
C     STRESS(1) = sigma_11
      STRESS(1) = STRESS_CLC(1,1,P1,EL1,D1,BETA1,ALPHA1,G1,F1,EMB1,TL1,
     1                       P2,EL2,D2,BETA2,ALPHA2,G2,F2,EMB2,TL2,
     2                       THETA,EM)
C     STRESS(2) = sigma_22
      STRESS(2) = STRESS_CLC(2,2,P1,EL1,D1,BETA1,ALPHA1,G1,F1,EMB1,TL1,
     1                       P2,EL2,D2,BETA2,ALPHA2,G2,F2,EMB2,TL2,
     2                       THETA,EM)
C     STRESS(3) = sigma_33 = 0 if 3D element in use
C     If a 2D element, this will be overwritten in the next line
      STRESS(3) = 0.D0
C     STRESS(NDI+1) = sigma12 = sigma21
      STRESS(NDI+1) = STRESS_CLC(1,2,P1,EL1,D1,BETA1,ALPHA1,G1,F1,EMB1,
     1                           TL1,P2,EL2,D2,BETA2,ALPHA2,G2,F2,
     2                           EMB2,TL2,THETA,EM)
C     All other stress components are zero
      IF (NSHR .GT. 1) THEN
      DO I=NDI+2,NTENS
            STRESS(I) = 0.D0
      END DO
      END IF
C
C ********************************************************************
C Calculate energy totals (for information only; does not affect
C analysis)
C ********************************************************************
C     Elastic Energy
      BETA1_INIT = BETA(P1_INIT, EL1_INIT)
      BETA2_INIT = BETA(P2_INIT, EL2_INIT)
      PHI_D1 = PHI_D(ENTERF_L1)
      PHI_D2 = PHI_D(ENTERF_L2)
      SSE = (1.D0/(4.D0*P1_INIT*P2_INIT*DSIN(THETA_INIT))) * (
     1      (ENTERF_K/ENTERF_A)*(DEXP(ENTERF_A*ENTERF_I) -
     2            ENTERF_A*ENTERF_I - 1.D0)
     3      + 0.5D0*STIFF1*(EL1-EL1_INIT)**2
     4      + 0.5D0*STIFF2*(EL2-EL2_INIT)**2
     5      + 0.5D0*BEND_K1*(BETA1 - BETA1_INIT)**2
     6      + 0.5D0*BEND_K2*(BETA2 - BETA2_INIT)**2
     7      + PHI_D1 + PHI_D2)
      SPD = SPD + (1.D0/(4.D0*P1_INIT*P2_INIT*DSIN(THETA_INIT))) *
     1            DABS((EM-EM_S)*(GAMMA_F_NEW - GAMMA_F))
C     Stabilization energy is stored as "creep dissipation" energy
      SCD = SCD + (1.D0/(4.D0*P1_INIT*P2_INIT*DSIN(THETA_INIT))) * (
     1            DABS(EM_S*(GAMMA - OLD_GAMMA)) +
     2            DABS(FS1*(P1 - OLD_P1)) + DABS(FS2*(P2 - OLD_P2)))
C
C ****************************************
C Numerical Determination of Material Jacobean
C ****************************************
C     Base strain value used if actual strain increment in a direction
C     is too small for a percentage of it to be an effective variation
      BASE_EPSILON = 1.D-6    ! Significantly affects convergence
C     Code applies positive strain variation of either 10%
```

```
C     of the strain increment from the load step in the direction of
C     the strain increment, or this base value, whichever has a greater
C     magnitude.
C
C VARIATION IN E11
C ----------------
C     Variational Deformation Gradient
      IF (DABS(0.1D0*DSTRAN(1)) .GT. BASE_EPSILON) THEN
            EPSILON = 0.1D0*DSTRAN(1)
      ELSE
            EPSILON = BASE_EPSILON
      END IF
      VAR_DFGRD(1,1) = DEXP(EPSILON)
      VAR_DFGRD(1,2) = 0.D0
      VAR_DFGRD(1,3) = 0.D0
      VAR_DFGRD(2,1) = 0.D0
      VAR_DFGRD(2,2) = 1.D0
      VAR_DFGRD(2,3) = 0.D0
      VAR_DFGRD(3,1) = 0.D0
      VAR_DFGRD(3,2) = 0.D0
      VAR_DFGRD(3,3) = 1.D0
C     Trial deformation gradient after variation
      TRIAL_DFGRD = MATMUL(VAR_DFGRD,DFGRD1)
C     Apply trial deformation gradient to find variated parameters
      VAR_G1 = MATMUL(TRIAL_DFGRD,G1_INIT)
      VAR_G2 = MATMUL(TRIAL_DFGRD,G2_INIT)
      VAR_STRETCH1 = DSQRT(DOT_PRODUCT(VAR_G1,VAR_G1))
      VAR_STRETCH2 = DSQRT(DOT_PRODUCT(VAR_G2,VAR_G2))
      VAR_P1 = VAR_STRETCH1 * P1_INIT
      VAR_P2 = VAR_STRETCH2 * P2_INIT
      VAR_G1 = VAR_G1 / VAR_STRETCH1
      VAR_G2 = VAR_G2 / VAR_STRETCH2
      VAR_THETA = DACOS(DOT_PRODUCT(VAR_G1,VAR_G2))
C     Initial L guesses = L(F1)
      VAR_L1 = EL1
      VAR_L2 = EL2
C     Caluclated variated lengths
      M_ERRCHK = 0
      CALL MINIMIZE_PHI(VAR_P1,VAR_L1,VAR_P2,VAR_L2,VAR_THETA,M_ERRCHK)
      IF (M_ERRCHK .EQ. 100) THEN
            PNEWDT = 0.5
            RETURN
      END IF
C     Determine the variated tensions and angles
      VAR_BETA1 = BETA(VAR_P1,VAR_L1)
      VAR_BETA2 = BETA(VAR_P2,VAR_L2)
      VAR_A1 = AMPLITUDE(VAR_P1,VAR_L1)
      VAR_A2 = AMPLITUDE(VAR_P2,VAR_L2)
      VAR_T1 = STIFF1*(VAR_L1 - EL1_INIT)
      VAR_T2 = STIFF2*(VAR_L2 - EL2_INIT)
      VAR_EMB1 = BEND_K1*(VAR_BETA1 - BETA(P1_INIT,EL1_INIT))
      VAR_EMB2 = BEND_K2*(VAR_BETA2 - BETA(P2_INIT,EL2_INIT))
      CALL LOCKING(1,VAR_P1,VAR_L1,VAR_P2,VAR_L2,VAR_THETA,
     1      VAR_D1,VAR_ALPHA1,VAR_ENTERF_L1)
      CALL LOCKING(2,VAR_P1,VAR_L1,VAR_P2,VAR_L2,VAR_THETA,
     1      VAR_D2,VAR_ALPHA2,VAR_ENTERF_L2)
      VAR_TL1 = T_L(VAR_ENTERF_L1)
```

```
      VAR_TL2 = T_L(VAR_ENTERF_L2)
      VAR_F1 = VAR_T1*DCOS(VAR_BETA1)
      VAR_F2 = VAR_T2*DCOS(VAR_BETA2)
      VAR_GAMMA = THETA_INIT - VAR_THETA
      VAR_GAMMA_E = VAR_GAMMA - GAMMA_F_NEW
      VAR_EM = SHEAR_K*VAR_GAMMA_E
      VAR_GAMMA_DOT = (VAR_GAMMA - OLD_GAMMA)/DTIME
C     Inertial Stabilization
      VAR_GAMMA_DOTDOT = (VAR_GAMMA_DOT - OLD_GAMMA_DOT)/DTIME
      VAR_EM_S = ROT_I1*ROT_I2*VAR_GAMMA_DOTDOT/(ROT_I1 + ROT_I2)
      VAR_EM = VAR_EM + VAR_EM_S
      VAR_BETA1_DOT = (VAR_BETA1 - OLD_BETA1)/DTIME
      VAR_BETA2_DOT = (VAR_BETA2 - OLD_BETA2)/DTIME
      VAR_BETA1_DOTDOT = (VAR_BETA1_DOT - OLD_BETA1_DOT)/DTIME
      VAR_BETA2_DOTDOT = (VAR_BETA2_DOT - OLD_BETA2_DOT)/DTIME
      VAR_FS1 = COMP_I1*VAR_BETA1_DOTDOT/(2.D0*VAR_A1)
      VAR_FS2 = COMP_I2*VAR_BETA2_DOTDOT/(2.D0*VAR_A2)
      VAR_F1 = VAR_F1 - VAR_FS1
      VAR_F2 = VAR_F2 - VAR_FS2
C     Calculate the variated stresses
C     STRESS(1) = sigma_11
      VAR_STRESS(1)=STRESS_CLC(1,1,VAR_P1,VAR_L1,VAR_D1,VAR_BETA1,
     1  VAR_ALPHA1,VAR_G1,VAR_F1,VAR_EMB1,VAR_TL1,VAR_P2,VAR_L2,VAR_D2,
     2  VAR_BETA2,VAR_ALPHA2,VAR_G2,VAR_F2,VAR_EMB2,VAR_TL2,VAR_THETA,
     3  VAR_EM)
C     STRESS(2) = sigma_22
      VAR_STRESS(2)=STRESS_CLC(2,2,VAR_P1,VAR_L1,VAR_D1,VAR_BETA1,
     1  VAR_ALPHA1,VAR_G1,VAR_F1,VAR_EMB1,VAR_TL1,VAR_P2,VAR_L2,VAR_D2,
     2  VAR_BETA2,VAR_ALPHA2,VAR_G2,VAR_F2,VAR_EMB2,VAR_TL2,VAR_THETA,
     3  VAR_EM)
C     STRESS(3) = sigma_33 = 0 if 3D element in use
C     If a 2D element in use, this will be overwritten in the next line
      VAR_STRESS(3) = 0.D0
C     STRESS(NDI+1) = sigma12 = sigma21
      VAR_STRESS(NDI+1)=STRESS_CLC(1,2,VAR_P1,VAR_L1,VAR_D1,VAR_BETA1,
     1  VAR_ALPHA1,VAR_G1,VAR_F1,VAR_EMB1,VAR_TL1,VAR_P2,VAR_L2,VAR_D2,
     2  VAR_BETA2,VAR_ALPHA2,VAR_G2,VAR_F2,VAR_EMB2,VAR_TL2,VAR_THETA,
     3  VAR_EM)
C
C     All other stress components are zero
      IF (NSHR .GT. 1) THEN
      DO I=NDI+2,NTENS
            VAR_STRESS(I) = 0.D0
      END DO
      END IF
C     Calculation of the Jacobian
      DO I=1,NTENS
            DDSDDE(I,1) = (VAR_STRESS(I) - STRESS(I))/EPSILON
      ENDDO
C
C VARIATION IN E22
C ----------------
C     Variational Deformation Gradient
      IF (DABS(0.1D0*DSTRAN(2)) .GT. BASE_EPSILON) THEN
            EPSILON = 0.1D0*DSTRAN(2)
      ELSE
            EPSILON = BASE_EPSILON
```

```
      END IF
      VAR_DFGRD(1,1) = 1.D0
      VAR_DFGRD(1,2) = 0.D0
      VAR_DFGRD(1,3) = 0.D0
      VAR_DFGRD(2,1) = 0.D0
      VAR_DFGRD(2,2) = DEXP(EPSILON)
      VAR_DFGRD(2,3) = 0.D0
      VAR_DFGRD(3,1) = 0.D0
      VAR_DFGRD(3,2) = 0.D0
      VAR_DFGRD(3,3) = 1.D0
C     Trial deformation gradient after variation
      TRIAL_DFGRD = MATMUL(VAR_DFGRD,DFGRD1)
C     Apply trial deformation gradient to find variated parameters
      VAR_G1 = MATMUL(TRIAL_DFGRD,G1_INIT)
      VAR_G2 = MATMUL(TRIAL_DFGRD,G2_INIT)
      VAR_STRETCH1 = DSQRT(DOT_PRODUCT(VAR_G1,VAR_G1))
      VAR_STRETCH2 = DSQRT(DOT_PRODUCT(VAR_G2,VAR_G2))
      VAR_P1 = VAR_STRETCH1 * P1_INIT
      VAR_P2 = VAR_STRETCH2 * P2_INIT
      VAR_G1 = VAR_G1 / VAR_STRETCH1
      VAR_G2 = VAR_G2 / VAR_STRETCH2
      VAR_THETA = DACOS(DOT_PRODUCT(VAR_G1,VAR_G2))
C     Initial L guesses = L(F1)
      VAR_L1 = EL1
      VAR_L2 = EL2
C     Caluclated variated lengths
      M_ERRCHK = 0
      CALL MINIMIZE_PHI(VAR_P1,VAR_L1,VAR_P2,VAR_L2,VAR_THETA,M_ERRCHK)
      IF (M_ERRCHK .EQ. 100) THEN
            PNEWDT = 0.5
            RETURN
      END IF
C     Determine the variated tensions and angles
      VAR_BETA1 = BETA(VAR_P1,VAR_L1)
      VAR_BETA2 = BETA(VAR_P2,VAR_L2)
      VAR_A1 = AMPLITUDE(VAR_P1,VAR_L1)
      VAR_A2 = AMPLITUDE(VAR_P2,VAR_L2)
      VAR_T1 = STIFF1*(VAR_L1 - EL1_INIT)
      VAR_T2 = STIFF2*(VAR_L2 - EL2_INIT)
      VAR_EMB1 = BEND_K1*(VAR_BETA1 - BETA(P1_INIT,EL1_INIT))
      VAR_EMB2 = BEND_K2*(VAR_BETA2 - BETA(P2_INIT,EL2_INIT))
      CALL LOCKING(1,VAR_P1,VAR_L1,VAR_P2,VAR_L2,VAR_THETA,
     1      VAR_D1,VAR_ALPHA1,VAR_ENTERF_L1)
      CALL LOCKING(2,VAR_P1,VAR_L1,VAR_P2,VAR_L2,VAR_THETA,
     1      VAR_D2,VAR_ALPHA2,VAR_ENTERF_L2)
      VAR_TL1 = T_L(VAR_ENTERF_L1)
      VAR_TL2 = T_L(VAR_ENTERF_L2)
      VAR_F1 = VAR_T1*DCOS(VAR_BETA1)
      VAR_F2 = VAR_T2*DCOS(VAR_BETA2)
      VAR_GAMMA = THETA_INIT - VAR_THETA
      VAR_GAMMA_E = VAR_GAMMA - GAMMA_F_NEW
      VAR_EM = SHEAR_K*VAR_GAMMA_E
      VAR_GAMMA_DOT = (VAR_GAMMA - OLD_GAMMA)/DTIME
C     Inertial Stabilization
      VAR_GAMMA_DOTDOT = (VAR_GAMMA_DOT - OLD_GAMMA_DOT)/DTIME
      VAR_EM_S = ROT_I1*ROT_I2*VAR_GAMMA_DOTDOT/(ROT_I1 + ROT_I2)
      VAR_EM = VAR_EM + VAR_EM_S
```

```
      VAR_BETA1_DOT = (VAR_BETA1 - OLD_BETA1)/DTIME
      VAR_BETA2_DOT = (VAR_BETA2 - OLD_BETA2)/DTIME
      VAR_BETA1_DOTDOT = (VAR_BETA1_DOT - OLD_BETA1_DOT)/DTIME
      VAR_BETA2_DOTDOT = (VAR_BETA2_DOT - OLD_BETA2_DOT)/DTIME
      VAR_FS1 = COMP_I1*VAR_BETA1_DOTDOT/(2.D0*VAR_A1)
      VAR_FS2 = COMP_I2*VAR_BETA2_DOTDOT/(2.D0*VAR_A2)
      VAR_F1 = VAR_F1 - VAR_FS1
      VAR_F2 = VAR_F2 - VAR_FS2
C     Calculate the variated stresses
C     STRESS(1) = sigma_11
      VAR_STRESS(1)=STRESS_CLC(1,1,VAR_P1,VAR_L1,VAR_D1,VAR_BETA1,
     1  VAR_ALPHA1,VAR_G1,VAR_F1,VAR_EMB1,VAR_TL1,VAR_P2,VAR_L2,VAR_D2,
     2  VAR_BETA2,VAR_ALPHA2,VAR_G2,VAR_F2,VAR_EMB2,VAR_TL2,VAR_THETA,
     3  VAR_EM)
C     STRESS(2) = sigma_22
      VAR_STRESS(2)=STRESS_CLC(2,2,VAR_P1,VAR_L1,VAR_D1,VAR_BETA1,
     1  VAR_ALPHA1,VAR_G1,VAR_F1,VAR_EMB1,VAR_TL1,VAR_P2,VAR_L2,VAR_D2,
     2  VAR_BETA2,VAR_ALPHA2,VAR_G2,VAR_F2,VAR_EMB2,VAR_TL2,VAR_THETA,
     3  VAR_EM)
C     STRESS(3) = sigma_33 = 0 if 3D element in use
C     If a 2D element in use, this will be overwritten in the next line
      VAR_STRESS(3) = 0.D0
C     STRESS(NDI+1) = sigma12 = sigma21
      VAR_STRESS(NDI+1)=STRESS_CLC(1,2,VAR_P1,VAR_L1,VAR_D1,VAR_BETA1,
     1  VAR_ALPHA1,VAR_G1,VAR_F1,VAR_EMB1,VAR_TL1,VAR_P2,VAR_L2,VAR_D2,
     2  VAR_BETA2,VAR_ALPHA2,VAR_G2,VAR_F2,VAR_EMB2,VAR_TL2,VAR_THETA,
     3  VAR_EM)
C
C     All other stress components are zero
      IF (NSHR .GT. 1) THEN
      DO I=NDI+2,NTENS
            VAR_STRESS(I) = 0.D0
      END DO
      END IF
C     Calculation of the Jacobian
      DO I=1,NTENS
            DDSDDE(I,2) = (VAR_STRESS(I) - STRESS(I))/EPSILON
      END DO
C
C VARIATION IN E33
C ----------------
C     Calculation of the Jacobian DDSDDE(i,3) = 0 if 3D element in use
      DO I=1,NTENS
            DDSDDE(I,3) = 0.D0
      END DO
C
C VARIATION IN E12
C ----------------
C     Variational Deformation Gradient
      IF (DABS(0.1D0*DSTRAN(NDI+1)) .GT. BASE_EPSILON) THEN
            EPSILON = 0.1D0*DSTRAN(NDI+1)
      ELSE
            EPSILON = BASE_EPSILON
      END IF
      VAR_DFGRD(1,1) = 0.5D0*(DEXP(EPSILON/2.D0) + DEXP(EPSILON/-2.D0))
      VAR_DFGRD(1,2) = 0.5D0*(DEXP(EPSILON/2.D0) - DEXP(EPSILON/-2.D0))
      VAR_DFGRD(1,3) = 0.D0
```

```
      VAR_DFGRD(2,1) = 0.5D0*(DEXP(EPSILON/2.D0) - DEXP(EPSILON/-2.D0))
      VAR_DFGRD(2,2) = 0.5D0*(DEXP(EPSILON/2.D0) + DEXP(EPSILON/-2.D0))
      VAR_DFGRD(2,3) = 0.D0
      VAR_DFGRD(3,1) = 0.D0
      VAR_DFGRD(3,2) = 0.D0
      VAR_DFGRD(3,3) = 1.D0
C     Trial deformation gradient after variation
      TRIAL_DFGRD = MATMUL(VAR_DFGRD,DFGRD1)
C     Apply trial deformation gradient to find variated parameters
      VAR_G1 = MATMUL(TRIAL_DFGRD,G1_INIT)
      VAR_G2 = MATMUL(TRIAL_DFGRD,G2_INIT)
      VAR_STRETCH1 = DSQRT(DOT_PRODUCT(VAR_G1,VAR_G1))
      VAR_STRETCH2 = DSQRT(DOT_PRODUCT(VAR_G2,VAR_G2))
      VAR_P1 = VAR_STRETCH1 * P1_INIT
      VAR_P2 = VAR_STRETCH2 * P2_INIT
      VAR_G1 = VAR_G1 / VAR_STRETCH1
      VAR_G2 = VAR_G2 / VAR_STRETCH2
      VAR_THETA = DACOS(DOT_PRODUCT(VAR_G1,VAR_G2))
C     Initial L guesses = L(F1)
      VAR_L1 = EL1
      VAR_L2 = EL2
C     Caluclated variated lengths
      M_ERRCHK = 0
      CALL MINIMIZE_PHI(VAR_P1,VAR_L1,VAR_P2,VAR_L2,VAR_THETA,M_ERRCHK)
      IF (M_ERRCHK .EQ. 100) THEN
            PNEWDT = 0.5
            RETURN
      END IF
C     Determine the variated tensions and angles
      VAR_BETA1 = BETA(VAR_P1,VAR_L1)
      VAR_BETA2 = BETA(VAR_P2,VAR_L2)
      VAR_A1 = AMPLITUDE(VAR_P1,VAR_L1)
      VAR_A2 = AMPLITUDE(VAR_P2,VAR_L2)
      VAR_T1 = STIFF1*(VAR_L1 - EL1_INIT)
      VAR_T2 = STIFF2*(VAR_L2 - EL2_INIT)
      VAR_EMB1 = BEND_K1*(VAR_BETA1 - BETA(P1_INIT,EL1_INIT))
      VAR_EMB2 = BEND_K2*(VAR_BETA2 - BETA(P2_INIT,EL2_INIT))
      CALL LOCKING(1,VAR_P1,VAR_L1,VAR_P2,VAR_L2,VAR_THETA,
     1      VAR_D1,VAR_ALPHA1,VAR_ENTERF_L1)
      CALL LOCKING(2,VAR_P1,VAR_L1,VAR_P2,VAR_L2,VAR_THETA,
     1      VAR_D2,VAR_ALPHA2,VAR_ENTERF_L2)
      VAR_TL1 = T_L(VAR_ENTERF_L1)
      VAR_TL2 = T_L(VAR_ENTERF_L2)
      VAR_F1 = VAR_T1*DCOS(VAR_BETA1)
      VAR_F2 = VAR_T2*DCOS(VAR_BETA2)
      VAR_GAMMA = THETA_INIT - VAR_THETA
      VAR_GAMMA_E = VAR_GAMMA - GAMMA_F_NEW
      VAR_EM = SHEAR_K*VAR_GAMMA_E
      VAR_GAMMA_DOT = (VAR_GAMMA - OLD_GAMMA)/DTIME
C     Inertial Stabilization
      VAR_GAMMA_DOTDOT = (VAR_GAMMA_DOT - OLD_GAMMA_DOT)/DTIME
      VAR_EM_S = ROT_I1*ROT_I2*VAR_GAMMA_DOTDOT/(ROT_I1 + ROT_I2)
      VAR_EM = VAR_EM + VAR_EM_S
      VAR_BETA1_DOT = (VAR_BETA1 - OLD_BETA1)/DTIME
      VAR_BETA2_DOT = (VAR_BETA2 - OLD_BETA2)/DTIME
      VAR_BETA1_DOTDOT = (VAR_BETA1_DOT - OLD_BETA1_DOT)/DTIME
      VAR_BETA2_DOTDOT = (VAR_BETA2_DOT - OLD_BETA2_DOT)/DTIME
```

```
      VAR_FS1 = COMP_I1*VAR_BETA1_DOTDOT/(2.D0*VAR_A1)
      VAR_FS2 = COMP_I2*VAR_BETA2_DOTDOT/(2.D0*VAR_A2)
      VAR_F1 = VAR_F1 - VAR_FS1
      VAR_F2 = VAR_F2 - VAR_FS2
C     Calculate the variated stresses
C     STRESS(1) = sigma_11
      VAR_STRESS(1)=STRESS_CLC(1,1,VAR_P1,VAR_L1,VAR_D1,VAR_BETA1,
     1  VAR_ALPHA1,VAR_G1,VAR_F1,VAR_EMB1,VAR_TL1,VAR_P2,VAR_L2,VAR_D2,
     2  VAR_BETA2,VAR_ALPHA2,VAR_G2,VAR_F2,VAR_EMB2,VAR_TL2,VAR_THETA,
     3  VAR_EM)
C     STRESS(2) = sigma_22
      VAR_STRESS(2)=STRESS_CLC(2,2,VAR_P1,VAR_L1,VAR_D1,VAR_BETA1,
     1  VAR_ALPHA1,VAR_G1,VAR_F1,VAR_EMB1,VAR_TL1,VAR_P2,VAR_L2,VAR_D2,
     2  VAR_BETA2,VAR_ALPHA2,VAR_G2,VAR_F2,VAR_EMB2,VAR_TL2,VAR_THETA,
     3  VAR_EM)
C     STRESS(3) = sigma_33 = 0 if 3D element in use
C     If a 2D element in use, this will be overwritten in the next line
      VAR_STRESS(3) = 0.D0
C     STRESS(NDI+1) = sigma12 = sigma21
      VAR_STRESS(NDI+1)=STRESS_CLC(1,2,VAR_P1,VAR_L1,VAR_D1,VAR_BETA1,
     1  VAR_ALPHA1,VAR_G1,VAR_F1,VAR_EMB1,VAR_TL1,VAR_P2,VAR_L2,VAR_D2,
     2  VAR_BETA2,VAR_ALPHA2,VAR_G2,VAR_F2,VAR_EMB2,VAR_TL2,VAR_THETA,
     3  VAR_EM)
C
C     All other stress components are zero
      IF (NSHR .GT. 1) THEN
      DO I=NDI+2,NTENS
            VAR_STRESS(I) = 0.D0
      END DO
      END IF
C     Calculation of the Jacobian
      DO I=1,NTENS
            DDSDDE(I,NDI+1) = (VAR_STRESS(I) - STRESS(I))/EPSILON
      END DO
C All other jacobian terms are zero
C -------------------------------
      IF (NSHR .GT. 1) THEN
      DO J=NDI+2,NTENS
            DO I=1,NTENS
                  DDSDDE(I,J) = 0.D0
            END DO
      END DO
      END IF
C ***********************************************
C Export the internal variables as state variables
C ***********************************************
      STATEV(1) = P1
      STATEV(2) = P2
      STATEV(3) = THETA1
      STATEV(4) = THETA2
      STATEV(5) = PHI_D1
      STATEV(6) = PHI_D2
      STATEV(7) = ENTERF_L1
      STATEV(8) = ENTERF_L2
      STATEV(9) = T1
      STATEV(10) = T2
      STATEV(11) = CFORCE
```

```
      STATEV(12) = EM
      STATEV(13) = BETA1
      STATEV(14) = BETA1_DOT
      STATEV(15) = BETA2
      STATEV(16) = BETA2_DOT
      STATEV(17) = GAMMA_F_NEW
      STATEV(18) = GAMMA_F_DOT_NEW
      STATEV(19) = GAMMA
      STATEV(20) = GAMMA_DOT
C
      RETURN
      END
```